Design of a Quantum Radar System with Sustainable Entanglement

Sürdürülebilir Dolanıklıkla Kuantum RADAR Sistemi Tasarımı

Ahmad SALMANOGLI KHIAVI

Assoc. Prof. Dr. Dinçer GÖKCEN

Supervisor

Submitted to

Graduate School of Science and Engineering of Hacettepe University

as a Partial Fulfillment to the Requirements

for the Award of the Degree of Doctor of Philosophy in Electrical and Electronics Engineering.

2021

ÖZET

Sürdürülebilir Dolanıklıkla Kuantum Radar Sistemi Tasarımı

Ahmad SALMANOGHLI KHIAVI

Doktora, Elektrik ve Elektronik Mühendisliği Bölümü

Tez Danışmanı: Doç. Dr. Dinçer GÖKCEN

Haz 2021, 116 sayfa

Bu çalışma, parçacıklar arasındaki kuantum dolanıklığı korumak amacıyla tam kuantum teorisini kullanarak, elektro-opto-mekanik veya optoelektronik dönüştürücü türleriyle çalışan kuantum radarlarda parçacıklar arasındaki dolanıklılık halinin sürdürülebilirliğine odaklanmaktadır. Kuantum radar, klasik bir radarla aynı şekilde mikrodalga fotonları kullanan bir kuantum uzaklık algılama sistemi olarak tanımlanmaktadır. Bu tezde tasarlanan kuantum radar, kuantum aydınlatma protokolü kurallarına uymaktadır. Buna göre, tasarlanan cihaz, algılamayı iyileştirmek ve tanımlamayı güçlü bir şekilde gerçekleştirmek amacıyla dolanık mikrodalga fotonlar kullanır. Kuantum mekaniği açısından bakıldığında, fotonlar gibi iki kuantum parçacığı birbiriyle etkileşmek üzere üretildiğinden ve özellikleri klasik olmayan bir şekilde birbirine bağlı olduğundan dolanıklık oluşmaktadır. Kuantum olanıklık halindeki parçacıklar arasında paylaşılan özellikler, aralarındaki mesafeden tamamen bağımsızdır. Ne yazık ki, parçacıklar arasındaki dolanma davranışı istikrarsızdır ve bu doğrultuda, parçacıklar arasındaki dolanma halini üretmek ve uzun süre korumak çalışmadaki en önemli amaçlardan biridir. Ek olarak, gürültü, hızlı bir bozulmaya neden olarak dolaşık durumdaki yapıları kolayca etkileyebilmektedir. Bahsedilen önemli hususların bilgisiyle, bu çalışma I. bölümde yer verildiği üzere kuantum radar operasyonlarının her aşamasında dolanıklılık durumlarını korumayı amaçlamaktadır. II. bölümde mikrodalga ve optik fotonlar arasındaki dolanıklığı oluşturmak için tipik bir dönüştürücü kullanılmıştır. Gerekli olan durumlarda dolaşan

mikrodalga fotonların yoğunlaştırılması III. bölümde anlatılmıştır. Son olarak atmosfere yoğunlaştırılmış foton yayılımı (zayıflatma ortamı) ele alınarak, hedeften foton saçılması olayı IV. bölümde gerçekleşmektedir. Her aşamada, ortam parametreleri dolaşık durumları kritik bir şekilde ortadan kaldırabilir. Bu doktora tezinde, dolaşık fotonları oluşturmak için temel bir yapı olarak iki farklı dönüştürücüye (elektro-opto-mekanik ve optoelektronik dönüştürücüler) sahip bir kuantum radar sisteminin dolanıklık davranışı özellikle vurgulanmaktadır. Bahsedilen dönüştürücüler, sırasıyla L-bandında (1.5 GHz'de mikrodalga boşluğu rezonansı) ve S-bandında (2.7 GHz'de mikrodalga boşluğu rezonansı) çalışacak şekilde tasarlanmış ve böylece, tutulan fotonlar ile geri dönen fotonlar arasındaki dolanıklığı tezin ana görevi olarak analiz edilmiştir.

Kuantum radar sisteminin tasarım aşamaları şu şekildedir:

I. Dönüştürücünün mikrodalga ve optik fotonlar arasında dolanıklık oluşturacak şekilde tasarımı; Bu tezde, özellikle yüksek kalitede bir kuantum radar sistemi tasarlayabilmek amacıyla sürdürülebilir dolaşık fotonlar oluşturarak uygun dönüştürücü tasarlamaya yoğunlaşılmıştır. Bu adımda, dönüştürücülerin kritik parametreleri arasındaki denge belirlenecektir.

II. Dolanık fotonları yükseltmek için yoğunlaştırıcı ortamın (klasik anlamda yükseltici) tasarımı; Bu aşama, geniş menzil tespiti vurgulandığından, klasik radarda birincil rol oynamaktadır.

III. Yayılma kanalının kayıplı bir ortam olarak modellenmesi ve dolanık modlar üzerindeki katkıda bulunan etkilerin incelenmesi.

IV. Hedeften yansıyan dolanık fotonların modellenmesi ve hedef parametrelerinin dolanıklık davranışları üzerindeki etkisi.

V. Kuantum yaklaşımı ile RCS'nin hesaplanması; bu adımda, "dipol yaklaşım yönteminin" RCS'yi analiz etmek için doğru ve eksiksiz bir yöntem olmadığı gösterilmiştir.

Anahtar Kelimeler: Kuantum radar, Kuantum Dolaşıklığı, kuantum teori, Optoelektronik Dönüştürücü, Elektro-opto-mekanik Dönüştürücü, Radar kesiti.

ABSTRACT

Design of a Quantum Radar System with Sustainable Entanglement

Ahmad SALMANOGLI KHIAVI

Doctor of Philosophy, Department of Electrical and Electronics Engineering

Supervisor: Assoc. Prof. Dr. Dinçer GÖKCEN

June 2021, 116 pages

This study mainly focuses on the sustainability of the entanglement in quantum radar working with different types of converters, either electro-opto-mechanical or optoelectronic converters, using full quantum theory at which the priority is to preserve the entanglement. The quantum radar is introduced as a quantum standoff detection system applying microwave photons the same as a classical radar. Quantum radar designed in this dissertation obeys the quantum illumination protocol. Accordingly, the device uses microwave entangled photons to improve detection and enhance identification strongly. From the quantum mechanical point of view, entanglement arises since two quantum particles, such as photons, are produced to interact with each other, and their properties are non-classically connected to each other. The shared properties between the entangled particles are independent of their inter-distance. Unfortunately, the entanglement behavior is so unstable, and more importantly, it is a crucial task to produce and preserve that for a long time. Additionally, the noise can easily affect the entangled states to cause a fast decaying. With knowledge of the crucial points mentioned, this study aimed to preserve the entangled states at each stage of the quantum radar operations, including I. Using a typical converter to create the entanglement between microwave and optical photons, II. Intensifying the entangled microwave photons (if it is necessary), III. Intensified photons propagation to the atmosphere (attenuation medium), IV. Photon scattering

from the target. At each stage, the medium parameters can critically kill the entangled states. This Ph.D. dissertation specifically emphasizes the entanglement behavior of a quantum radar system with two different converters (electro-opto-mechanical and optoelectronics converters) as a basic substrate to generate the entangled photons. The converters mentioned will be designed to operate at L-band (microwave cavity resonate at 1.5 GHz) and S-band (microwave cavity resonate at 2.7 GHz), respectively. Thus, we will try to analyze the entanglement between retained photons with the returned photons as the main task of the thesis.

The steps of the design of the quantum radar system are as follows:

I. Design of the converter to generate entanglement between microwave and optical photons; in this dissertation, we specifically focus on designing the suitable converter to generate sustainable entangled photons to introduce a quantum radar system with high quality. In this step, the trade-off between critical quantities of the converters will be determined.

II. Design of the intensifying medium (amplifier in the classic sense) to amplify the entangled photons; This stage plays a primary role in the classical radar since the large range detection is emphasized.

III. Modeling the propagation channel as a lossy medium and study the contributed effects on the entangled modes

IV. Modeling the entangled photons reflected from the target and target's parameters effect on their entanglement behavior

V. Calculation of the RCS via the quantum approach; in this step, we show that the "dipole approximation method" is not a complete method to analyze the RCS.

Keywords: Quantum Radar, Entanglement, Quantum theory, Optoelectronic Converter, Electro-opto-mechanical Converter, Radar cross-section.

ACKNOWLEDGEMENTS

One of the most amazing journeys that I have ever experienced in my life was my Ph.D journey; it was the first chapter of my scientific story. Yes, Ph.D is not the end of the story, it is a starting point. I have learned a lot of things in this way and constructed my background to strongly start the next chapter! I learned: How to be patient, How to change the way, How to manage the idea, How to effectively express the thought. However, I'm sure, I couldn't support these tasks and move in this way alone. For this reason, I want to thank anyone that helps me:

First of all, I would like to thank my esteemed, smart, patient and supportive supervisor Dr. D. Gökcen for his consistent support, guidance during the running of my project, and valuable supervision during my Ph.D degree. I specially thank Prof. H. S. Geçim for four years' forgettable help and support. I also thank Dr. M. E. Taşgın for his friendly mentorship; in fact, my Quantum knowledge foundation is due to his help and effort. Additionally, I would like to thank my friends, colleagues and Dr. D. Gökcen's research team.

Further, I am also thankful to the Faculty of Engineering and its entire member's staff for all the guidance and help.

My special friend and my life's friend, Zeinab Bayat, I simply couldn't have done this without you, special thanks. I'm sure this long journey could not be finished without your support and help.

Finally, thanks to my parents who set me off in this hard, but interesting and beautiful way a long time ago.

The END of a Beautiful Journey…

CONTENTS

FIGURES

SYMBOLS AND ABBREVIATIONS

Symbols

$\hbar$	Reduced Planck's constant
$\lambda(\lambda_c)$	Wavelength
k_B	Boltzmann's constant
ζ	quantum efficiency
μ_0	Permeability of the free space
ε_0	Permittivity of the free space
ω	Angular frequency
$\chi^{(2)}$	Second-order susceptibility
(2η)	Symplectic eigenvalue
c	Speed of light in free space
κ_{atm}	Atmosphere attenuation factor
m_{eff}	Effective mass of the electron-hole
ω_{eg}	Photodetector gap-related frequency
ω_{oc}	Optical cavity angular frequency
ω_m	Microresonator angular frequency
γ_m	Microresonator decay rate
κ_t	Target decay rate
κ_a	Active medium amplification factor

Abbreviations

BS	Beam splitter
CM	Classical mechanics
JPC	Josephson parametric converter
LIDAR	Light detection and ranging
MC	Microwave cavity
MoM	Method of moment
MR	Microresonator
OC	Optical cavity
OPDC	Optical parameter down converter
PD	Photodetector
PEC	Perfect conductor
QED	Quantum electrodynamics
QD	Quantum dot
QM	Quantum mechanics
QMoM	Quantum method of moment
QRCS	Quantum radar cross-section
RADAR	Radio detection and ranging
RCS (CRCS)	Radar Cross Section
RWA	Rotating wave approximation
SNR	Signal to noise ratio
VD	Varactor diode

1. INTRODUCTION

Recently, the quantum phenomenon has been used as a novel idea in sensors to improve their capabilities and specifications [1-2]. The following studies exemplify the utilization of quantum phenomena in sensors: quantum radar systems [1-4], image resolution enhancement [5-7], quantum illumination [8-9], quantum communication [9-10], increasing the responsivity of plasmonic photodetector [11], engineering the decay rate of plasmonic systems [12], and also modification of Raman signals [13]. However, in the following, the emphasis is laid on the quantum radar that operates as classic radar using quantum phenomena to enhance some performances.

A "quantum radar" system, shown in Figure 1.1, is traditionally introduced as a sensing system utilizing the entangled microwave photons regarding "quantum illumination protocol" to enhance the radar performances, including detection, identification, and resolution [1,4,14-21]. This phenomenon (entanglement) is created through the interaction of two photons, resulting in an interrelated property independent of the distance between particles. [5, 19]. Using microwave photons via quantum radar enables an effective penetration in the atmospheric medium to minimize the losses as classical radar. It has been shown that quantum radars using the entanglement phenomenon strongly improve some crucial quantities such as the "signal to noise ratio" (SNR) and detection probability compared to a classical radar [1, 2, 14-18]. Additionally, it has been investigated that the "effective visibility" of a target can be enhanced when the quantum radar is employed [1]. Also, countermeasures like jamming are efficiently quenched by a quantum radar [1, 2]. The points mentioned above emphasize that quantum radar advantages are just because of the entanglement property. Nonetheless, it is clear that entanglement is fragile, and it is also challenging to produce and preserve that and can be easily affected by the noise sources [12, 13]. Moreover, in a quantum radar system, entanglement is naturally strongly distorted because of the losses introduced due to the atmosphere channel, as well as scattering from the target. Thus, the entanglement fragility becomes worse since employed by quantum radar to propagate into free space to detect the target. This critical issue has been studied in detail [14, 15]. For instance, Ref [14] focuses on

"microwave-optical entanglement", and examines the entanglement affected by "quantum noise" and "quantum Brownian noise". As a significant result, the mentioned work shows that the radar system using "quantum illumination protocol" has a lower probability of error than the coherent-state system. Quantum illumination radar system refers to the quantum radar that utilizes the quantum illumination protocol.

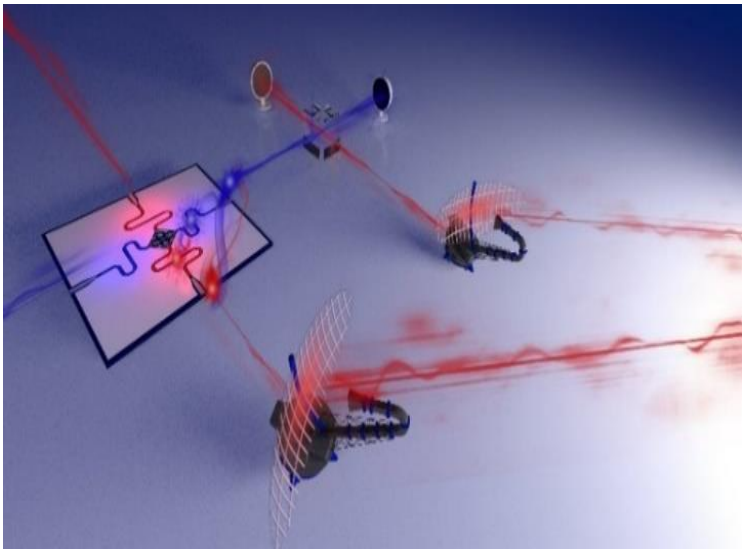

Figure 1.1. A schematic of a quantum radar containing transmission of the entangled photons and backscattering photons detection [16].

One of the exciting works contributed to the "quantum radar" system concentrates on the entangled microwave photons generation using "Josephson parametric converter" (JPC) [16]. The system defined in [16] is schematically depicted in Figure 1.2. After the generation of the entangled states, the entangled photons are amplified to increase the probability of the detection. The entanglement generation and conservation at low operational temperatures is the crucial factor in the system discussed above. Some other interesting works focus on the converters generating the entangled microwave photons [9, 10]. In published works, a typical "electro-opto-mechanical" converter is employed at which the optical cavity couples to the microwave cavity via microresonator operating with frequency in the range of MHz. Thus, the photons induced thermally are strongly increased due to the low-frequency operation and then confined the entangled photons. Therefore, studies [14-18] mentioned above specifically limit the operational temperature at 15 mK.

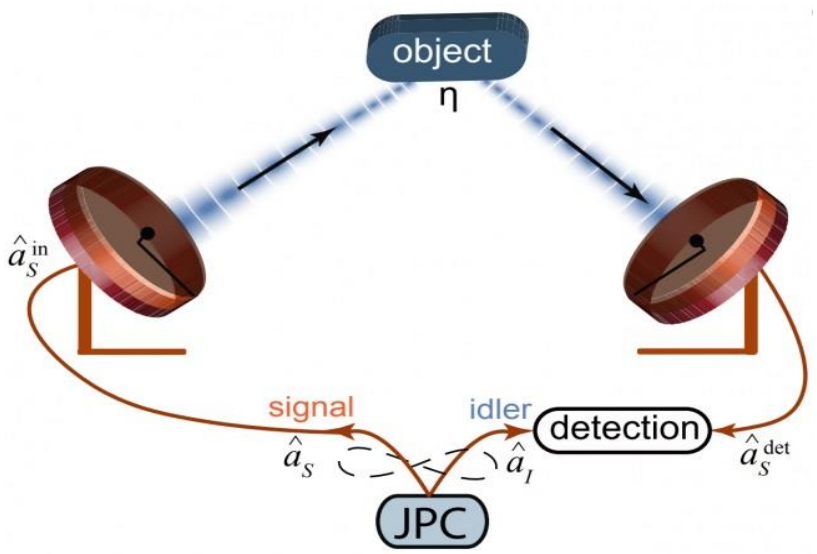

Figure 1.2. Using JPC nonlinearity to generate entangled photons in a typical Quantum Radar [16].

In this Ph.D. dissertation, with knowledge of the above-cited studies, a quantum radar with the aim of entanglement preserving is designed and analyzed by employing full quantum theory to answer some critical questions:

I. By which approach is it possible to manipulate subsystems coupling in the converter to create entanglement between photons at high temperature? [22- 27]

II. Is it possible to define and design a converter more robust in entangled photon generation by increasing the temperature?

III. How and by which design can one eliminate the low-frequency part of the electro-opto-mechanical part that is the original issue of the generation of the thermal photons?

IV. What is the critical temperature that the design system can generate the entangled photons?

V. How the active, passive mediums and also scattering from a target can affect the entangled states?

As the primary goal, the entanglement properties preservation is highly emphasized at each design step. A typical design for a quantum illumination radar system is initiated in this dissertation by an electro-opto-mechanical converter (Figure 1.3). This system contains three coupled subsystems as “optical cavity” (OC), “microresonator” (MR), and “microwave cavity” (MC) to cause the MC modes to become entangled with OC modes. The term “cavity

(e.g., optical or microwave)" is a space where the related modes (optical or microwave) can resonate.

To provide entangled states, the subsystems mentioned above are coupled to each other. OC modes are coupled to MR via the enforced optical pressure, and then the contributed effect is transferred to MC via the changing the capacitance. The system equation of motion is analyzed with the quantum canonical quantization approach by which the entanglement between the fluctuations of the contributed modes is investigated. By engineering the system, the OC and MC modes, which contain optical and microwave photons, become entangled. It will be shown that the designed electro-opto-mechanical system has some drawbacks, such as operating at shallow temperatures and a strong influence of the thermal noise. Then, another converter is introduced to fix the problem. Another system that the dissertation focused on is the optoelectronic-based quantum radar to generate entangled states. In the same way, the optoelectronic converter containing OC, MC, and photodetector (PD) cavities is theoretically designed with full quantum theory. In fact, the low-frequency operating MR subsystem is replaced with an optoelectronic-based component such as PD operating at high frequency. Operating at high frequency strongly limits the thermally excited photons, representing one of the critical cases that destroy the mode's entanglement. Using the optoelectronic converter shows that it is possible to create entanglement between photons at high temperatures. Also, "Simon-Peres-Horodecki criterion" is applied to calculate the cavities modes of entanglement.

After generating the entangled photons, to complete the process to detect the target, the created entangled photons are intensified (in the first system) and propagated into a real medium to interact with a target. Accordingly, quantum electrodynamic theory is utilized to model the intensification of the signal, propagation through the atmosphere channel, and also scattering from the target's surface. In this theory, the quantum electromagnetic field interacts with the quantum field of atoms. It is because all real mediums such as active medium for amplification, passive medium for attenuation, or the target that reflects the incident photons, made of atoms. It is the atoms that interact with the electromagnetic fields. So the atoms are considered as the scattering agents. From the quantum electrodynamics perspective, the interaction between matter and light is given by a term in energy that couple the particle field with the quantum electromagnetic field.

Notably, at each step, the entanglement between the OC mode (idler) kept in the laboratory should be evaluated with the signal that returned and detected by the detector. The main aim is to design a system by which the retained and returned signals is remained entangled after the photon detection. This task is a crucial one, and in fact, for a real quantum radar system, the returned signals completely lost the entanglement between modes. That means that the correlation between retained and returned signals rather than its entanglement should be calculated.

Another vital task studied in this dissertation is radar cross-section calculation with the canonical conjugate method. In this task, it will be proved that the dipole approximation method is not a complete one. The system's dynamics equations are analyzed using the theory of "quantum electrodynamics (QED)".

Following a brief introduction about the new converter emphasized in this study, the major design steps of a typical quantum radar are presented, and then the introduction section will be completed with some critical points about the optoelectronic converter design.

The major design steps are considered as:

I. Optical entangled photons generation,

II. Using converter to create microwave photons entanglement

III. Intensifying the microwave cavity photons,

IV. Propagating the microwave photons in the atmosphere,

V. Scattering the photons from a target

VI. Analyzing the retained and returned fields entanglement

Traditionally, the converter illustrated in Figure 1.3 is used in a quantum radar to generate the entangled photons by engineering the coupling between subsystems. It can be shown that this system cannot operate at high temperatures due to the effect of the MR in the system. In other words, there is no more degree of freedom in the previous design to manipulate the system to support the generation of the entangled states at high temperatures. Thus, it is necessary to introduce another plan to fix the problem.

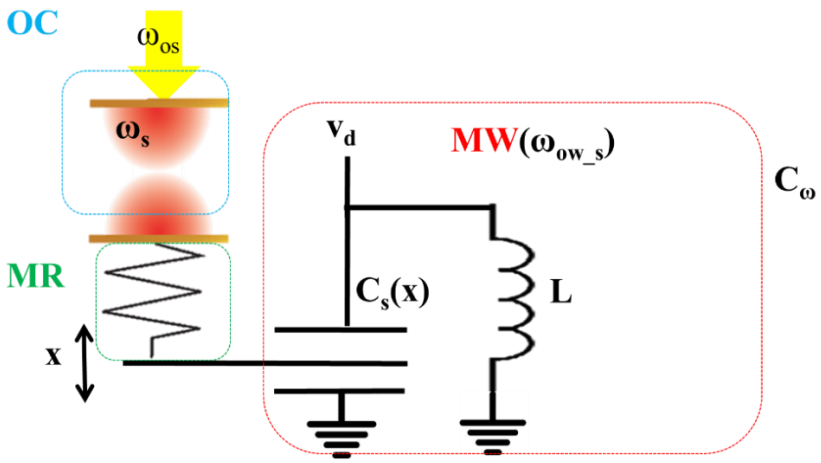

Figure 1.3. Electro-opto-mechanical converter containing three coupled subsystems as OC, MC, and MR [18].

In the second design that the present dissertation emphasizes, the MR subsystem is removed and replaced that with an optoelectronic converter to solve the problem. The optoelectronics converter is utilized to modify the interconnection between cavities. In fact, the mechanical part is removed from the "electro-opto-mechanical" converter [27-31], and rather than, the optoelectronic elements are employed to establish coupling between MC and OC modes [26]. This system is schematically illustrated in Figure 1.4. The exciting idea contributed to the design relates to the subsystems used operating at high frequency. That leads to subside the photons induced due to the thermal effect and the associated noises. It is shown that by engineering the coupling between converter's subsystems, the entanglement modes are strongly increased.

In the same way with the first design, QED is used to analyze the quantum radar systems, amplifier, propagation in the atmosphere, and target's scattering [29,30], and the dynamic equation of the quantum illumination radar are derived using "Heisenberg-Langevin" equations [31,32]. The indicating equations are usually used to analyze any quantum systems and derive the "equation of motion" of the designed system. For a typical system with an associated Hamiltonian (H), the Heisenberg equations are defined using $d\hat{a}/dt = -(j/\hbar)\,[\hat{a},H]$, where $\hat{a}$ is the considered operator. However, to thoroughly analyze a quantum system, it needs to consider the system's interaction with the environment that the system is embedded into. In other words, the Heisenberg equations require other factors such as noises that affect

the system. These terms obeying the Langevin equations called the “Langevin noise operators”. The mentioned operators are added to the equation of the system motion (Heisenberg equations) to complete the analysis. At last, the “Simon-Peres-Horodecki separability criterion” is used for separability calculation between the continuous variable modes [33-36].

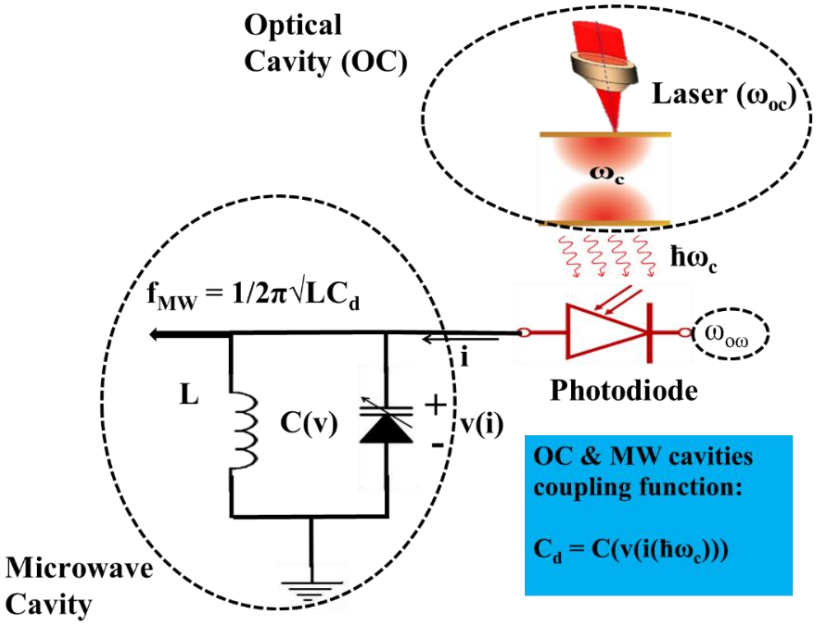

Figure 1.4. Optoelectronic converter contains OC, optoelectronic device [22].

In the following, before concentrating on the main materials of the work, which is quantum theory and the related backgrounds to design the system, it is necessary to shortly and briefly discuss the classical radar and its subsystems. It is because any quantum radar uses the classical radar approach for operation. Nonetheless, we have to focus on the dissertation's main point, which is entanglement sustainability in a quantum radar. This dissertation mainly emphasizes designing a system to generate and preserve the entanglement at high temperatures.

2. CLASSICAL RADAR (a short Review on classical radar subsystems)

The term *RADAR* is an acronym for detection and ranging with the radio wave. Radar as a sensing system employs radio frequency waves to analyze the range, angle, and velocity of objects. Radars are commonly used to detect aircraft, missiles, and ships [37-39]. A radar system is depicted in Figure 2.1 with a block diagram. It, in essence, consists of a transmitter to produce electromagnetic waves, an antenna to amplify the signal and broadcast that, a receiving antenna with the same role and a receiver to detect the backscattering signal (returned fields) from the target, and finally, a processor to analyze properties of the target. In radar applications, the radio waves, which can be continuous or pulsed, issue electromagnetic waves from the transmitter, reflect the wave of the object, then return to the receiver, and finally, after some processing, give some info about the object location, speed and also its properties [38, 39].

There are also others systems functioning similar to the radar but employing the other spectra of the electromagnetic spectrum like visible light. One crucial example is LIDAR ("Light detection and ranging"), which uses infrared spectrum with high-intensity photons. Any detection system, either radar or LIDAR, operates essentially based on the reflection from a target. In essence, if an electromagnetic wave travels through one material and meets another one, the wave will scatter due to the dielectric constant discrepancy in the boundary. That means that any solid object will usually scatter or reflect radio or infrared waves from the target surface. It is only valid for materials with high conductivity as metal and carbon fiber. However, radar absorbing materials have been used for military applications containing resistive and magnetic substances to strongly reduce radar reflection [37-39]. This kind of subject has been discussed explicitly in radar cross-section calculations. The scattering of radar waves from target depends on a variety of parameters consisting of wavelength, target's shape, the angle of wave propagation, and more importantly, depends on the materials of the target. For instance, if the wavelength is comparable with- or shorter than the target size, LIDAR, or laser radar applications, the wave will be backscattered in the same way as a reflection by a mirror. In contrast, if the incident wavelength becomes longer enough regarding the size of the target, the related visibility can be strongly distorted because of the poor reflection. With regard to the points mentioned above, the "Low-

frequency radar technology" is employed just for the detection of the target, not for its identification. That is why the low-frequency radar system cannot identify two close targets from each other; that is contributed to the radar system resolution. Thus, for increasing the radar resolution, the wave's wavelength should be shorter enough. The reflective targets for a short wavelength have angles around 90° between surfaces that reflect the incident wave. To know generally about a classical radar system performance, in the following, the radar range equation is introduced by which one can find the relationship between quantities and also find which quantity can affect the other.

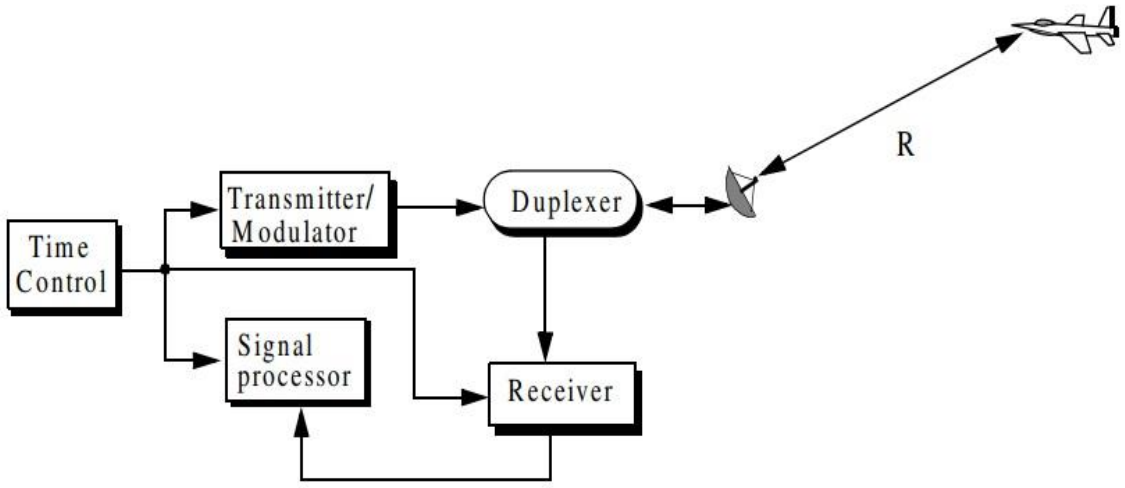

Figure 2.1. Illustration of radar subsystems with block diagrams; time control, transmitter, receiver, signal processing, and duplexer [37].

2.1 Radar range equation

A wave is propagated toward the target in a classical radar system, and some portion of the incident wave is reflected. Here, the detector's receiving power is analyzed and determined by which factors the receiving power will be affected. The receiving antenna gets the backscattering power P_r as [37-39]:

$$P_r = \frac{P_t G_t A_r}{\left(4\pi R_t R_r\right)^2}\left[A_{rs}\sigma F^4 G_{ts}\right],\ A_r = \frac{\lambda_t^2 G_r}{4\pi} \tag{2.1}$$

where P_t, G_t, A_r, A_{rs}, λ_t, G_r, σ, F, R_t, and R_r are transmitter power, transmitting antenna's gain, target effective area, receiving effective antenna aperture, transmitted wavelength, receiving antenna gain, radar cross-section, the factor of pattern propagation, transmitter-target distance,

and also target-receiver distance, respectively. In some cases, the transmitter and receiver are placed at the same location where $R_t = R_r$; then the term $R_t^2 R_r^2$ in Eq. 2.1 can be substituted with R^4.This reveals that the receiving power decreases with the range fourth power, which means that the detecting signals from a distant target are relatively small. The factor F relates to the interference in the route that the pulse is transmitted to detect the target. However, $F = 1$ means that transmission is in a vacuum without any interference; this is impossible due to the environmental effect. To better understand the radar range equation, one can consider Figure 2.2, in which the relationship among parameters is clearly shown.

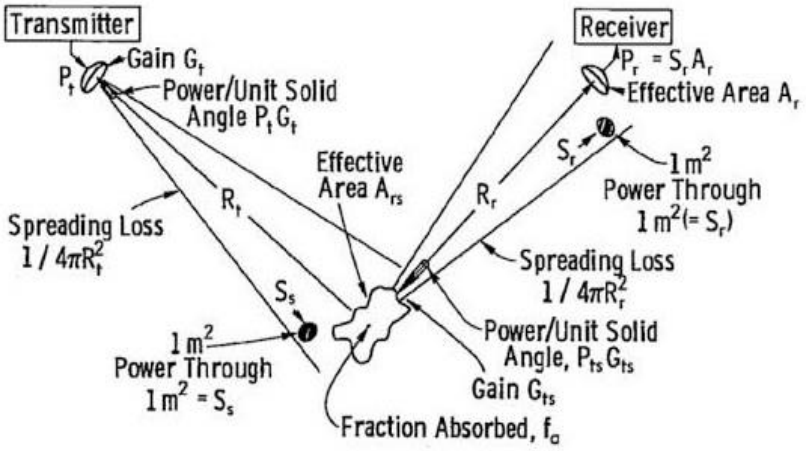

Figure 2.2. Bistatic radar range equation parameters; transmitter antenna gain (G_t), traget effective area (A_{rs}), fraction absorbed (f_a), spreading loss, receiver effective area (A_r) [38].

From this figure, one can understand the step-by-step of radar performance. The operation starts with the transmitter to generate the microwave photons; the microwave photons are amplified and broadcasted via an antenna with gain G_t toward the area for detection. After the propagation of the signals, the signals suffer a loss due to propagation loss in real medium as $1/4\pi R_t^2$ and then interact with the target. All signals cannot reflect toward the radar detector due to the effective area of the target A_{rs} and absorption by the target f_a. However, the backscattering signal suffers one more time due to the effect of the propagation loss as $1/4\pi R_r^2$. Another effect based on the schematic is the effective area of the receiver, which means that all of the backscattering signals cannot be detected, and it is the effective area of the detector A_r that confined it.

2.1.1. Antenna

A radar system requires a device to amplify the signal and spread it out in all directions to broadcast radio signals. Likewise, a transmitter's antenna, the receiver's antenna collects the backscattering signals equally from all directions and amplifies them again [39, 40]. The mentioned device is called an antenna. However, for a monostatic radar, an antenna is used to propagate and collect the signals.

Recently the radar systems have been tended to use omnidirectional broadcast antennas, with directional antenna as a receiver to cover various directions. The directional antenna is specifically employed to reduce the noise.

More importantly, in the receiver, the maximum return signals can be detected via an antenna at angles correctly aligned toward the target. Thus, the antenna has a significant impact on the radar system. The broadcasting signals and receiving signals are amplified, and an effective area of the receiving antenna is essential in detecting backscattered signals.

2.1.2. Noise

Noise is an essential factor that confines the radar system performance [37-39], [41, 42]. Noise as an internal source basically refers to random variations of the signal generated by electronic devices and also applied by the environment. Backscattered signals (returned signals) from the target based on Eq. 1 decline rapidly as distance increases. That means that the amplitude of the returned signals is strongly decreased. Thus, the detector's generated noise can strongly introduce a radar range limitation because the returned signal amplitude is comparable with the applied noise level. The remote targets generate so faint signal for detection, and due to the noise effect, the original signal cannot be detected. Usually, a detector requires a signal exceeding by at least the defined SNR as:

$$SNR = P_r / P_N = \frac{P_t G^2 \lambda^2 \sigma}{(4\pi)^3 R^4 k_B T_0 B F} \tag{2.2}$$

where P_N, T_0, B, and F are receiver noise power, absolute temperature (300 K), the bandwidth receiver, and noise figure, respectively.

In the following, it will be suitable to discuss the noises shortly and their types generated and confined the electronic-based systems and radar. In the radar system, noise appears as stochastic

variations attached to the backscattered signal detected via the receiver. Thus, it becomes more challenging to recognize the signal from the noise if the power of the desired signal is so low. Actually, "noise figure F" is a criterion to measure the noise arisen by a receiver compared to an ideal receiver, and the radar system designers have tried to minimize that factor. Some noises strongly affect the radar systems, such as shot noise [41], flicker noise [42], and thermal noise [22]. "Shot noise" generated by electrons in the device occurs in all detectors and receivers. This noise is the primary source in most receivers and can firmly be confined by low-temperature operation. Another type of noise is flicker noise or 1/f noise generated by electron transit through amplification devices. This type of noise is dominant in low and very low frequency. Additionally, noise can be externally generated like the background natural thermal radiation which surrounds the target. The "thermal noise" is expressed by k_BTB; one can consider the thermal noise effect in Eq. 2 on SNR. In modern radar systems, especially in quantum radar, the internal noises are typically equal to (or lower than) the thermally-induced noise, meaning that 1/f noise and shot noise can be ignored entirely.

Therefore, in the following, due to the subject of this dissertation which is the design of a quantum illumination radar, the focus is briefly shortly laid on the quantum noise that is arisen due to the quantization. When a photodetector is utilized in the receiver, it receives the incoming signal as a quantized photon, leading to the quantum noise and current fluctuation. In other words, whenever discrete particles detect at random times, so some fluctuations occur in the rate of detected photons. The numbers of arrivals discrete photons at time duration (t_d) can be supposed to have a distribution like a "Poisson distribution" [22, 41]. Thus, the current 'i' and its fluctuation $<\delta i^2>$ are calculated as [22, 41]:

$$\begin{aligned} & i = \frac{e}{t_d} n \longrightarrow I = \frac{e}{t_d} < n > \\ & < \delta i^2 >= \frac{e^2}{{t_d}^2} < \delta n^2 > \xrightarrow{\delta n = < n >} = \frac{e}{t_d} I \xrightarrow{t_d = 1/2B} < \delta i^2 >= 2eIB \end{aligned} \tag{2.3}$$

where e, B, and I are the electron charge, receiver bandwidth, the average current I = <i>, respectively. Also, <n> is the photons average number and $<\delta n^2>$ is photons number fluctuation. The other significant parameter that has to be involved in Eq. 2.3 is the quantum efficiency of receiver ζ. The quantum efficiency determines the probability by which every received discrete photon creates a free electron. With including ζ, the fluctuation of the current is re-written as:

$$< \delta i^2 >= 2e\zeta BI \quad (2.4)$$

Eq. 2.4 shows the dependency of the current fluctuation to receiver quantum efficiency, its bandwidth which is arisen due to the quantization. In the design of quantum radar, the effect of the quantum noise is considered, and also thermally excited photons. It is shown that these factors are crucial that can strongly restrict the retained and returned signals entanglement. However, it is noteworthy to indicate that the quantum noise will arise after detecting the signals. In contrast, thermally excited photons (thermal noise) can be found anywhere in the quantum radar system, such as in converter, amplifier, propagation channel, and also scattering from the target. That means that the thermal noise in quantum radar that works with the low-level photons is so critical than other types of noises. However, the simulation of a quantum radar needs to comprehensively analyze the thermal noise at each design level.

2.1.3. Radar Cross Section (RCS)

RCS is a criterion of how a typical target can be detected by a radar or detection system [43-50]. A larger RCS of an object means that the object is more easily detectable. By incidence of a wave toward a target, the illuminated target backscattered a limited rate of the radar's incident waves backscattering to the detector. This is because of the effective target area and target material. Generally, the scattering waves by a target depend on some factors such as [47,48]:

1. the material of the target
2. the real target size
3. the relative size of the target with regarding the incident signal wavelength
4. the polarization of the transmitted and the received signals
5. the angle at which the radar's wave incidents on a portion of the target, and that strongly depends on the target's shape and its orientation
6. the reflected angle by which the scattered beam leaves the target

From the classical picture, RCS is essential for the detection of the targets; nonetheless, the strength of incident pulses and also the distance between radar system and target are not factors that affect the calculation of RCS; it is since RCS is arisen by the target's reflectivity property. For example, the RCS of some simple geometrics is theoretically calculated and illustrated in Figure 2.3.

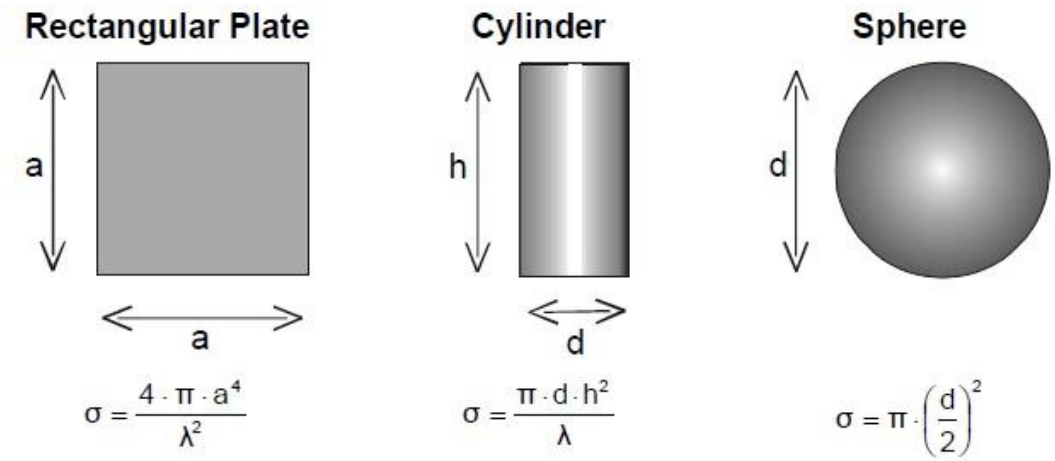

Figure 0.3. RCS of some simple geometric shape analysis with exact method [37].

In from quantum picture, some other factors intuitively depend on analyzing approach that can affect RCS. We will come back to this subject later and compare RCS analysis in the classical realm with the case elaborated in the quantum area and study the advantages and disadvantages of the considered methods.

2.2. A short comparison between classical radar and quantum radar (a generic view on performance)

After a short discussion about classical radar, before focusing on quantum illumination radar and quantum phenomena, it is better to discuss the classical radar's disadvantages. It is a list of advantages of quantum radar that can be used for comparison with classical radar.

1. Non-classical correlation utilized by quantum illumination radar is so complete than the classical correlation; it is just a difference between single-photon correlation and wave front correlation [1-3].
2. SNR is a critical case in the classical radar system [15]; this factor will be strongly enhanced in the quantum radar due to the effect of quantum phenomena.
3. Radar cross-section is improved using quantum illumination radar [51]; using a quantum-based approach gives us some freedom to enhance the associated parameters.

4. Interaction between transmitted wave and medium can be completely analyzed in quantum radar [18]; it means that the quantum theory approach is so complete than the classic theory.
5. Due to the non-classicality used in quantum radar, this type of radar is hardly ever decoyed [1,16].
6. Increasing the detection sensitivity by using the entanglement [16]. The preservation of the entanglement between retained and returned signals is so challenging.
7. Quantum entanglement has been employed to enhance the imaging resolution [5].
8. Able to solve the problem of traditional radar trade-off between resolution and detection range [1,2].
9. Stealthy target detection [1] by quantum radars.
10. Identification of the target materials [1] can be considered as another advantage of quantum radar.

Now, we are ready to start with the quantum radar and initially focus on providing some general information about quantum radar. Thus, some useful tools employed by the quantum theory should be introduced, such as quantum mechanics and quantum physics. These will be considered as the indispensable elements to design the quantum radar.

3. QUANTUM RADAR (a generic definition)

Quantum radar is introduced as a sensing system using either microwave photons or optical photons and utilizing quantum phenomena (i.e., entanglement) to improve target detection and recognition processes. Quantum radar is a remote sensing device that employs quantum entanglement and quantum detections. If quantum radar operates well, it will allow the sensing device to detect its own signal even when strongly affected by the background noise. Thus, quantum radar can detect stealth aircraft, can completely remove the jamming attempts, and can operate in areas containing background noise. Some prototype design of a quantum radar has been proposed [1, 16].

Quantum radar offers an approach by which it can improve the classical radar system's detection, identification, and resolution. Using the entanglement in quantum radar leads to enhancing the target detection capabilities. The operation of the system relies on the photon's quantum states to preserve the entanglement between states. The basic concept of the quantum illumination radar system illustrated in Figure 3.1 is as follows: creating the entangled optical photons and split them in half using a beam splitter. One half, called "signal beam", coupled to a microwave cavity to affect the associated cavity modes in such a way as to preserve the original quantum state. This can be done using either an electro-opto-mechanical converter [14, 15] or an optoelectronic-based system [18, 22] to produce entangled microwave photons. Then microwave signal is broadcasted and received like a classical radar system operating based on the microwave signals. When the backscattered signal (returned signals) is received, it has to be converted back into optical photons and calculate its correlation with the other half "idler beam" of the original entangled beam. The existing nonclassicality correlation between the backscattering photons from the target and the photons (idler) held inside the radar improves signal detection. With such property, quantum illumination radar offers the possibility of strongly improving the detecting, identifying, and resolving small targets [16, 18].

Even though most of the entanglement between photons is lost due to "quantum decoherence" when the microwave photons broadcast toward the target and back; however, it may remain

enough quantum correlations between the returned signal and the idler [18]. Some studies reported that quantum illumination radar employing entanglement photons could significantly increase the resolution over non-entangled photons [1]. Furthermore, the target's visibility is increased when observed with the entangled microwave photons instead of some classical microwave photons [1]. However, in this dissertation, we mainly focus on the sustainability of the entanglement in the designed quantum radar. For this reason, the focus lies in improving the design of the converters traditionally employed by the designer and, at first, producing the entangled microwave photons at high temperatures and then preserving that. The introducing converter is an optoelectronic-based converter that completely employs the high-frequency operation elements. Thus, it is shown that microwave photons entanglement generation at high temperatures becomes possible. It will be an astonishing achievement by which the retuned signals remained entangled with the retained signals. In fact, this is the main aim of this Ph.D. dissertation.

3.1. Quantum Mechanics

It is significant to note that quantum radar essentially operates like a classical radar but significantly differs in the type of signals utilized by the quantum radar. In principle, entangled microwave photons are utilized by quantum radar. It is known that quantum entanglement is a physical source for an application in communication, and thus, it is no longer merely an exposition of quantum mechanics. It should be noted that constructing and detecting the entanglement is crucial in every application. To fundamentally know about the entanglement mathematics and physics, it needs some quantum mechanics tools to deal with, to understand the subject completely [30,52]. In contrast to "Newtonian mechanics", "Quantum mechanics" is a group of mathematical postulates describing the microscopic particles and their interaction. For this reason, it is necessary to shortly introduce some of the quantum mechanics postulations and tools that have been utilized in this thesis. In the following, a short introduction about the Lagrangian is presented [52,53] and Hamiltonian mechanics [30,52,53].

3.1.1. The mechanics of Lagrangian

One can generally consider a system with "n" particles; each particle in classical mechanics is characterized by its position at any time "t" and the related velocity [52,53]. That means the initial condition of a classical system containing particles is the related particles' position and velocity.

Lagrangian mechanics starts with constructing a set of generalized position q_i (i = 1, 2, … N) that describes the classical particles. The associated velocity of the particles is indicated by dq_i/dt. Thus, the Lagrangian mechanic is described by a single function as:

$$L(q,\dot{q};t) = L(q_1, q_2, ...q_N, \dot{q}_1, \dot{q}_2, ..., \dot{q}_N, ; t) \tag{3.1}$$

The Lagrangian is the difference between a system's kinetic and potential energies and is generally presented as:

$$L(q,\dot{q};t) = \frac{1}{2}\sum_{n=1}^{N}\left\{ m_n \frac{d^2 q_n}{dt^2} - V(q_n)\right\} \tag{3.2}$$

Eq. 3.2 defines the Lagrangian for N particles whose kinetic and potential energies are included. However, one can derive the associated Hamiltonian from the Lagrangian. In the next part, the Hamiltonian mechanics is shortly discussed.

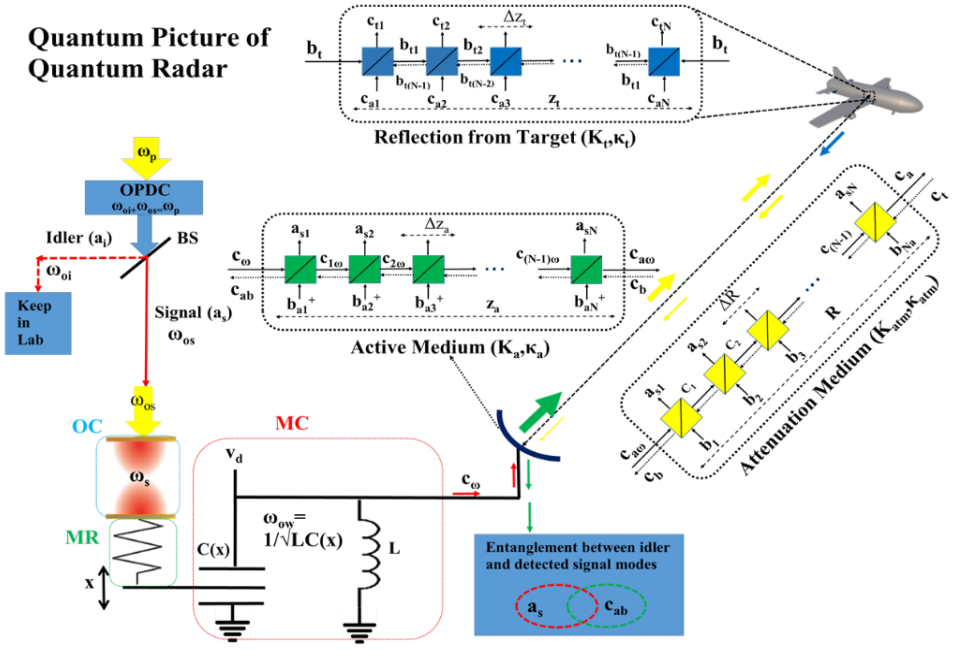

Figure 3.1. General schematic of a quantum radar system; 1. Creation of the entangled optical photons (signal and idler) 2. An electro-opto-mechanical subsystem to generate entangled photons, 3. Microwave photons propagation in the atmosphere to target detection, 4. Scattering from the target [18].

3.1.2. The mechanics of Hamiltonian

In a general way, one can define the Hamiltonian using the Lagrangian defined in Eq. 3.1. With Lagrangian $L(q_n, dq_n/dt; t)$ the momentum p canonically conjugate to q is introduced as [30, 52, 53]:

$$p_n = \frac{\partial L(q_n, \dot{q}_n; t)}{\partial \dot{q}_n} \tag{3.3}$$

It should be noted that the canonical momentum may differ from the mechanical momentum. Thus, using the Legendre transformation, one can define the Hamiltonian by:

$$H(q, p; t) = \sum_{n=1}^{N} \left\{ p_n \frac{dq_n}{dt} \right\} - L(q, \dot{q}; t) \tag{3.4}$$

From Eq. 3.4, the space of q_n and p_n is referred to as phase space. Taking the differential of Hamiltonian with respect to p, q, and t:

$$dH(q, p; t) = \sum_{n=1}^{N} \left\{ \frac{\partial H}{\partial q_n} dq_n + \frac{\partial H}{\partial p_n} dp_n \right\} - \frac{\partial H}{\partial t} dt \tag{3.5}$$

Therefore, using the Euler-Lagrange equation, one can obtain the Hamiltonian equations as:

$$\frac{dq_n}{dt} = \frac{\partial H}{\partial p_n}, \frac{dp_n}{dt} = -\frac{\partial H}{\partial q_n}, \frac{\partial H}{\partial t} = -\frac{\partial L}{\partial t} \tag{3.6}$$

In Hamiltonian mechanics, the system is presented by points (q,p) in phase space on a path that satisfies the equation of motion derived by Hamiltonian.

Also, one can consider the time evolution of dynamical variable H(q,p,t) defined by:

$$\frac{dA(q, p; t)}{dt} = \sum_{n=1}^{N} \left\{ \frac{\partial A}{\partial q_n} \frac{dq_n}{dt} + \frac{\partial A}{\partial p_n} \frac{dp_i}{dt} \right\} + \frac{\partial A}{\partial t} = \sum_{n=1}^{N} \left\{ \frac{\partial A}{\partial q_n} \frac{dH}{dp_n} - \frac{\partial A}{\partial p_n} \frac{dH}{dq_n} \right\} + \frac{\partial A}{\partial t} \tag{3.7}$$

where *A* is a typical variable. From Eq. 3.7, the Poisson bracket is presented as:

$$\{A, H\} = \sum_{n=1}^{N} \left\{ \frac{\partial A}{\partial q_n} \frac{dH}{dp_n} - \frac{\partial A}{\partial p_n} \frac{dH}{dq_n} \right\} \tag{3.8}$$

Finally, the time evolution of A can be defined as:

$$\frac{dA}{dt} = \{A, H\} + \frac{\partial A}{\partial t} \tag{3.9}$$

In classical mechanics, the Poisson bracket plays the same role that the commutation relation plays in quantum mechanics. Upon quantization, the dynamical variable in Hamiltonian mechanics is replaced by operators in quantum mechanics as:

$$CM: \{q_n, q_m\} = 0, \{p_n, p_m\} = 0, \{q_n, p_m\} = \delta_{nm},$$
$$QM: \left[\hat{q}_n, \hat{q}_m\right] = 0, \left[\hat{p}_n, \hat{p}_m\right] = 0, \left[\hat{q}_n, \hat{p}_m\right] = j\hbar\delta_{nm}, \tag{3.10}$$

where CM and QM stand for classical and quantum mechanics, respectively. In the following, some suitable tools used in quantum mechanics will be introduced.

3.1.3 Bra-Ket notation and Pauli matrixes

All of the systems designed in this thesis will be defined as a matrix form and Bra-Ket notation (Ket notation |x> and Bra notation <x|) introduced by Paul Dirac for quantum mechanics [52,53]. A Bra vector x in a finite Hilbert space (can be defined as complete inner product space) is defined as a row vector:

$$< x| = \begin{bmatrix} x_1 & x_2 & . & . & x_n \end{bmatrix} \tag{3.11}$$

Also, |x> "Ket vector" is the vector conjugate transposition in Eq. 3.11 ($|x> = <x|^T$). One can use the "Bra-Ket" vector to define "inner product" as:

$$< x \mid y >= \begin{bmatrix} x_1 & x_2 & . & . & x_n \end{bmatrix} . \begin{bmatrix} y_1 \\ y_2 \\ . \\ . \\ y_n \end{bmatrix} = x_1 y_1 + x_2 y_2 + ... + x_n y_n \tag{3.12}$$

Also, the outer product can be evaluated as:

$$\mid y >< x \mid = \begin{bmatrix} y_1 \\ y_2 \\ . \\ . \\ y_n \end{bmatrix} \begin{bmatrix} x_1 & x_2 & . & . & x_n \end{bmatrix} = \begin{bmatrix} y_1 x_1 & y_1 x_2 & . & . & y_1 x_n \\ y_2 x_1 & y_2 x_2 & . & . & y_2 x_n \\ . & . & . & & \\ . & . & & . & \\ y_n x_1 & y_n x_2 & & & y_n x_n \end{bmatrix} \tag{3.13}$$

Any Ket vectors such as |φ> can be expressed based on some orthonormal basis functions as $|\varphi> = \sum \lambda_n |x_n>$, where λ_n and $|x_n>$ are eigenvalue and eigenvector (basis function) of the system, respectively.

Another essential property of quantum mechanics is the Pauli matrixes. Four Pauli matrices, addressed in Eq. 3.14, are a basis in the space of Hermitian matrices.

$$I = \begin{bmatrix} 1 & 0 \\ 0 & 1 \end{bmatrix}, \sigma_z = \begin{bmatrix} 1 & 0 \\ 0 & -1 \end{bmatrix}, \sigma_x = \begin{bmatrix} 0 & 1 \\ 1 & 0 \end{bmatrix}, \sigma_y = \begin{bmatrix} 0 & j \\ -j & 0 \end{bmatrix} \tag{3.14}$$

For an atom with two-level energies containing ground state |g> and excited state |s> the Pauli matrixes can be re-expressed as: I = |g><g|+|s><s|, σ_z = |s><s|-|g><g|, σ_x= |s><g|+|g><s|, and σ_y= j(|s><g|-|g><s|). In this definition, |g> and |s> are the quantum states that will be shortly discussed later.

3.1.4. Quantum state

For each physical system, one can introduce a Hilbert space that describes its states, and a unit vector in that space defines each system's state. Systems are defined based on the associated states. In other words, it is the states of the system that define the system operations. From the classical point of view, that is called "Eigen-state". There are two types of states: pure and mixed states [53]. When the state associated with a system is unknown, such as $|x_n>$ in which "n" can be changed, and that is predicted to be one of a collection of states, that type of state is called a mixed state. In contrast, a single state such as |x> is regarded as a pure state and known. In reality, due to the system interaction with the environment, the noise usually causes a pure state to convert to a mixed state, so this study emphasizes working with the mixed state. One useful tool to represent the states, either pure state or mixed state, is the density matrix by which one can unify the representation of both pure and mixed states. For a pure state, the density matrix is defined as $\rho = |x><x|$, while for a mixed state, it can be defined as $\rho = \sum \lambda_n |x_n><x_n|$. The latter statement shows that the representation is not unique.

3.1.5. Evolution

The quantum system evolution is defined using pure state, mixed state, and density matrix representation. If the system has no interaction with its implemented space, the system's pure state at initial time t_0 relates to its pure state at time t as $|\varphi(t)> = U|\varphi(t_0)>$, where U is a "unitary matrix" [52, 53]. However, in the general case, a quantum system time evolution is defined using "Schrödinger equation" by:

$$j\hbar \frac{\partial |\varphi>}{\partial t} = H|\varphi> \longrightarrow |\varphi(t)>= e^{[\frac{-jHt}{\hbar}]} |\varphi(t_0)> \quad (3.15)$$

where H is the system Hamiltonian (time-independent). From Eq. 3.15, the unitary matrix can be easily calculated with regard to the system Hamiltonian.

3.1.6. Observable and measurement

Observability considers as a measurable system property. There is a significant difference between observabilities in quantum and classical physics. In classical physics, the observer doesn't change the observables when attempting to measure them. But the condition is so different for microscopic particle and quantum systems. From Copenhagen interpretation [52], particles cannot be considered as observables before measurement. That means the state of a quantum particle is stochastically collapsed when one tries to measure the states. In quantum mechanics, every observable is attained by considering the Hamiltonian. For example, one can consider a pure state $|x>$; the observable that can be measured contains eigenvalue and orthonormal eigenvectors as $H = \sum \lambda_n |x_n><x_n|$, where λ_n is the eigenvalue and $|x_n>$ are the orthonormal eigenvectors. The measurement outcome is λ_n, and the system collapses $|x_n>$. For example, consider a system A collapses $|x_1>$ with measurement outcome λ_1 and the other system named B collapse $|x_1>$ with λ_2, then one can conclude that $[A,B] = 0$. This indicates that with regard to the basis vector collapsed by A and B, A and B become diagonalized, then A and B commute with each other. In contrast, $[A,B] \neq 0$ means no basis vector collapsed by two systems to be diagonalized by that basis vector. The commutation relation, responsible for quantum fluctuation, is a critical factor by which a classical system is distinct from a quantum system.

3.1.7. Constructing a quantum system from classical mechanics

There are two general methods to construct a quantum system from a classical one. The first method is based on producing a Hilbert space, a set of contributed observable and Hamiltonian of classical mechanics. The second method is based on the direct calculation of the probability amplitude from a classical mechanic's system in the Lagrangian approach [30, 52, 53]. For example, a classic system with the relating Hamiltonian H(q,p) on a "phase space" can be defined as:

$$\{q_n, p_m\} = \delta_{nm}, and \frac{\partial A_p(q,p)}{\partial t} = \{A_p(q,p), H(q,p)\} \tag{3.16}$$

Using the first method suggests that the corresponding quantum system is introduced as:

$$\begin{cases} Classical\,Variable & & Quantum\,Observable \\ q & \rightarrow & Q \\ p & \rightarrow & P \\ a(q,p) & \rightarrow & A_p(Q,P) \\ \{a,b\} & \rightarrow & \frac{-j}{\hbar}\left[A_p, B_p\right] \end{cases} \tag{3.17}$$

It is clear from Eq. 3.17 that the Poisson bracket relations between a and b as {a,b} for the classic system becomes canonical commutation relation as [$\mathbf{A_p}$,$\mathbf{B_p}$] for the quantum system. In this dissertation the bold alphabet is used to indicate the operator and also bold-italic alphabet stands for the vector.

3.2. A short introduction to quantum physics

Quantum physics, in essence, contains some properties, which have no relevance in classical physics. The properties such as photoelectric effect [54], Wave-Particle Duality [55, 56], Compton effect [57], and so forth cannot be effectively and completely defined by the classical physics rules. However, one of the interesting phenomena in quantum physics, the main idea behind a quantum radar, is entanglement [5, 19, 30]. In fact, entanglement is a crucial property to enhancing the quantum illumination radar performance [1, 16, 18]. Here in the following, some other valuable properties of quantum physics which have been widely utilized in quantum radar will be addressed.

3.2.1. Quantization of the Electromagnetic mode

Before quantizing the electromagnetic fields, it is useful to start with the free space electromagnetic fields definition classically by Maxwell's equations as [30]:

$$\begin{cases} \nabla.\vec{E} = 0 \\ \nabla.\vec{B} = 0 \\ \nabla \times \vec{B} = \dfrac{\partial \vec{D}}{\mu_0 \partial t} \\ \nabla \times \vec{E} = -\dfrac{\partial \vec{B}}{c \partial t} \end{cases} \tag{3.18}$$

In this equation, $\boldsymbol{B}$ is the magnetic flux, and $\boldsymbol{D}=\varepsilon_0\boldsymbol{E}$ is the electric displacement field. Eq. 3.18 can be reduced to:

$$\begin{aligned} \nabla^2 \vec{E} - \frac{\partial^2 \vec{E}}{c^2 \partial t^2} = 0 \\ \nabla^2 \vec{B} - \frac{\partial^2 \vec{B}}{c^2 \partial t^2} = 0 \end{aligned} \tag{3.19}$$

Eq. 3.19 explicitly defines the electromagnetic waves. From electromagnetic theory, it is well-known that inside an empty cavity that is electromagnetically excited, just a discrete number of frequencies can be alive [30, 53]. Each of those discrete frequencies corresponds to the electromagnetic modes. In contrast to inside the cavity, there is a continuum of infinite numbers of electromagnetic modes in free space, which can be addressed. Now consider a finite optical cavity with length L_0 and cross-section of A, and also it is supposed that an electric field is polarized in x-direction containing discrete mode as [30]:

$$\overrightarrow{E_x}(z,t) = \sum_n \sqrt{\frac{2\nu_n m_n}{V\varepsilon_0}} A_n(t) \sin(k_n z) \tag{3.20}$$

where ν_n, V, A_n, and k_n are cavity Eigen-frequency, mode amplitude, and wavenumber, respectively. In this equation, $V = L_0 A$, $k_n = n\pi/ L_0$, and $\nu_n = n\pi c/ L_0$, and also m_n is to create an analogy between the simple harmonic oscillator and a single-mode electromagnetic. From Eq. 3.20, it is possible to calculate the magnetic field component perpendicular to the electric field at each point in space as:

$$\overrightarrow{H_y}(z,t) = \sum_n \sqrt{\frac{2\upsilon_n m_n}{V\varepsilon_0}} \sqrt{\frac{\varepsilon_0}{k}} \frac{dA_n(t)}{dt} \cos(kz) \tag{3.21}$$

The classical Hamiltonian for the cavity is introduced as:

$$H = \int_V dv \left\{ \varepsilon_0 \overrightarrow{E_x}^2(z,t) + \mu_0 \overrightarrow{H_y}^2(z,t) \right\} \tag{3.22}$$

where **H** (without any subscripts) is the Hamiltonian of the system, and $\boldsymbol{H_y}$ defines the magnetic field with polarization in y-direction. By replacing Eq. 3.20 and Eq. 3.21, in Eq. 3.22, the system Hamiltonian is quantized in terms of mode numbers as:

$$H = \frac{1}{2}\sum_n m_n \upsilon_n^{\,2} A_n^{\,2} + m_n \left(\frac{dA_n}{dt}\right)^2 \rightarrow H = \frac{1}{2}\sum_n m_n \upsilon_n^{\,2} A_n^{\,2} + \frac{p_n^{\,2}}{m_n} \tag{3.23}$$

where $\mathbf{p_n}$ is the canonical momentum of n^{th} mode. Eq. 3.23 expresses the Hamiltonian of the system as a discrete number of independent oscillator energies. That means that each electromagnetic field's mode is equivalent to a simple mechanical harmonic oscillator mode.

3.2.2. Electromagnetic mode quantization

For quantization of an electromagnetic field, it initially needs to replace the classical fields with the quantum operators as ***E***—**E** and ***H***—**H**. The classical field replaced with quantum operator should satisfy Maxwell's equations; that means the relations that are true in classical electrodynamics should be held in quantum electrodynamics. To quantize the Hamiltonian expressed in Eq. 3.23, $\mathbf{A_n}$ and $\mathbf{p_n}$ as the operators should obey the commutation relation $[\mathbf{A_n}, \mathbf{p_n}'] = j\hbar\delta_{nn'}$, which means that there is no a basis vector such as $|\varphi\rangle$ collapsed by $\mathbf{A_n}$ and $\mathbf{p_n}$, to be diagonalized. In other words, $\mathbf{A_n}$ and $\mathbf{p_n}$, cannot be measured simultaneously. Using the canonical transformation to define creation ($\mathbf{a}^+$) and annihilation (**a**) operators, the quantum fields (the quantized electric and magnetic fields), classically expressed in Eq. 3.20 and Eq. 3.21, can be represented as the form of quantized version as [30]:

$$\begin{aligned} E(r,t) &= \sum_{\vec{k},n} e_{\vec{k}}^{(n)} \sqrt{\frac{\omega_n}{2V\varepsilon_0}} \left\{ \hat{a}_{\vec{k},n} e^{j[-\omega_k t + \vec{k}.\vec{r}]} + \hat{a}_{\vec{k},n}^{+} e^{j[\omega_k t - \vec{k}.\vec{r}]} \right\} \\ B(r,t) &= \sum_{\vec{k},n} \frac{\vec{k} \times e_{\vec{k}}^{(n)}}{\omega_n} \sqrt{\frac{\omega_n}{2V\varepsilon_0}} \left\{ \hat{a}_{\vec{k},n} e^{j[-\omega_k t + \vec{k}.\vec{r}]} + \hat{a}_{\vec{k},n}^{+} e^{j[\omega_k t - \vec{k}.\vec{r}]} \right\} \end{aligned} \tag{3.24}$$

where $\boldsymbol{e_k}^{(n)}$ is the polarization vector. In this dissertation, bold letters are used to indicate a vector. The annihilation and creation operator **a** and $\mathbf{a}^+$ satisfy the commutation relation as $[\mathbf{a_{k,n}}, \mathbf{a^+_{k',n'}}] = \delta_{\mathbf{kk'}}\delta_{nn'}$. Thus, the quantum Hamiltonian for free space electromagnetic wave is introduced based on the "annihilation and creation operators" as [30]:

$$H = \sum_{\vec{k},n} \hbar\omega_{\vec{k}} \left(\hat{a}_{\vec{k}n}^{+} \hat{a}_{\vec{k}n} + \frac{1}{2} \right) \tag{3.25}$$

In the relations mentioned above, $\boldsymbol{k} = (k_x,k_y,k_z)$ is the wave vector. By considering the periodic conditions that are $k_x = 2\pi n_x/L$, $k_y = 2\pi n_y/L$, and $k_z = 2\pi n_z/L$; in these relationships, n_x, n_y, and n_z are integers, and a set of numbers (n_x, n_y, n_z) defines a mode of electromagnetic.

For most applications in quantum sensors such as quantum radar, the electromagnetic radiations move as a beam in a straight line. Thus, it is applicable to utilize the continuous mode quantization of the fields instead of the discrete cavity modes presented in Eq. 3.25. Thus, "sum" in the relations should be converted to "integral" as [30]:

$$\sum_{\vec{k}} \rightarrow \frac{2V}{(2\pi)^3}\int dV^3$$
$$a \rightarrow \sqrt{\frac{(2\pi)^3}{V}}a \; and \; a^+ \rightarrow \sqrt{\frac{(2\pi)^3}{V}}a^+ \qquad (3.26)$$

Therefore, the "creation and annihilation operators" can be simply indicated by $\mathbf{a(\omega)}$ and $\mathbf{a^+(\omega)}$ in the continuous form.

3.2.3. Quantum superposition

Superposition in the quantum realm means that a physical system, always, can be in a superposition of two or more states. In the classical sense, a system with two different states as $|\varphi_1\rangle$ and $|\varphi_2\rangle$ has been established in a state either at $|\varphi_1\rangle$ or $|\varphi_2\rangle$. In contrast with the classical picture, in quantum, the system state is defined as $\{|\varphi_1\rangle + |\varphi_2\rangle\}/0.7070$. This means that the state of the system is both $|\varphi_1\rangle$ and $|\varphi_2\rangle$ at the same time. Of course, if one measures the quantum system to define its state, the quantum waves function collapses, and it just measures $|\varphi_1\rangle$ or $|\varphi_2\rangle$. Thus, it is found that actual measurement changes a probabilistic quantum system (both $|\varphi_1\rangle$ and $|\varphi_2\rangle$) to a deterministic one ($|\varphi_1\rangle$ or $|\varphi_2\rangle$). Using the materials mentioned above, in the following, the entanglement as a key factor is defined as an essential factor to enhance the quantum radar performance.

3.2.4. Entanglement (General definition)

To generally define entanglement [5, 30, 53], two quantum systems are supposed with two different states as $|\Psi_1\rangle$ and $|\Psi_2\rangle$, both in superposition states according to:

$$\begin{cases} |\psi_1\rangle = \frac{1}{\sqrt{2}}\{|V_1\rangle + |H_1\rangle\} \\ |\psi_2\rangle = \frac{1}{\sqrt{2}}\{|V_2\rangle + |H_2\rangle\} \end{cases} \quad (3.27)$$

If the systems are separable or independent, their total states become [5, 30, 53]:

$$\begin{aligned} |\psi_1\rangle \otimes |\psi_2\rangle &= \frac{1}{\sqrt{2}}\{|V_1\rangle + |H_1\rangle\} \otimes \frac{1}{\sqrt{2}}\{|V_2\rangle + |H_2\rangle\} \\ |\psi_1\psi_2\rangle &= \frac{1}{2}\{|V_1\rangle|V_2\rangle + |V_1\rangle|H_2\rangle + |H_1\rangle|V_2\rangle + |H_1\rangle|H_2\rangle\} \end{aligned} \quad (3.28)$$

In Eq. 3.28, it is shown that the measurement of the state of "system 1", has no effect on "system 2" state and vice versa. For example, if a measurement is done and system 1 is in $|V_1\rangle$; using this information, one cannot deduce the state of system 2, which can be either $|V_2\rangle$ or $|H_2\rangle$.

However, quantum physics allows the generation of states not as an independent case, which is the products of two states, but if the system is entangled, the associated state is defined as [5, 30, 53]:

$$|\psi_1\psi_2\rangle = \frac{1}{\sqrt{2}}\{|V_1\rangle|H_2\rangle + |H_1\rangle|V_2\rangle\} \quad (3.29)$$

Considering Eq. 3.29, if one measures the related system states, and for example, the result is $|V_1\rangle$, then the other system state can be immediately known, which is $|H_2\rangle$. That is true even though the system 1 and 2 be far away from each other. By two Eq. 3.28 and Eq. 3.29, the difference between two separable and entangled states is expressed.

"Entanglement" is a well-known term used in "quantum theory" [30], describing the way that quantum particles can become "non-classically correlated". This is mathematically shown in Eq. 3.29. Quantum particles, as photons and electrons, can interact with each other and establish a type of connection, which can be non-classically correlated in some sense; It has been mentioned in the quantum realm that those particles are entangled with each other.

Entanglement is a real phenomenon, which has been theoretically and experimentally demonstrated [5,19,33]. The mechanism behind the entanglement has not ever been fully explained by any classical theory. One interesting theory proposes that "all particles on earth were once compacted tightly together and, as a consequence, maintain a connectedness" [58].

Much current research has been focusing on how to efficiently employ the potential of entanglement to enhance the classical systems in different applications, such as improving quantum radar performance [1-4], enhancing the resolution of an imaging system [5-7], systems using "quantum illumination protocol" [8], quantum communication [9-10], plasmonic photodetector responsivity [11], plasmonic systems [12], and Raman signals [13]. In the next part, the generation of the optical entangled photons will be shortly discussed. This is the main point that the quantum illumination radar operation starts.

3.2.5. Generation of entangled optical photons

As a general definition, entanglement is established (Figure 3.2a) as two quantum particles, such as photons, interact with the conservation of the frequency and wave vector. Their interrelated properties are independent of the distance between them [5, 19, 33]. Figure 3.2a shows that the entanglement is created at the intersection of the output photons profile. For simplicity and traceability, a few numbers of the profiles are displayed. The production of the entangled photons (called signal and idler) needs a laser interaction with a nonlinear material (OPDC: optical parameter down converter) by which the output photons become entangled. That process is schematically depicted in Figure 3.2b. The generated output photons have different wave vectors ($\boldsymbol{K_s}$, $\boldsymbol{K_i}$) and frequencies (ω_s,ω_i). The wave vectors and frequencies are related to the pumping frequency and wave vector, associated with the energy and momentum conservation. Accordingly, two important conditions to satisfy entanglement are energy and momentum conservation, illustrated in Figure 9b. That means that $\boldsymbol{K_{pump}} = \boldsymbol{K_s} + \boldsymbol{K_i}$ and $\omega_{pump} = \omega_s + \omega_i$. In the following, some theoretical derivations are presented by which one can find how the energy and momentum conservation are employed to define the entangled photons state. The state defined for entangled photons is presented in a different way than a single photon.

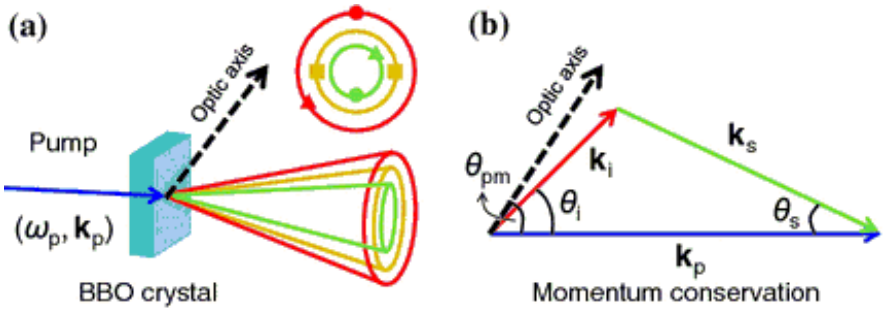

Figure 3.2. An illustration of the generation of the entangled optical photons, b momentum conservation that supports the generation of the entangled photons [80].

Subsequently, the state of the entangled photons is theoretically derived. In a nonlinear material, the second-order susceptibility $\chi^{(2)}$ plays an important role. The nonlinear interaction Hamiltonian (second-order) is expressed as [5, 19, 33]:

$$H_{\text{int}}(t) = \varepsilon_0 \int_v d^3r \chi^{(2)} \{\hat{E}_{inc}(r,t).\hat{E}_s(r,t).\hat{E}_i(r,t)\} \tag{3.30}$$

where $\mathbf{E_{inc}}$, $\mathbf{E_s}$, $\mathbf{E_i}$, and v are incident laser field, signal field, idler field, and the interaction volume, respectively. To simplify Eq. 3.30, one can express the electrical field in the Fourier domain, and the equation is re-written as [5, 19, 33]:

$$H_{\text{int}}(t) = \varepsilon_0 \int_v d^3r \chi^{(2)} \int d^3k_s d^3k_i \{\hat{E}_{inc}^{(+)} e^{j(\omega_{inc}t - \vec{k}_{inc}.\vec{r})}.\hat{E}_s^{(-)} e^{j(\omega_s t - \vec{k}_s.\vec{r})}.\hat{E}_i^{(-)} e^{j(\omega_i t - \vec{k}_i.\vec{r})}\} + H.C. \tag{3.31}$$

In Eq. 3.31, H.C. indicates the "Hermitian conjugate". To simplify, the incident wave is supposed as a plane wave with a wave vector $\boldsymbol{k_{inc}}$ and frequency ω_{inc}. Also, the supposing volume in the integration is assumed to be so large. Applying the mentioned assumptions, Eq. 3.31 is simplified as [5, 19, 33]:

$$H_{\text{int}}(t) = \varepsilon_0 \int d^3k_s d^3k_i \chi^{(2)} \delta(k_{inc} - k_s - k_i) \{\hat{E}_{inc}^{(+)}.\hat{E}_{sct}^{(-)}.\hat{E}_{ph}^{(-)} e^{j(\omega_{inc} - \omega_s - \omega_i)t}\} + H.C. \tag{3.32}$$

Thus, one can use the "first-order perturbations" to calculate the entangled photons state (signal and idler) [19]:

$$|\phi> = (-j/\hbar) \int dt.H_{\text{int}}(t)|0> \tag{3.33}$$

Substituting $H_{int}(t)$ into Eq. 3.33, the state of the entangled pair is calculated as [5, 19, 33]:

$$|\phi_e>=(\frac{-j}{\hbar})\int dt.\{\varepsilon_0\int d^3k_s d^3k_i \chi^{(2)}\delta(k_{inc}-k_s-k_i)\{\hat{E}_{inc}^{(+)}.\hat{E}_{sct}^{(-)}.\hat{E}_{ph}^{(-)}e^{j(\omega_{inc}-\omega_s-\omega_i)t}\}+H.C.\}|0>$$

$$|\phi_e>=(\frac{-j\varepsilon_0}{\hbar})\int d^3k_s d^3k_i \delta(\Delta_k).\delta(\Delta_\omega)[\hat{E}_{inc}^{(+)}.\hat{E}_{sct}^{(-)}.\hat{E}_{ph}^{(-)}]\}|0>, \quad (3.34)$$

$$\Delta_k=k_{inc}-k_s-k_i, \Delta_\omega=\omega_{inc}-\omega_s-\omega_i$$

A classical laser beam is considered, and the field of signal and idler is quantized as $\mathbf{E_s}^{(-)} = j\times\sqrt{(\hbar\omega_s/(2\varepsilon_0 v))}\times \mathbf{a_s}^+$, $\mathbf{E_i}^{(-)} = j\times\sqrt{(\hbar\omega_i/(2\varepsilon_0 v))}\times \mathbf{a_i}^+$, where $\mathbf{a_s}^+$ and $\mathbf{a_i}^+$ are signal and idler photons creation operators, respectively. Finally, by substituting the quantized form of $\mathbf{E_s}^{(-)}$ and $\mathbf{E_i}^{(-)}$ in Eq. 3.34 and by slow varying parameters absorbing, the entangled photon state is deduced as [5, 19, 33]:

$$|\phi_e>=A_0 a_s^+ a_i^+|0>, A_0=\left\{\frac{j}{2v}\delta(\Delta_k).\delta(\Delta_\omega).E_{inc}.\sqrt{\omega_s\omega_i}\right\} \quad (3.35)$$

This equation clearly shows that the signal and idler photons became entangled at both frequency and wave vector because of the "delta function" in the relationship.

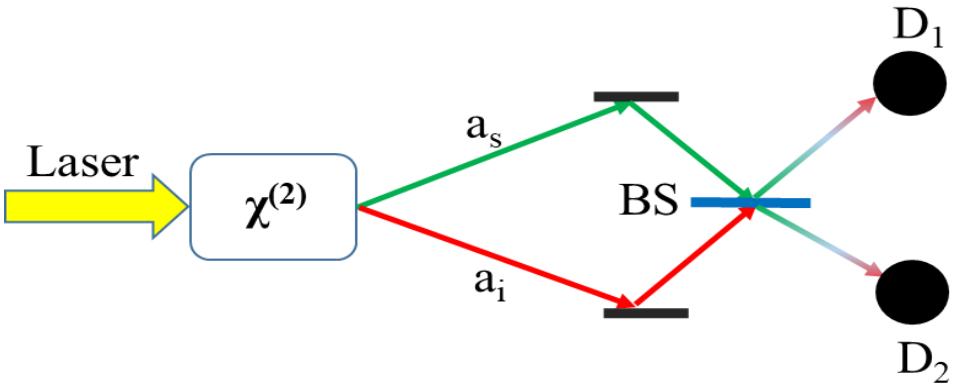

Figure 3.3. Setup for analyzing the entanglement between optical photons; interaction of laser with a nonlinear material and generation of signal (a_s) and idler (a_i) and using BS to mix the states and detect the mixed states.

However, one can practically study the entanglement between the generated photons due to the high-intensity laser interaction with an OPDC. Therefore, one can consider the setup illustrated in Figure 3.3. The generated signal and idler photons are merged using a 50-50 beam splitter, which means that each path after beam-splitter (BS) contains the signal and idler field. Eventually, the coincidence detection of the sensitive single-photon detectors D_1 and D_2

determine when the emitted photons are entangled or separable [5, 19]. In this set up the distance between detectors from BS is a critical factor by which the detection of the entangled photons can be easily accomplished. In the next part, some theoretical methods to study the entanglement between modes are presented.

3.2.6. Entanglement analyzing methods and procedures

After a short discussion about the entangled optical photons generation and quantum state of the entangled photons theoretically derived in Eq. 3.35, Simon's two-mode entanglement criterion is introduced [33]. The criterion is derived with regard to the negativity of a bipartite system partial transposes. The mentioning criterion establishes a necessary and sufficient condition to analyze the separability of the Gaussian state [33, 59-60]. Gaussian state is considered as a simple class of a continuous variable system. That is a state whose "Wigner function (quasi-probability distribution)" to be as a Gaussian state [60]. Using Wigner distribution leads the quantum operators to contribute to their "phase space" variables [36]. It is clear to show that the designed converters quantum ensembles "density matrix" is a Gaussian state and can be expressed in the form of "Wigner distribution" for a single-mode coherent-squeezed state. The related mean and variance information are just sufficient to describe the state of the system. Therefore, it is possible for us to use Simon's separability criterion [33], as a generalized form of the "Peres-Horodecki criterion" to measuring the entanglement between two modes. For instance, two separable states are expressed by two subsystems density matrices regarding the summation of the tensor products as [33]:

$$\rho = \sum_{n} P_n \rho_1^n \otimes \rho_2^n \tag{3.36}$$

where ρ_1, ρ_2 are subsystem's density matrix and P_n stands probability, while the entangled states cannot be remarked as the form of Eq. 3.36, and the behaviors of the subsystems correlate non-trivially to each other. For measuring the entanglement of two-mode using "Peres-Horodecki criterion", a two-mode Gaussian state is necessary to be defined through which one can completely characterize the corresponding correlation matrix elements as:

$$V_{nm} = \frac{1}{2} < \hat{Y}_n \hat{Y}_m + \hat{Y}_m \hat{Y}_n > - < \hat{Y}_n >< \hat{Y}_m >, Y = [x_1, p_1, x_2, p_2],$$
$$x_{n\_out} = (a_{n\_out} + a_{n\_out}{}^{+}), p_{i\_out} = 1/\, j\sqrt{2}\,(a_{n\_out} - a_{n\_out}{}^{+}) \tag{3.37}$$

Since the correlation matrix ($V_{4\times4}$ = [A_v, C_v; C_v^T, B_v]) is calculated, the measurement of the two-output modes separability can be accomplished. In the correlation matrix, A_v, B_v, and C_v are 2×2 matrixes that the elements are examined from V_{nm} as:

$$A_v = \begin{bmatrix} <X_1^2> - <X_1>^2 & 0.5\times <X_1P_1 + P_1X_1> - <X_1><P_1> \\ 0.5\times <X_1P_1 + P_1X_1> - <X_1><P_1> & <P_1^2> - <P_1>^2 \end{bmatrix}$$
$$B_v = \begin{bmatrix} <X_2^2> - <X_2>^2 & 0.5\times <X_2P_2 + P_2X_2> - <X_2><P_2> \\ 0.5\times <P_2X_2 + X_2P_2> - <P_2><X_2> & <P_2^2> - <P_2>^2 \end{bmatrix} \quad (3.38)$$
$$C_v = \begin{bmatrix} 0.5\times <X_1X_2 + X_2X_1> - <X_1><X_2> & 0.5\times <X_1P_2 + P_2X_1> - <X_1><P_2> \\ 0.5\times <P_1X_2 + X_2P_1> - <P_1><X_2> & 0.5\times <P_1P_2 + P_2P_1> - <P_1><P_2> \end{bmatrix}$$

Finally, the "Peres-Horodecki criterion" simple form to evaluate the separability of the continuous states [33, 59] given by:

$$\lambda_{SPH} = \det(A_v)\det(B_v) + (0.25 - |\det(C_v)|)^2 - tr(A_v J C_v J B_v J C_v^T J) - 0.25\times(\det(A_v) + \det(B_v)) \geq 0 \quad (3.39)$$

In this equation J = [0, 1; -1, 0]. In addition to Eq. 3.39, there is another method to analyze the two-mode entanglement employing the Symplectic eigenvalue [59] as:

$$\eta = 1/\sqrt{2} \times \sqrt{\sigma_v(V) - \sqrt{\sigma_v(V) - 4\det(V)}}, \quad \sigma_v(V) = \det(A_v) + \det(B_v) - 2\det(C_v) \quad (3.40)$$

A bipartite Gaussian system is separable if Symplectic eigenvalue satisfies 2η>1 [59-60] and, also, the strength of violation of this criterion (2η>1) is expressed as the two-mode entanglement measuring. Thus, to investigate the two-mode entanglement affected by the system, it is sufficient to calculate the correlation matrix elements in Eq. 3.38.

So far, all of the necessary elements to design a typical quantum radar were discussed. In the following, the emphasis was laid on quantum radar designing and how one can manipulate the critical quantities to improve the modes entanglement. It is noteworthy to mention that the main goal of this dissertation is to design a quantum radar system employing different types of converters to maximally preserve the entanglement between transmitting and backscattering modes.

4. DESIGN OF QUANTUM RADAR USING QED

Quantum radar, in essence, generalizes the concept of the classical radar employing a relatively small amount of incident photons. The main reason to develop quantum radar is benefiting the quantum phenomenon for system sensitivity enhancing [1, 62]. It is challenging to jam on a quantum radar operating with entanglement phenomenon [62]. In a general sense, one can define a quantum radar system as a standoff sensing system that employs microwave photons as well as quantum phenomena to enhance the capability to detect, identify and recognize the desired target.

Quantum sensing systems are classified with regard to the type of quantum phenomena utilized by the system: **(1)** The quantum sensor transmits un-entangled photons; this type of quantum radar is called single-photon quantum radar. This system operates as same as a classical radar. As illustrated in Figure 4.1, the quantum system transmits a single-photon pulse toward the target, and then the target backscatters the captured photons toward the detector. One of the advantages of this system is that when the target is illuminated by a single photon, the related RCS is strongly increased. **(2)** The quantum sensor transmits classical photons and uses a quantum-based photodetector to enhance detection capability; as an example, one can notice the operation of a typical quantum RADAR [63]. This type of system uses some shorter wavelengths such as laser to attain much better spatial resolution. In contrast, it loses the advantage of an easy penetration through the fog or clouds as radar does. **(3)** The quantum sensor transmits entangled photons and attempts to detect the backscattered entangled photons. This type of quantum radar is the case that we will discuss in detail in this dissertation. In this system schematically depicted in Figure 4.2, the entangled photons (signal and idler) are produced at the first stage. The signal photons are transmitted in the atmosphere to detect a target, while the idler is preserved in the laboratory. The backscattering photons from a target are detected, and then non-classical correlations between states cause to enhance the detection performance.

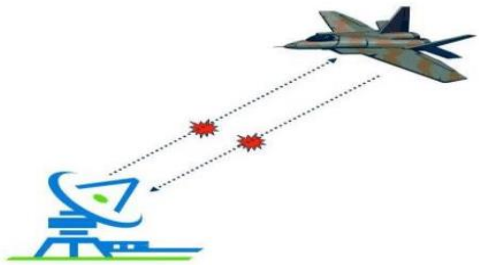

Figure 4.1. Quantum radar using a single photon to detect the target [1].

In the next step, the design of the quantum radar system using quantum electrodynamics theory (QED) will be presented. It should be noted that the main aim is to particularly attract attention to improve the retained and returned modes entanglement. Thus, the concentration set on the design of the different types of converters to enhance the entanglement and ignore the processes after the detector in which everything becomes classic. In particle physics, “QED” (introduced by Feynman for the first time) is the electrodynamics of the “relativistic quantum field theory”. Fundamentally, it presents how light and matter interact with each other and establishes full compatibility between “quantum mechanics” and “special relativity”. QED is technically described as a “perturbation theory” of the “electromagnetic quantum vacuum” [61]. Thus, to design a quantum radar using QED, two different subsystems are studied to generate the microwave photons entangled with the optical photons (the idler fields that are kept in the laboratory). The work initially starts with the design of the electro-opto-mechanical converter, and in the next part, the optoelectronic converter will be investigated to produce entangled photons. The goal is to study the difference between two subsystems and compare the subsystems with each other to select the best one to use in the quantum radar system. In fact, this thesis emphasizes the design of a quantum radar to maintain a sustainable entanglement. As the entanglement is basically so fragile and easily leak away because of the effect of the noises and environment.

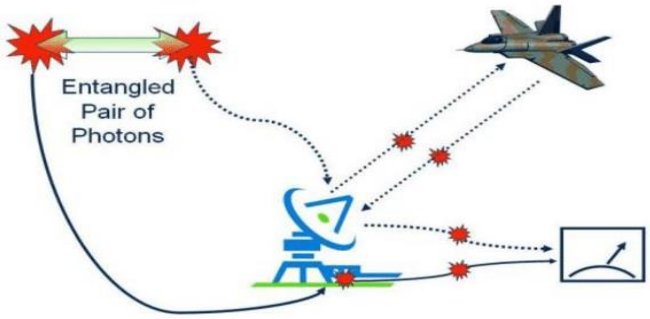

Figure 4.2. Quantum radar using entanglement for detection [1].

4.1. Design of an electro-opto-mechanical converter for a typical quantum radar

Quantum radar using microwave photons, the same as a "classical radar", is defined as a detector employing entanglement to enhance radar performance, such as detection and resolution capabilities [1,62]. Notably, entanglement is an unstable quantity, and it is difficult to have two entangled particles alive for a long time. The points mentioned above emphasize to carefully study the entanglement behavior at each level of the designed system, including: (I) process of the entanglement creation, (II) entangled photons amplifying, (III) atmosphere channel effect on propagation wave, and (IV) backscattering photons from the target. It will be shown that each step mentioned above, such as active medium as an amplifier, atmosphere as a lossy channel, and also target scattering, can kill the entanglement. In the following, a system (like an electro-opto-mechanical converter) is designed using QED to generate the entangled microwave photons. In this step, it is obligatory to find the parameters that make a strict trade-off between each other and engineer them to increase the entanglement sustainability. In a quantum radar that employs an electro-opto-mechanical converter, three subsystems are employed, such as optical cavity, microresonator, and microwave cavity coupling one another to induce the entanglement between cavities mode. In the mentioned converter, the optical cavity mode resonates with an optical frequency around 10^{14} Hz, the micro-cavity mode resonates in the range of GHz (L-band), and the microresonator mode resonates with a low frequency around 10 MHz. It will be shown that the low operating frequency of the microresonator leads to a critical problem of maintaining the entanglement between modes high temperatures. It is related to the point that at such a low operating frequency, the generation of the thermally excited photons becomes so high. That factor restricts the entanglement between modes and leads to leak away of the entanglement. Therefore, in the second system, the mechanical parts operating at low frequency are removed

and replaced them with some optoelectronic-based elements to solve the problem. Let's initiate the story with the design of the electro-opto-mechanical converter to produce the entangled microwave photons.

4.1.1. System definition

A typical quantum radar system (same as an interferometry with a long arm) is depicted in Figure 3.1. The quantum radar process to produce optical photons (signal and idler) entangled with each other initiates by laser interaction with a nonlinear material [5,19]. It is stated in section 3.2.5 that due to the nonlinearity of OPDC, the two generating photons can be entangled. One of them is called signal, and the other is called the idler. These photons are operated in the optical range, and clearly the quantum radar that we want to design operates in the same way as a classical radar. That means that it is necessary to generate the microwave photons entangling with the idler photons. The idler photons kept in the lab are used to analyze the correlation with the backscattering photons from the target. Thus, the signal is used to excite the tripartite system in an electro-opto-mechanical converter [18,22-27] to produce the entanglement. A traditional electro-opto-mechanical converter containing OC, MR, and MC cavities coupled to each other is schematically illustrated in Figure 4.3. For system modeling, all of the interactions between cavities are theoretically derived using the canonical conjugate method [29,64]. This is a full quantum-based method to describe the interaction between cavities in the system completely.

The process begins with the excitation of the OC with a signal that can generate some quantized optical modes inside the cavity. The OC output modes are connected to MR via optical pressure. The optical pressure effect leads to MR resonance with a frequency at MHz range. To derive the coupling between OC and MR, the interaction between OC output fields with the atom's field are considered. In the canonical conjugate theory, MR is regarded as a matter consisting of N simple harmonic oscillator. It is shown that there are some critical parameters by which one can engineer the system to manipulate the coupling between OC and MR. These parameters will exhibit a critical role in enhancing the entanglement between modes. Subsequently, MR resonator oscillation alters the MC capacitance through which the microwave cavity resonant frequency is changed. This point indicates that MR couples to MC through a capacitive change.

In fact, it is MR simple oscillators that can couple to MC cavity. All of the coupling coefficients will be theoretically derived and presented in the next section.

From the latter mentioned points, it is found in the tripartite system OC, MC, and MR modes coupling engineers the cavities mode in the system. In other words, OC modes can couple to MC modes through MR coupling effect. Since the modes of cavities coupled to the other inside the system, thus, by engineering the electro-opto-mechanical converter's parameters, the non-classical correlation between cavities modes can be established [22-27]. Engineering converter's parameter means that one can manipulate: I. Coupling factor among cavities; II. The cavity decaying rate; III. The frequency resonance of cavity; IV. OC and MC driving field. All of the mentioned engineering tasks lead to the point that it is possible to make OC and MC modes entanglement. Establishing entanglement between the cavities mode and its preservation are critical points that one has to be considered in the designed system. Preserving the entanglement is very important in a quantum radar system. It is because the entanglement between modes inside the "electro-opto-mechanical converter" system can be manipulated. It means that after transmission of the photons in the atmosphere toward the target, there are no degrees of freedom to change and enhance the entanglement. In fact, it is the effects of the real medium such as thermally excited photons, scattering from atmospheric particles, absorption by the target, and so forth that can destroy the entanglement between modes. Therefore, in this Ph.D. dissertation, our attention specifically emphasizes converter system engineering and designing a new system: I. To enhance the entanglement between modes; II. To preserve the generation of the entanglement at a high temperature around 5K~50K; III. To reduce the system complexity; IV. To readily manipulate the coupling between cavities in the converter.

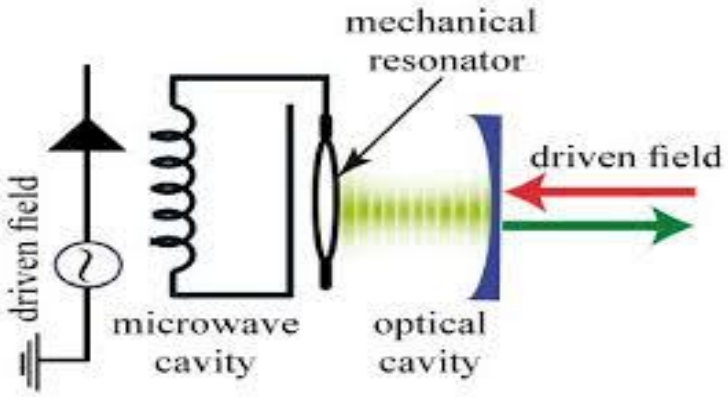

Figure 4.3. Electro-opto-mechanical converter [14] containing OC, MC, and MR subsystems coupling to each other.

The schematically illustrated quantum radar in Figure 3.1 clearly shows that MC modes initially enter an active medium to amplify the entangled photons and then broadcast toward the target. Here, as an assumption the active medium (amplifier in the classic sense) should enhance the intensity of the entangled photons. However, it is so clear that this task is so challenging [65], and using an amplifier will cause to disturb the entanglement.

In the following, for simplicity, the relationships among quantum radar different level modes are depicted in Figure 4.4. As illustrated in Figure 4.4, the output mode of MC **(**C_{ω}**)**, latterly entangled with the OC mode (a_s), is initially intensified by an active medium. After amplifying the entangled photons, these photons are broadcasted into a lossy channel to detect a target. The modeling of the active medium using QED is shown in Figure 4.4. For this, N beam-splitters (BS) is considered as the amplifying agent to fully model the active medium. Regarding the "quantum electrodynamics theory", the photons excited due to the thermal effect in the inverted state are employed to amplify the photons [28]. Generally, one has to study the entanglement between the active medium output modes ($C_{a\omega}$) with the OC modes. It emphasizes the active medium effect on the correlation between modes. It is noteworthy to mention that, as the main task of this dissertation, the focus emphasizes on preserving the non-classicality of the transmitting photons in the designed quantum radar. Thus, some parameters need to manipulate and enhance the entanglement between modes. In the active medium, supposing that makes possible to improve the entanglement between modes, the fundamental parameters include the

active medium amplification factor (κ_a), the contributed wave vector (K_a), and the medium length. However, in reality, it is clear that any real medium can kill the entanglement between photons. Nonetheless, recently, it has been shown that the entangled photons can be amplified. Using JPC [16], nonlinearity properties lead to amplify the entangled photons. Thus, it seems that our assumptions and approach to intensify the entangled photons were correct. However, this task is so challenging to be established in practice. To simulate the active medium, N discrete BS are used by which the interaction between incident field and medium particles is modeled. Each BS has two inputs; one of them deals with the desired incident photons, and the other is for thermally excited photons. Therefore, at each step the effect of the thermally excited photon (noise effect) should be noted. Also, the BS has two outputs by which one can mode the transmitted photons (desired photons) and the photons that are coupled to the environment as a noise. The active medium is schematically illustrated in Figure 4.4, whose Z_a and ΔZ are the active medium length and BS length, respectively. The relationship between active medium input and output modes will be discussed in the theory and background section in detail.

Subsequently, the active medium output modes $C_{a\omega}$ is sending out in the atmosphere to find the target. Using N discrete scattering agents as BS, the atmospheric medium is modeled through which the amplitude and phase of the propagating photons will be manipulated. The modeling is schematically shown in Figure 4.4. It is shown that the length of channel R (transmitter-target distance) significantly influences the attenuation medium output modes (C_a) and the wave vector (κ_{atm}) imaginary part. Other crucial factors affecting the entanglement between modes in the atmosphere are the uncontrollable natural effects such as temperature and pressure [1], [28]. As a result, the channel strongly limits the quantum radar applications in which the entanglement is a crucial factor and, unfortunately, easily destroyed by the atmosphere. Also, we have no degree of freedom to engineer the atmosphere parameters. One of the quantum radar system's advantages is to use microwave photons for target detection (like the classical radar) rather than optical photons. The atmospheric medium strongly destroys the optical photons that propagate with a frequency higher than 1000 THz. Therefore, it is noteworthy to mention that to reduce the atmospheric effect on the entanglement between photons, it is necessary to use such tripartite system schematically illustrated in Figure 4.3 to generate the entangled microwave photons. Thus, it is microwave photons that broadcast toward the target like a classic radar system. In this

dissertation, the backscattering photons from the target are analyzed in detail. In the same way, "quantum electrodynamics theory" is used to model the scattering from a target. Reflection, in essence, is introduced as an electromagnetic field interaction with the quantum field of the target's atoms. The component of the target's material is the other crucial parameter that the incident photons can be severely influenced. Thus, the C_t and OC modes entanglement can be strongly affected. It is shown in Figure 4.4 that output modes from the atmosphere are coupled to the target in parallel. Also, the model considers the effect of the noise, b_t, which is issued due to the target materials specifications. In the following, the relationship between C_a and C_t is theoretically derived by which one can calculate the scattering effect from a target on the entanglement between modes.

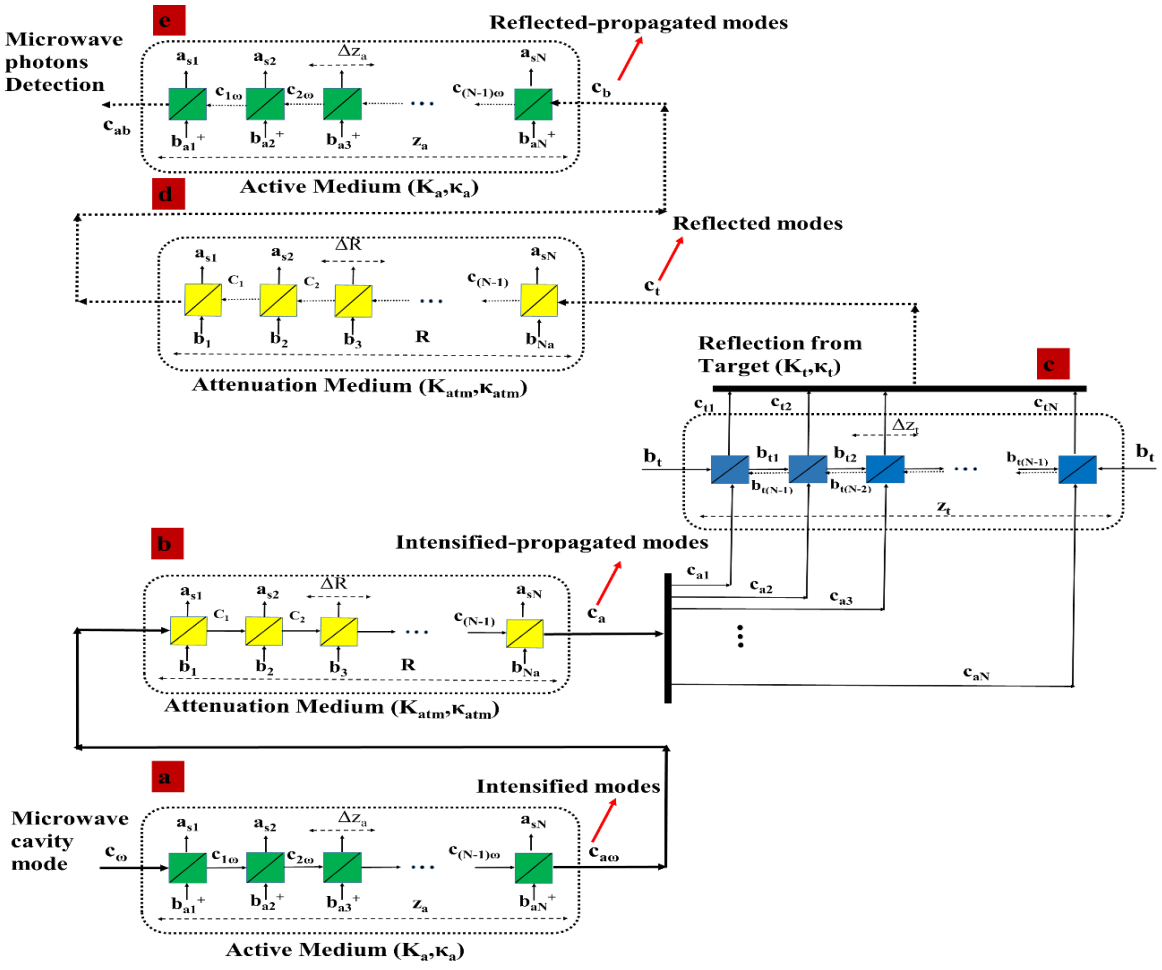

Figure 4.4. An illustration of the relationship between the modes $\mathbf{c_\omega}$, $\mathbf{c_{a\omega}}$, $\mathbf{c_a}$, $\mathbf{c_t}$, $\mathbf{c_b}$, $\mathbf{c_{ab}}$, and the mediums in a quantum radar.

Subsequently, the backscattering photons return to the atmosphere, and finally, they should be amplified one more time before the detection. Therefore, it is necessary to consider the atmosphere effects as a lossy channel on the return photons non-classicality one more time. For the sake of simplicity, all of the mode relationships in different mediums are completely depicted in Figure 4.4.

In the following, we theoretically design an "electro-opto-mechanical converter" system as the main part of a quantum radar system and engineer the system parameters to generate the entanglement photons and, more importantly, to conserve photons non-classicality with regarding the effect of the real lossy mediums.

4.1.2. Design of an electro-opto-mechanical converter to generate the entangled microwave photons

It is discussed that the quantum radar employing the microwave photons entanglement to broadcast toward the unknown target rather than optical photons. This means that it needs a device to produce microwave photons entangled with the initially generated entangling optical photons. In this dissertation, two different systems as the electro-opto-mechanical and optoelectronic-based converters are studied to produce the entanglement. Herein, the equation of motion of the "electro-opto-mechanical" converter is theoretically studied and derived using "Heisenberg-Langevin equations".

To analyze the system, "Quantum electrodynamics theory" is used [29, 30]. First of all, analysis of the converter dynamics equation of the system motion is initiated; that is a subsystem of a typical quantum radar illustrated schematically in Figure 3.1. With regard to the standard approach in QED, the system associated with Lagrangian is defined. The converter addressed in Figure 3.1 has three different parts as OC, MR, and MC coupling each other. Thus, it needs to define the contributed subsystems Lagrangian and also coupling Lagrangian among the subsystems. For this, the total Lagrangian of the electro-opto-mechanical system is given by:

$$
\begin{aligned}
L_{OC} &= \frac{\varepsilon_0}{2}(\dot{A}^2 - \omega_c{}^2 A^2) \\
L_{MR} &= \frac{1}{2} m \dot{X}^2 - \frac{1}{2} m \omega_m{}^2 X^2 \\
L_{MC} &= \frac{1}{2} C(x) \dot{\phi}^2 - \frac{1}{2L} \phi^2 + \frac{1}{2} C_d (v_d - \dot{\phi})^2 \\
L_{OC-MR} &= -\alpha_c A \dot{X}
\end{aligned}
\tag{4.1}
$$

In this equation, L_{MC}, L_{MR}, $L_{OC,}$ and $L_{OC\text{-}MR}$ are, respectively, MC, MR, OC, and OC-MR interaction Lagrangian. The letters with dots above stand for time derivation. Also, the Lagrangian related to MC-MR interaction is defined via C(x) in $L_{MC.}$

In Eq. 4.1, α_c, ω_m, ω_c, v_d, C(x), C_d and m are the interaction coefficient of OC-MR, angular frequency of MR, angular frequency of OC, driving field of MC, variable capacitor, fix capacitor, and the mass of MR resonator, respectively. Additionally, the parameters **A**, **X**, and **Φ** are vector potential, MR resonator position, and magnetic flux operators, respectively.

In the next step, the contributed Hamiltonian should be defined to clarify the dynamic equation of the system. Thus, the conjugate momentum of the **A**, **X**, and **Φ** are defined regarding the classical conjugate variables [26], and consequently, the "creation and annihilation operators" are introduced. After that, the system's Hamiltonian [18] is re-expressed using the creation and annihilation operators by:

$$
\begin{aligned}
H_{OC} &= \hbar \omega_c \hat{a_c}^+ \hat{a_c} \\
H_{MR} &= \frac{\hbar \omega_m}{2} (\hat{P_x}^2 + \hat{q_x}^2) \\
H_{MC} &= \hbar \omega_\omega \hat{c_\omega}^+ \hat{c_\omega} - jV_d C_d \sqrt{\frac{\hbar \omega_\omega}{2C_t}} (\hat{c_\omega} - \hat{c_\omega}^+) \\
H_{OC-MR} &= \hbar \sqrt{\frac{\alpha_c{}^2 \omega_m}{2\varepsilon_0 \omega_c m}} (\hat{a_c}^+ + \hat{a_c}) \hat{P_x} \\
H_{MC-MR} &= C_p C_t \frac{\hbar \omega_\omega}{2} \sqrt{\frac{\hbar}{\omega_m m}} \hat{q_x} (\hat{c_s} - \hat{c_s}^+)^2 \\
H_{oc-drive} &= j\hbar E_c (\hat{a_c}^+ e^{(-j\omega_L t)} - \hat{a_c} e^{(j\omega_L t)})
\end{aligned}
\tag{4.2}
$$

In Eq. 4.2, ($\mathbf{a_c}^+$, $\mathbf{a_c}$), and ($\mathbf{c_\omega}^+$, $\mathbf{c_\omega}$) stand for OC and MC contributed creation and annihilation operators, respectively. In the last term, E_c is the OC driving field [22- 24]. Also, C_p and C_t are calculated using $C_p = C'(x)/[C(x) + C_d]^2$ and $C_t = C_d+C(x_0)$, where x_0 stands for MR resonator equilibrium position. In Eq. 4.2, the second term in H_{MC} indicates the external source cavity driving. In this equation, the cavity interaction Hamiltonian is explicitly defined. Thus, it is clear how and by which parameters one can manipulate the interaction between cavities through which it is shown that the entanglement among modes is dramatically changed. In this design, the MC modes oscillate with $\omega_{\omega,}$ which is around 1.5 GHz. That means the designed converter operates at L-band. The designed system's dynamics are routinely derived using "Heisenberg-Langevin equations" [18, 21]. Also, as an important part, one has to notice the interaction of the system-environment with which the noise and damping rate effects are included. By considering the latter point, including the noise effect, the equation of motion of the system becomes:

$$\begin{aligned}
\dot{a}_s &= -(i\Delta_c + \kappa_c)\hat{a}_c - jG_1\hat{P}_x + E_c + \sqrt{2\kappa_s}\,\hat{a}_{in} \\
\dot{\hat{c}}_\omega &= -(i\Delta_\omega + \kappa_\omega)\hat{c}_\omega + j\Delta_{o\omega 1}G_2\hat{q}_x\hat{c}_\omega + E_\omega + \sqrt{2\kappa_\omega}\,\hat{c}_{in} \\
\dot{q}_x &= \omega_m\hat{P}_x + G_1(\hat{a}_c^+ + \hat{a}_c) \\
\dot{P}_x &= -\gamma_m\hat{P}_x - \omega_m\hat{q}_x + \Delta_\omega G_2\hat{c}_\omega^+\hat{c}_\omega + \hat{b}_{in}
\end{aligned} \tag{4.3}$$

In this equation, κ_c, γ_m, κ_ω, Δ_c, and Δ_ω are the OC, MR, MC damping rate, and detuning frequencies, respectively. Also, $G_1 = \sqrt{(\alpha_c^2\omega_m/2\varepsilon_0 m\omega_c)}$, $G_2 = C_pC_t\sqrt{(\hbar/m\omega_m)}$ and E_ω is the MC driving field [22- 24]. Eq. 4.3 is a nonlinear equation that cannot be easily solved in terms of the contributed operators. To solve this equation, the equation should be initially linearized; this is done by selecting a fix point where the cavities of the system are driven and operated with and then calculate the slight fluctuation around the DC point. That is a fair assumption to select a strong driven field, and then one has to concentrate on the quantum field fluctuation close to the constant point (driven field) [22, 27]. Thus, the mode of cavities is expressed based on new quantities as a superposition of DC, and AC (fluctuating) terms resulted in the form of: $\mathbf{a_c} = A_s+\boldsymbol{\delta}\mathbf{a_c}$, $\mathbf{c_\omega} = C_s+\boldsymbol{\delta}\mathbf{c_\omega}$, $\mathbf{q_x} = X_s+\boldsymbol{\delta}\mathbf{q_x}$, and $\mathbf{P_x} = P_s+\boldsymbol{\delta}\mathbf{p_x}$. In these expressions, the capital alphabet with subscript "s" stands for fix point (DC), and presubscription "δ" stands for the quantum

fluctuation very close to the fix point. With substituting new quantities in Eq. 4.3 and regarding just the stationary terms, the results are expressed as:

$$\begin{aligned}
&-(j\Delta_c+\kappa_c)A_s - jG_1P_s + E_c = 0\\
&-(j\Delta_\omega+\kappa_\omega)C_s + j\Delta_{o\omega 1}G_2X_sC_s + E_\omega = 0\\
&\omega_m P_s + 2G_1\,\mathrm{Re}\{A_s\} = 0\\
&-\gamma_m P_s - \omega_m X_s + \Delta_\omega G_2\,|C_s|^2 = 0
\end{aligned} \tag{4.4}$$

For solving Eq. 4.4, it is usually supposed $\mathrm{Re}\{A_s\}>>1$ and also $|C_s|>>1$. The system-driven fix points A_s, C_s, P_s, and X_s are determined with solving Eq. 4.4 as:

$$\begin{aligned}
&P_s = \frac{2G_1\,\mathrm{Re}\{A_s\}}{\omega_m},\ X_s = \frac{-\gamma_m P_s + \Delta_\omega G_2\,|C_s|^2}{\omega_m}\\
&A_s = \frac{E_c - jG_1P_s}{(j\Delta_c+\kappa_c)},\ C_s = \frac{j\Delta_{o\omega 1}G_2X_sC_s + E_\omega}{(j\Delta_\omega+\kappa_\omega)}
\end{aligned} \tag{4.5}$$

Eq. 4.5 shows the DC point that the cavities are driven. However, it is necessary to calculate the small fluctuation around them in the following. It can be easily shown that the modes fluctuations are not affected by the DC points selection in Eq. 4.5. Eventually, the cavities mode fluctuation, which is limited very close to the DC point, is given by:

$$\begin{aligned}
&\dot{\hat{\delta a}}_c = -(j\Delta_c+\kappa_c)\,\hat{\delta a}_c - jG_1\,\hat{\delta p}_x + \sqrt{2\kappa_s}\,\hat{\delta a}_{in}\\
&\dot{\hat{\delta c}}_\omega = j\Delta_{o\omega 1}G_2\{\hat{\delta q}_x C_s + X_s\,\hat{\delta c}_\omega\} + \sqrt{2\kappa_{cs}}\,\hat{\delta c}_{in} - (j\Delta_\omega+\kappa_\omega)\,\hat{\delta c}_\omega\\
&\dot{\hat{\delta q}}_x = \omega_m\,\hat{\delta p}_x + G_1(\hat{\delta a}_c^{+} + \hat{\delta a}_c)\\
&\dot{\hat{\delta p}}_x = -\gamma_m\,\hat{\delta p}_x + \Delta_\omega G_2\{\hat{\delta c}_\omega^{+} C_s + C_s^{*}\,\hat{\delta c}_\omega\} - \omega_m\,\hat{\delta q}_x + \hat{\delta b}_{in}
\end{aligned} \tag{4.6}$$

Eq. 4.6 is a linearized coupled equation in which the quantum fluctuation of the cavity modes is involved. By solving this equation, modes separability and their entanglement are determined. The cavities mode interaction in the converter creates CV entanglement, which is the quantum correlation among intra-cavity field quadrature operators [12,13,19]. In fact, it is the coupling factor that can engineer the correlation among cavities mode. In Eq. 4.6, $\boldsymbol{\delta p_x}$ couples to $\boldsymbol{\delta a_c}$ by G_1, $\boldsymbol{\delta c_\omega}$ is manipulated by $\boldsymbol{\delta q_x}$ via factor $C_sG_2\Delta_{o\omega 1}$, $\boldsymbol{\delta q_x}$ is changed by the alteration of $\boldsymbol{\delta X_c}$, and finally, $\boldsymbol{\delta p_x}$ is altered due to the change of $\boldsymbol{\delta q_x}$ and $\boldsymbol{\delta c_\omega}$. Thus, this is the role of a quantum radar engineer who determines the factors in such a way that the modes become correlated. The effect

of the mentioned factors on the entanglement between mods will be studied and investigated in detail in the following section. In Eq. 4.6, OC and MC cavity modes are expressed based on only annihilation operator, while for MR, the related quadrature operators are expressed. Thus, one can easily derive the quadrature operators for OC and MC cavities, and eventually, the system equation of motion using QED theory in the matrix form is expressed as:

$$\begin{bmatrix} \dot{\delta q}_x \\ \dot{\delta p}_x \\ \dot{\delta X}_c \\ \dot{\delta Y}_c \\ \dot{\delta X}_\omega \\ \dot{\delta Y}_\omega \end{bmatrix} = \underbrace{\begin{bmatrix} 0 & \omega_m & G_1\sqrt{2} & 0 & 0 & 0 \\ -\omega_m & -\gamma_m & 0 & G_m & 0 & 0 \\ 0 & 0 & -\kappa_c & \Delta_c & 0 & 0 \\ 0 & -G_1\sqrt{2} & -\Delta_c & -\kappa_c & 0 & 0 \\ G_{11} & 0 & 0 & 0 & -\kappa_{\omega 1} & \Delta_{\omega 1} \\ G_{22} & 0 & 0 & 0 & -\Delta_{\omega 1} & -\kappa_{\omega 1} \end{bmatrix}}_{A_{i,j}} \times \underbrace{\begin{bmatrix} \delta q_x \\ \delta p_x \\ \delta X_c \\ \delta Y_c \\ \delta X_\omega \\ \delta Y_\omega \end{bmatrix}}_{u(0)} + \underbrace{\begin{bmatrix} 0 \\ \delta b_{in} \\ \sqrt{2\kappa_c}\delta X_c{}^{in} \\ \sqrt{2\kappa_c}\delta Y_c{}^{in} \\ \sqrt{2\kappa_\omega}\delta X_\omega{}^{in} \\ \sqrt{2\kappa_\omega}\delta Y_\omega{}^{in} \end{bmatrix}}_{n(t)}$$

$$G_m = \sqrt{2}G_2\Delta_\omega C_s, G_{22} = \sqrt{2}G_2\Delta\omega \mathrm{Re}\{C_s\}, \kappa_{\omega 1} = \kappa_\omega + G_2\Delta_\omega \mathrm{Im}\{q_s\} \quad (4.7)$$

$$G_{11} = -\sqrt{2}G_2\Delta\omega \mathrm{Im}\{C_s\}, \Delta_{\omega 1} = \Delta_\omega - G_2\Delta_\omega \mathrm{Re}\{q_s\}$$

One can consider the general form of the solution of Eq. 4.7, which is "$u(t) = \exp(A_{nm}t)u(0) + \int(\exp(A_{nm}s).n(t-s))ds$", where n(.) define the system contributed noise. The familiar correlation function is applied to characterize the noises in the system as [19-23]:

$$\begin{aligned} &< a_{in}(s)\, a_{in}^{*}(s') >= [N(\omega_c)+1]\delta(s-s'); < a_{in}^{*}(s)\, a_{in}(s') >= [N(\omega_c)]\delta(s-s') \\ &< \hat{c}_{in}(s)\, \hat{c}_{in}^{*}(s') >= [N(\omega_\omega)+1]\delta(s-s'); < \hat{c}_{in}^{*}(s)\, \hat{c}_{in}(s') >= [N(\omega_\omega)]\delta(s-s') \\ &< \hat{b}_{in}(s)\, \hat{b}_{in}^{*}(s') >= [N(\omega_m)+1]\delta(s-s'); < \hat{b}_{in}^{*}(s)\, \hat{b}_{in}(s') >= [N(\omega_m)]\delta(s-s') \end{aligned} \quad (4.8)$$

In Eq. 4.8, $N(\omega) = [\exp(\hbar\omega/k_BT)-1]^{-1}$ characterizes the mean of thermal photon numbers in the equilibrium state. Eq. 4.7 results in the fluctuation of cavity modes and is used to analyze the entanglement of the cavity modes. In the quantum radar application, the OC and MC modes entanglement get the highest priority. That is why we deliberately focus on analyzing the MC and OC modes correlation. For this reason, all of the factors destroying entanglement between modes are studied. The entanglement between modes is evaluated using "Simon-Peres-Horodecki criterion" of the continuous mode given in Eq. 3.39. The criterion in Eq. 3.39 is the bipartite Gaussian states separability necessary and sufficient condition. Thus, it should be supposed that all of the cavities states are Gaussian. Also, A_v, B_v, and C_v in Eq. 3.39 are

correlation and cross-correlation matrix elements [A_v, C_v; C_v^T, B_v]. The elements of the mentioned matrix in Eq. 3.40 are re-expressed for OC-MC modes as:

$$A_v=\begin{bmatrix} <\delta X_c^2>-<\delta X_c>^2 & 0.5\times<\delta X_c\delta Y_c+\delta Y_c\delta X_c>-<\delta X_c><\delta Y_c> \\ 0.5\times<\delta X_c\delta Y_c+\delta Y_c\delta X_c>-<\delta X_c><\delta Y_c> & <\delta Y_c^2>-<\delta Y_c>^2 \end{bmatrix}$$

$$B_v=\begin{bmatrix} <\delta X_\omega^2>-<\delta X_\omega>^2 & 0.5\times<\delta X_\omega\delta Y_\omega+\delta Y_\omega\delta X_\omega>-<\delta X_\omega><\delta Y_\omega> \\ 0.5\times<\delta Y_\omega\delta X_\omega+\delta X_\omega\delta Y_\omega>-<\delta Y_\omega><\delta X_\omega> & <\delta Y_\omega^2>-<\delta Y_\omega>^2 \end{bmatrix} \quad 4.10)$$

$$C_v=\begin{bmatrix} 0.5\times<\delta X_c\delta X_\omega+\delta X_\omega\delta X_c>-<\delta X_c><\delta X_\omega> & 0.5\times<\delta X_c\delta Y_\omega+\delta Y_\omega\delta X_c>-<\delta X_c><\delta Y_\omega> \\ 0.5\times<\delta Y_c\delta X_\omega+\delta X_\omega\delta Y_c>-<\delta Y_c><\delta X_\omega> & 0.5\times<\delta Y_c\delta Y_\omega+\delta Y_\omega\delta Y_c>-<\delta Y_c><\delta Y_\omega> \end{bmatrix}$$

For each two-mode entanglement evaluation, matrix elements should be constructed and uses the criterion expressed in Eq. 3.39 to analyze the correlation between modes. Up to now, the equation of motion of the electro-opto-mechanical converter was analytically derived applying "canonical quantization method" and "Heisenberg-Langevin equations". In the following, "Simon-Peres-Horodecki criterion" is employed as a major criterion for figuring out the cavity modes entanglement. As the primary goal of this thesis, the converter mentioned above must be engineered in such a way to enhance the OC-MC modes entanglement sustainability. However, as an application of a radar system, it needs to broadcast the entangled microwave photons toward a target. That means the entangled photons, before finding the target, should experience the atmospheric medium. It is clear that the propagation of a signal through the atmosphere leads to disperse in the signal, same as a classical radar. Thus, one can use an amplifier to intensify the signal and then propagate the amplified signal into the atmosphere. Nonetheless, it is clear that the amplifying of the entangled photons to produce more photons with the same non-classicality is so critical. With knowledge about this point, it is supposed that one can amplify the entangled photons as same as a classical approach. Also, after scattering from the target, the scattered photons meet the atmosphere again, get amplified, and are finally detected. In the next step, these effects are considered and theoretically analyzed the effect of the active medium (amplifier), attenuation medium (atmosphere), and the target scattering on the correlation between modes.

4.1.3. Entangled photons Amplification: The effect of active medium

This part concentrates on showing the active medium effects on intensifying microwave photons using QED. Figure 4.5 demonstrates the schematic of the active medium. The main idea emphasizes preserving the entanglement behavior of the entangled photons, although they should endure the active medium effect to intensify the microwave photons. Using an active medium

leads to intensifying the entangled photons to create more photons with non-classicality. From Figure 4.5, it is clear that the active medium's input is a microwave photon, $\mathbf{c_{\omega}}$, and the medium's output is $\mathbf{c_{a\omega}}$. Analyzing the entanglement between $\mathbf{c_{a\omega}}$ and $\mathbf{c_{\omega}}$ is one of the primary purposes of the study. It will show that the active medium is an indispensable part of a quantum radar before the propagation of the signals into the atmosphere and detection of the target. Thus, it is essential to find an effective method by which it becomes possible to amplify the entangled microwave photons.

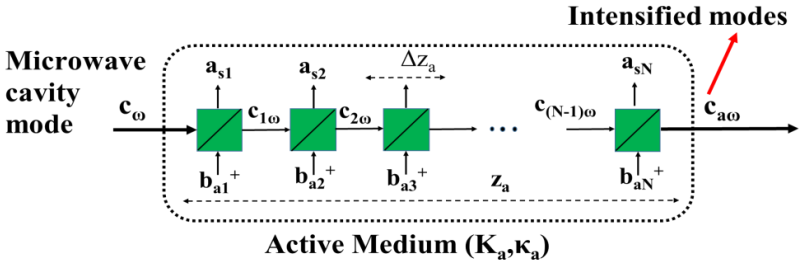

Figure 4.5. Active medium modeling with series connection of BS.

The active medium is modeled using BS connected in series. In this connection, each BS operating as an active agent amplifies the incoming photons fundamentally using harmonic oscillator inverting. It is contributed to the "thermally excited photons $b_a \rightarrow b_a^+$", where b_a is the related operator [18, 28]. Therefore, the microwave signals are amplified since propagating through the active medium due to the interaction with the inverted atom population. The mentioned interaction refers to the interaction between atomic quantum and electromagnetic fields. One of the essential factors to enhance the system's efficiency is the coupling factor of the incident and atom's field interaction. In this modeling, BS plays a critical role to especially note. The BS is modeled as an intensifying agent in terms of its inputs ($c_{\omega n}$, b_a^+) and outputs ($c_{\omega(n+1)}$, a_{sn}), where subscript n and a_{sn} indicate the BS number in medium and output mode, respectively. The BS input and output operators are given as [28]:

$$\begin{aligned} \hat{c}_{(n+1)\omega} &= t(\omega)\hat{c}_{n\omega}(\omega) + r(\omega)\hat{b}_{an}^{+}(\omega) \\ \hat{a}_{sn} &= r(\omega)\hat{c}_{n\omega}(\omega) + t(\omega)\hat{b}_{an}^{+}(\omega) \end{aligned} \tag{4.11}$$

In this equation, r(ω) and t(ω) are the complex reflection and transmission coefficients at frequency ω, respectively. In the present modeling, all of the input and output single modes

satisfy the commutation relation as $[\mathbf{c_{n\omega}}(\omega), \mathbf{c_{n\omega}}^{+}(\omega')] = \delta(\omega - \omega')$, $[\mathbf{c_{(n+1)\omega}}(\omega), \mathbf{c_{(n+1)\omega}}^{+}(\omega')] = \delta(\omega - \omega')$ and $[\mathbf{b_n}(\omega), \mathbf{b_m}^{+}(\omega')] = \delta_{mn}\delta(\omega - \omega')$.

The calculation of the active medium's effect on the input and output modes entanglement requires an expression of the output with regard to the input operators (relationship between $\mathbf{c_{a\omega}}$ and $\mathbf{c_{\omega}}$). This is obtained for a single BS in Eq. 4.11. Also, this equation can be modified by considering the effect of the beam propagation phase with the wave vector real-part $K_a = \omega n(\omega)/c$, as:

$$\begin{aligned} \hat{c}_{(n+1)\omega}(\omega) &= t(\omega)e^{[jK_a\Delta_{za}]}\hat{c}_{n\omega}(\omega) + r(\omega)\hat{b}_{an}^{+}(\omega) \\ \hat{a}_{sn} &= r(\omega)\hat{c}_{n\omega}(\omega) + t(\omega)e^{[jK_a\Delta_{za}]}\hat{b}_{an}^{+}(\omega) \end{aligned} \tag{4.12}$$

where $n(\omega)$ is the active medium real refractive index. The focus is laid on the intensified signal $\mathbf{c_{\omega(n+1)}}(\omega)$ to analyze the sustainability of the entanglement regarding the active medium effects. The relation between the input and output mode operators for N discrete-series BS is introduced as:

$$\hat{c}_{a\omega}(\omega) = t(\omega)e^{[jK_a\Delta_{za}]N}\hat{c}_{\omega}(\omega) + r(\omega)\sum_{n=1}^{N}\left\{t(\omega)e^{[jK_a\Delta_{za}]}\right\}^{(N-n)}\hat{b}_{an}^{+}(\omega) \tag{4.13}$$

Also, the imaginary part of the wave vector is regarded as $\kappa_a(\omega) = |r(\omega)|^2/2\Delta_{za}$ [28]. The expectation value of the thermally excited photons, which operate, in essence, like a noise, obeying the same relation of Eq. 4.8. It can be observed from Eq. 4.13 that N beam-splitter is employed in the discrete form with $N = z_a/\Delta_{za}$, where z_a is the active medium length, and Δ_{za} is the single BS length. One can convert the discrete model to a continuous one by approaching N to infinity in order to model a real amplifier. Eq. 4.13 can be re-written in the continuous form as:

$$\hat{c}_{a\omega}(\omega) = e^{[jK_a + \kappa_a(\omega)]z_a}\hat{c}_{\omega}(\omega) + j\sqrt{2\kappa_a(\omega)}\int_0^{z_a} dz e^{[jK_a + \kappa_a(\omega)](z_a - z)}\hat{b}_{a}^{+}(\omega, z) \tag{4.14}$$

where $\mathbf{c_{a\omega}}(\omega)$ is the output mode operator of the active medium. From Eq. 4.14, the first term indicates the MC output mode intensifying by the active medium, and also, the second term stands for the noise operator effects. The active medium's operator continuous form is examined based on the MC mode. Thus, it is possible to investigate the active medium-related parameter effects on the modes $\mathbf{c_{a\omega}}$ and $\mathbf{a_s}$ entanglement. Thus, with changing the active medium parameters such as length, the wave vector real and imaginary parts, and also the applied thermally excited photons, the output modes correlation are strongly manipulated.

The entanglement analysis for modes $\mathbf{c_{a\omega}}$ and $\mathbf{c_{\omega}}$ needs to define the quadrature operator of the active medium output modes as:

$$\begin{aligned}\delta\hat{X}_{a\omega} &= \frac{\hat{c_{a\omega}}(\omega)+\hat{c_{a\omega}}^{+}(\omega)}{2} = e^{\kappa_a(\omega)z_a}\left\{\delta\hat{X}_{\omega}\cos(K_a z_a)-\delta\hat{Y}_{\omega}\sin(K_a z_a)\right\} \\ &+\sqrt{2\kappa_a(\omega)}\int_0^{z_a} dz e^{\kappa_a(\omega)(z_a-z)}\left\{\delta\hat{Y}_b(\omega,z)\cos(K_a(z_a-z))-\delta\hat{X}_b(\omega',z')\sin(K_a(z_a-z))\right\} \\ \delta\hat{Y}_{a\omega} &= \frac{\hat{c_{a\omega}}(\omega)-\hat{c_{a\omega}}^{+}(\omega)}{2j} = e^{\kappa_a(\omega)z_a}\left\{\delta\hat{Y}_{\omega}\cos(K_a z_a)+\delta\hat{X}_{\omega}\sin(K_a z_a)\right\} \\ &+\sqrt{2\kappa_a(\omega)}\int_0^{z_a} dz e^{\kappa_a(\omega)(z_a-z)}\left\{\delta\hat{X}_b(\omega,z)\cos(K_a(z_a-z))+\delta\hat{Y}_b(\omega',z')\sin(K_a(z_a-z))\right\}\end{aligned} \quad (4.15)$$

where $\delta X_b = \{\mathbf{b}(\omega,z)+ \mathbf{b_m}^{+}(\omega',z')\}/2$ and $\delta Y_b = \{\mathbf{b}(\omega,z)- \mathbf{b_m}^{+}(\omega',z')\}/2j$. It is clear from Eq. 4.15 that the quadrature operator of the active medium mode is presented based on the MC output mode operators. Similar to the latter stage that the OC and MC modes entanglement was studied through the construction of the matrix elements A_v, B_v, C_v, and D_v via Eq. 4.10 and then using Eq. 3.39 to analyze the entanglement between modes in the same way. It should notably be considered the differences between two mode quadrature operators, $<\delta X_{\omega}^2>$ and $<\delta X_{a\omega}^2>$. In other words, to analyze the entanglement of $\mathbf{c_{a\omega}}$ and $\mathbf{a_s}$, the matrix A is the same with Eq. 4.10, while matrix B and C should be re-expressed as:

$$\begin{aligned}A_v &= \begin{bmatrix} <\delta X_c^2>-<\delta X_c>^2 & 0.5\times<\delta X_c\delta Y_c+\delta Y_c\delta X_c>-<\delta X_c><\delta Y_c> \\ 0.5\times<\delta X_c\delta Y_c+\delta Y_c\delta X_c>-<\delta X_c><\delta Y_c> & <\delta Y_c^2>-<\delta Y_c>^2 \end{bmatrix} \\ B_v &= \begin{bmatrix} <\delta X_{a\omega}^2>-<\delta X_{a\omega}>^2 & 0.5\times<\delta X_{a\omega}\delta Y_{a\omega}+\delta Y_{a\omega}\delta X_{a\omega}>-<\delta X_{a\omega}><\delta Y_{a\omega}> \\ 0.5\times<\delta Y_{a\omega}\delta X_{a\omega}+\delta X_{a\omega}\delta Y_{a\omega}>-<\delta Y_{a\omega}><\delta X_{a\omega}> & <\delta Y_{a\omega}^2>-<\delta Y_{a\omega}>^2 \end{bmatrix} \\ C_v &= \begin{bmatrix} 0.5\times<\delta X_c\delta X_{a\omega}+\delta X_{a\omega}\delta X_c>-<\delta X_c><\delta X_{a\omega}> & 0.5\times<\delta X_c\delta Y_{a\omega}+\delta Y_{a\omega}\delta X_c>-<\delta X_c><\delta Y_{a\omega}> \\ 0.5\times<\delta Y_c\delta X_{a\omega}+\delta X_{a\omega}\delta Y_c>-<\delta Y_c><\delta X_{a\omega}> & 0.5\times<\delta Y_c\delta Y_{a\omega}+\delta Y_{a\omega}\delta Y_c>-<\delta Y_c><\delta Y_{a\omega}> \end{bmatrix}\end{aligned} \quad (4.16)$$

For instance, in the following, the expectation value of $<\delta X_{a\omega}^2>$, $<\delta X_{a\omega}\delta X_C>$ and $<\delta X_{a\omega}\delta Y_C>$ are calculated as:

$$
\begin{aligned}
<\delta\hat{X}_{a\omega}{}^2> &= e^{2\kappa_a(\omega)z_a}\Big\{<\delta\hat{X}_{\omega}{}^2>\cos^2(K_a z_a)+<\delta\hat{Y}_{\omega}{}^2>\sin^2(K_a z_a)-\cos(K_a z_a)\sin(K_a z_a)\\
&\quad(<\delta\hat{X}_{\omega}><\delta\hat{X}_{\omega}>+<\delta X_{\omega}><\delta\hat{X}_{\omega}>)\Big\}\\
&\quad+2\kappa_a(\omega)\Big\{\int_0^{z_a}dz'e^{\kappa_a(\omega)(z_a-z')}.\int_0^{z_a}dze^{\kappa_a(\omega)(z_a-z)}\Big\{\cos^2(K_a(z_a-z))<\hat{\delta Y}_b(\omega,z)\hat{\delta Y}_b(\omega',z')>\\
&\quad+\sin^2(K_a(z_a-z))<\hat{\delta X}_b(\omega,z)\hat{\delta X}_b(\omega',z')>-\cos(K_a(z_a-z))\sin(K_a(z_a-z))\\
&\quad\Big[<\hat{\delta Y}_b(\omega,z)\hat{\delta X}_b(\omega',z')>+<\hat{\delta X}_b(\omega,z)\hat{\delta Y}_b(\omega',z')>\Big]\Big\}\Big\}
\end{aligned}
\tag{4.17}
$$

$$
\begin{aligned}
<\hat{\delta X}_{a\omega}\hat{\delta X_C}> &= e^{2\kappa_a(\omega)z_a}\Big\{<\hat{\delta X}_{\omega}\hat{\delta X_C}>\cos(K_a z_a)-<\hat{\delta Y}_{\omega}\hat{\delta X_C}>\sin(K_a z_a)\Big\}\\
<\hat{\delta X}_{a\omega}\hat{\delta Y_C}> &= e^{2\kappa_a(\omega)z_a}\Big\{<\hat{\delta X}_{\omega}\hat{\delta Y_C}>\cos(K_a z_a)-<\hat{\delta Y}_{\omega}\hat{\delta Y_C}>\sin(K_a z_a)\Big\}
\end{aligned}
\tag{4.18}
$$

Other expectation values, e.g., $<\mathbf{\delta Y_{a\omega}}^2>$, $<\mathbf{\delta Y_{a\omega}\delta X_C}>$ and $<\mathbf{\delta Y_{a\omega}\delta Y_C}>$ and so on should be calculated in the same way. The calculation of the entanglement of modes is routinely examined by Eq. 3.39. The simulation results reveal that the designed active medium amplifies both entangled and separable photons. In fact, the entangled photons are amplified through the incident with atom's fields interaction. This occurs at a few specific frequencies. However, in an actual condition, it seems that an amplifier will disturb the photons-related non-classicality. Additionally, naturally, the entanglement between modes is completely distorted at a lot of detuning frequencies. The mentioning points will be discussed in the following section.

4.1.4. The atmosphere effect on the propagation of the entangled photons

In the latter step, an amplifier (classic sense) was designed utilizing QED theory due to the amplification of the microwave cavity signal. It was supposed that the entangled microwave photons can be intensified to generate more photons with preserving entanglement behavior. It will be shown that the existence of the active medium to increase the number of entangled photons before the propagation in the atmosphere is an indispensable step. For that, the relationship between the microwave cavity mode and active medium output was theoretically derived. It is noteworthy to mention that the active medium can intensify the propagating photons by a factor depending on the properties of the real medium.

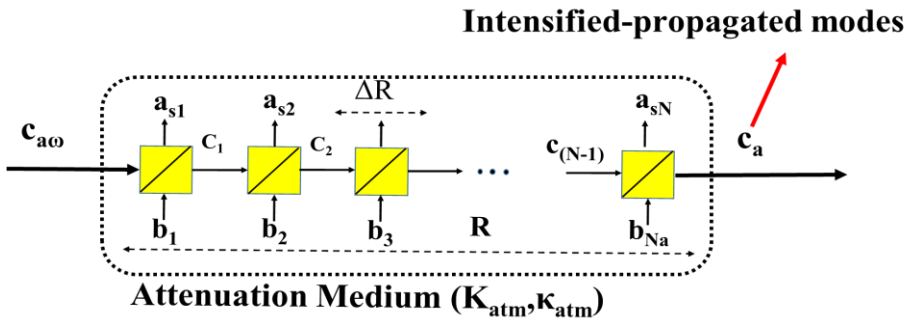

Figure 4.6. Attenuation (atmosphere) medium modeling with series connection of BS.

After microwave photons amplification, the photons enter the atmospheric medium (attenuation medium) for target detection. From the classical point of view, one can use some statistical models to analyze the properties of the atmosphere as a real and uncontrollable medium, which have a critical effect on the propagating signal [1]. It is known that the atmosphere randomly changing properties is the most critical feature of that medium. Nevertheless, a quantum radar profits one of the major advantages of a classic radar which employs microwave photons for propagating into the atmosphere [1, 66]. In the following, the attenuation medium using quantum electrodynamics will be modeled. For this reason, we focus on the quantum picture in which the mentioned medium is modeled by a specific package containing the scattering centers. These centers behave functionality with atmosphere-related variables, including pressure, temperature, and altitude. The discussing scattering centers in the atmosphere quantum electrodynamiclly are modeled using BS depicted in Figure 4.6. In this medium, the thermally excited photons which have a critical effect can be expressed as a function of the atmospheric conditions. In addition, it will be revealed that the factor mentioned above strongly impact the entanglement behavior.

The simulation of the atmosphere medium initiates by modeling the scattering agents with a series connection of BS. For n^{th} BS, the inputs and outputs are, respectively, ($c_{a\omega n}$ and b_n) and ($c_{a\omega(n+1)}$ and a_{sn}). The BS input and output operators can be introduced as [1, 28]:

$$\begin{aligned} \hat{c}_{(n+1)} &= t(\omega)\hat{c}_n(\omega) + r(\omega)\hat{b}_n(\omega) \\ \hat{a}_{sn} &= r(\omega)\hat{c}_n(\omega) + t(\omega)\hat{b}_n(\omega) \end{aligned} \tag{4.19}$$

Generally, the input and output single modes obey the commutation relation $[\mathbf{c_n}(\omega), \mathbf{c_n}^{+}(\omega')] = \delta(\omega - \omega')$. By considering the effect of the beam propagation phase with the real part of the wave vector $K_{atm} = \omega n_{atm}(\omega,R)/c$, Eq. 4.19 is re-expressed as:

$$\hat{c}_{(n+1)}(\omega) = t(\omega)e^{[jKatm\Delta R]}\hat{c}_n(\omega) + r(\omega)\hat{b}_{an}^{+}(\omega)$$
$$\hat{a}_{sn} = r(\omega)\hat{c}_n(\omega) + t(\omega)e^{[jKatm\Delta R]}\hat{b}_{an}^{+}(\omega) \quad (4.20)$$

where $n_{atm}(\omega,R)$ is the atmosphere real refractive index dependent on the atmosphere altitude. The output mode operator of the atmosphere channel is expressed for N discrete and series BS, in terms of the input operator given by:

$$\hat{c}_a(\omega) = t(\omega)e^{[jKatm\Delta_R]N}\hat{c}_{a\omega}(\omega) + r(\omega)\sum_{n=1}^{N}\left\{t(\omega)e^{[jKatm\Delta_R]}\right\}^{(N-n)}\hat{b}_n(\omega) \quad (4.21)$$

Also, the wave vector imaginary part is regarded as $\kappa_{atm}(\omega)= |r(\omega)|^2/2\Delta R$ [28]. The discrete form presented in Eq. 4.21 is rearranged in the continuous form as:

$$\hat{c}_a(\omega) = e^{[jKatm-\kappa_{atm}(\omega)]R}\hat{c}_{a\omega}(\omega) + j\sqrt{2\kappa_{atm}(\omega)}\int_0^R dz e^{[jKatm+\kappa_{atm}(\omega)](R-z)}\hat{b}(\omega,z) \quad (4.22)$$

where $\mathbf{c_a}(\omega)$ is the attenuation medium output modes operator. Eq. 4.22 expresses the effect of the attenuation channel. Clearly seen from the equation that the input mode is exponentially attenuated due to the scattering agent's effect, and also the noise effect is shown. Changing the atmosphere conditions leads to a change of $\kappa_{atm,}$ meaning that the output modes correlation is strongly affected. Also, the entanglement between modes is severely manipulated by the atmosphere noise effect, and additionally, the atmosphere length from the radar to the target R is a critical factor to disturb the nonclassicality correlation between the modes. The input operator in Eq. 4.22 $\mathbf{c_{a\omega}}(\omega)$ is the active medium output which can be manipulated and controlled with the related medium's properties.

In the following, the entanglement between $\mathbf{c_a}(\omega)$ and $\mathbf{a_s}$ is studied to demonstrate how the atmosphere can affect the entanglement between modes. For the calculation of the entanglement between two modes, the quadrature operator of the attenuation medium output modes is generally needed to be defined as:

$$\delta\hat{X}_a = \frac{\hat{c_a}(\omega)+\hat{c_a}^{+}(\omega)}{2} = e^{-\kappa_{atm}(\omega)R}\left\{\delta\hat{X}_{a\omega}\cos(K_{atm}R) - \delta\hat{Y}_{a\omega}\sin(K_{atm}R)\right\}$$
$$-\sqrt{2\kappa_{atm}(\omega)}\int_0^{z_a} dz e^{-\kappa_{atm}(\omega)(R-z)}\left\{\delta\hat{Y}_b(\omega,z)\cos(K_{atm}(R-z)) + \delta\hat{X}_b(\omega',z')\sin(K_{atm}(R-z))\right\}$$
$$\delta\hat{Y}_a = \frac{\hat{c_a}(\omega)-\hat{c_a}^{+}(\omega)}{2j} = e^{-\kappa_{atm}(\omega)R}\left\{\delta\hat{Y}_{a\omega}\cos(K_{atm}R) + \delta\hat{X}_{a\omega}\sin(K_{atm}R)\right\} \quad (4.23)$$
$$+\sqrt{2\kappa_{atm}(\omega)}\int_0^{z_a} dz e^{-\kappa_{atm}(\omega)(R-z)}\left\{\delta\hat{X}_b(\omega,z)\cos(K_{atm}(R-z)) - \delta\hat{Y}_b(\omega',z')\sin(K_{atm}(R-z))\right\}$$

In Eq. 4.23, the attenuation medium quadrature mode operators are presented. Similarly, entanglement between attenuation medium output modes and the modes kept in the laboratory can be studied. For this purpose, one has to calculate the correlation matrix elements for the new quantitates such as $<\delta\mathbf{X_a}^2>$, $<\delta\mathbf{X_a}\ \delta\mathbf{X_c}>$, $<\delta\mathbf{Y_a}^2>$ and so forth. Finally, to analyze the entanglement of c_a and a_s, matrix A_v is established in the same way with Eq. 4.10, while matrix B_v and C_v should be re-arranged based on the new quantities as:

$$A_v = \begin{bmatrix} <\delta X_c^2> - <\delta X_c>^2 & 0.5\times <\delta X_c\delta Y_c + \delta Y_c\delta X_c> - <\delta X_c><\delta Y_c> \\ 0.5\times <\delta X_c\delta Y_c + \delta Y_c\delta X_c> - <\delta X_c><\delta Y_c> & <\delta Y_c^2> - <\delta Y_c>^2 \end{bmatrix}$$
$$B_v = \begin{bmatrix} <\delta X_a^2> - <\delta X_a>^2 & 0.5\times <\delta X_a\delta Y_a + \delta Y_a\delta X_a> - <\delta X_a><\delta Y_a> \\ 0.5\times <\delta Y_a\delta X_a + \delta X_a\delta Y_a> - <\delta Y_a><\delta X_a> & <\delta Y_a^2> - <\delta Y_a>^2 \end{bmatrix} \quad (4.24)$$
$$C_v = \begin{bmatrix} 0.5\times <\delta X_c\delta X_a + \delta X_a\delta X_c> - <\delta X_c><\delta X_a> & 0.5\times <\delta X_c\delta Y_a + \delta Y_a\delta X_c> - <\delta X_c><\delta Y_a> \\ 0.5\times <\delta Y_c\delta X_a + \delta X_a\delta Y_c> - <\delta Y_c><\delta X_a> & 0.5\times <\delta Y_c\delta Y_a + \delta Y_a\delta Y_c> - <\delta Y_c><\delta Y_a> \end{bmatrix}$$

It seems to be possible to analyze the two modes entanglement using Eq. 3.39 through calculation of A_v, B_v, and C_v matrix in Eq. 4.24. It will be shown that the entanglement between modes is strongly affected by changing the attenuation medium properties. This significant issue will be discussed in detail using simulations and modeling.

4.1.5. Scattering from a target

After analyzing the effect of the active and attenuation mediums on the nonclassical correlation relation between modes, it is now time to investigate the target reflection effects on the incident microwave photons. Herein, to analyze the mentioned effect of the QED theory is used as same as the previous sections. Figure 4.7 depicts the model analyzing the reflection effect. In quantum picture, reflection from a target is defined as the scattering of the incident photons from the

target's atom. The process basically is the incident field and atoms' field interacting. However, the photons excited thermally in the system play a destructing role during the incident photons scattering from the target, leading to leaking away of the modes entanglement.

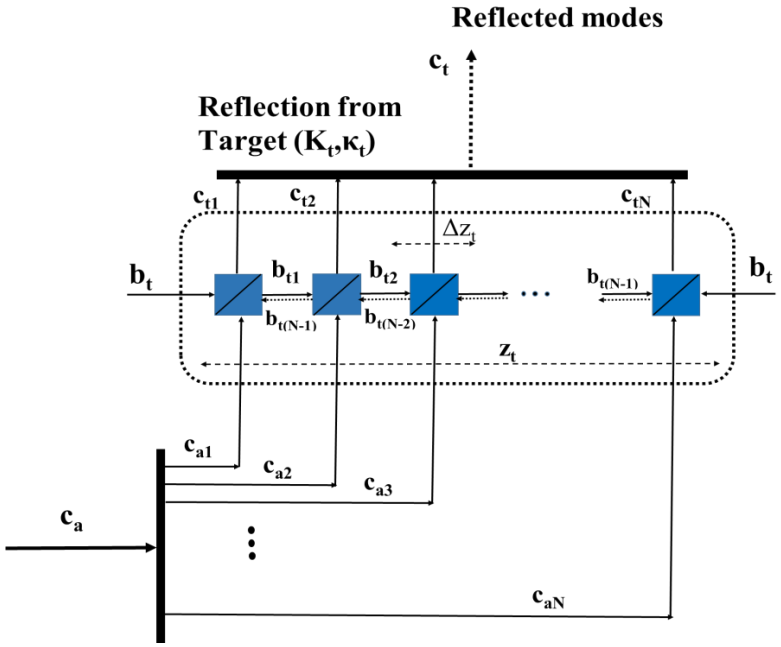

Figure 4.7. A schematic illustration of the scattering modes from the target modeled with the series connection of BS.

In Figure 4.7, it is clear that C_a is the input mode and C_t is the output mode. It needs to find a compact relationship between them to analyze the effect of the target properties on the output signal. In the same way, n^{th} BS is considered as a scattering agent, and the relationship between input and output is given by:

$$\begin{aligned} \hat{c_{tj}} &= t(\omega)\hat{c_{aj}}(\omega) + r(\omega)\hat{b_{tj}}(\omega) \\ \hat{a_{sj}} &= r(\omega)\hat{c_{aj}}(\omega) + t(\omega)\hat{b_{tj}}(\omega) \end{aligned} \tag{4.25}$$

By involving the beam interaction phase with the wave vector real part $K_t = \omega n_t(\omega)/c$, Eq. 4.25 is re-expressed as:

$$\begin{aligned} \hat{c_{tj}} &= t(\omega)e^{[iKt\Delta z_t]}\hat{c_{aj}}(\omega) + r(\omega)\hat{b_{tj}}(\omega) \\ \hat{a_{sj}} &= r(\omega)\hat{c_{aj}}(\omega) + t(\omega)e^{[iKt\Delta z_t]}\hat{b_{tj}}(\omega) \end{aligned} \tag{4.26}$$

where $n_t(\omega)$ is the target's real refractive index. Therefore, the reflected mode operator from the target can be expressed for N discrete BS in terms of the attenuation channel output $\mathbf{C_{a\omega}}(\omega)$ operator as:

$$\hat{c_t}(\omega) = \left\{ t(\omega)e^{[\,jKt\Delta z_t\,]} + r^2(\omega)\sum_{n=1}^{N-1} \left\{ t(\omega)e^{[\,jKt\Delta z_t\,]} \right\}^{(n-1)} \right\} \hat{c_a}(\omega) + r(\omega)t(\omega)e^{[\,jKt\Delta z_t\,]N}\, \hat{b_t}(\omega) \tag{4.27}$$

In Eq. 4.27, all b_{tj}, j = 1, 2, …are expressed in terms of b_t. By considering the infinite number of BS, and using the attenuation medium's relationship between transmission and reflection coefficients satisfying "$|t(\omega)|^2+|r(\omega)|^2 = 1$", the continuous form of Eq. 4.27 is given by:

$$\hat{c_t}(\omega) = \left\{ t(\omega)e^{[\,jKt\Delta z_t\,]} + 2\kappa_t(\omega)\sqrt{\Delta z_t}\int_0^{z_t} dz \left\{ t(\omega)e^{[\,jKt-\kappa_t(\omega)]} \right\}^{(z_t-z)} \right\} \hat{c_a}(\omega) + j\sqrt{\kappa_t(\omega)\Delta z_t}\, e^{[\,jKt-\kappa_t(\omega)]z_t}\, \hat{b_t}(\omega) \tag{4.28}$$

The incident photons scattering from a target are introduced in Eq. 4.28; the first term stands for the target's material wavenumber imaginary part, while the second expression indicates the influences of photons excited thermally. In fact, using Eq. 4.28, one can address RCS modeling with BS using QED and the parameters that affect RCS. Additionally, the entanglement is affected by the phase raising because of the noise presented in the second term. Finally, to study the entanglement between $\mathbf{c_t}(\omega)$ and $\mathbf{a_s}$, it needs to define the quadrature operator of the reflection output modes $\mathbf{c_t}(\omega)$, which is introduced as:

$$\begin{aligned}
\delta\hat{X}_t &= e^{-\kappa_t(\omega)\Delta z_t} \left\{ \delta\hat{X}_a \cos(K_t\Delta z_t) - \delta\hat{Y}_a \sin(K_t\Delta z_t) \right\} - \sqrt{\kappa_t(\omega)\Delta z_t}\, e^{-\kappa_t(\omega)\Delta z_t} \left\{ \delta\hat{Y}_b(\omega,z)\cos(K_t z_t) + \delta\hat{X}_b(\omega,z) \right. \\
&\left. \sin(K_t\Delta z_t) \right\} + 2\sqrt{\Delta z_t}\,\kappa_t(\omega)\int_0^{z_t} dz e^{-\kappa_t(\omega)(z_t-z)} \left\{ \delta\hat{X}_a(\omega)\cos(K_t(z_t-z)) + \delta\hat{Y}_a(\omega)\sin(K_t(z_t-z)) \right\} \\
\delta\hat{Y}_t &= e^{-\kappa_t(\omega)\Delta z_t} \left\{ \delta\hat{Y}_a \cos(K_t\Delta z_t) + \delta\hat{Y}_a \sin(K_t\Delta z_t) \right\} - \sqrt{\kappa_t(\omega)\Delta z_t}\, e^{-\kappa_t(\omega)\Delta z_t} \left\{ -\delta\hat{X}_b(\omega,z)\cos(K_t z_t) + \delta\hat{Y}_b(\omega,z) \right. \\
&\left. \sin(K_t\Delta z_t) \right\} + 2\sqrt{\Delta z_t}\,\kappa_t(\omega)\int_0^{z_t} dz e^{-\kappa_t(\omega)(z_t-z)} \left\{ \delta\hat{Y}_a(\omega)\cos(K_t(z_t-z)) + \delta\hat{X}_a(\omega)\sin(K_t(z_t-z)) \right\}
\end{aligned} \tag{4.29}$$

where $\delta X_t = \mathbf{c_t}(\omega) + \mathbf{c_t}^{+}(\omega)\ /2$ and $\delta Y_t = \mathbf{c_t}(\omega) - \mathbf{c_t}^{+}(\omega)\ /2j$. Eq. 4.29 shows that the quadrature operators contributed to the target reflection are expressed in terms of the attenuation medium operators. Now, one can study the OC and reflection output modes entanglement. For this purpose, the correlation matrix Av, B_v, and C_v have to be calculated for the new quantities as given below.

$$A_v=\begin{bmatrix} <\delta X_c{}^2>-<\delta X_c>^2 & 0.5\times<\delta X_c\delta Y_c+\delta Y_c\delta X_c>-<\delta X_c><\delta Y_c> \\ 0.5\times<\delta X_c\delta Y_c+\delta Y_c\delta X_c>-<\delta X_c><\delta Y_c> & <\delta Y_c^2>-<\delta Y_c>^2 \end{bmatrix}$$

$$B_v=\begin{bmatrix} <\delta X_t{}^2>-<\delta X_t>^2 & 0.5\times<\delta X_t\delta Y_t+\delta Y_t\delta X_t>-<\delta X_t><\delta Y_t> \\ 0.5\times<\delta Y_t\delta X_t+\delta X_t\delta Y_t>-<\delta Y_t><\delta X_t> & <\delta Y_t^2>-<\delta Y_t>^2 \end{bmatrix} \quad (4.30)$$

$$C_v=\begin{bmatrix} 0.5\times<\delta X_c\delta X_t+\delta X_t\delta X_c>-<\delta X_c><\delta X_t> & 0.5\times<\delta X_c\delta Y_t+\delta Y_t\delta X_c>-<\delta X_c><\delta Y_t> \\ 0.5\times<\delta Y_c\delta X_t+\delta X_t\delta Y_c>-<\delta Y_c><\delta X_t> & 0.5\times<\delta Y_c\delta Y_t+\delta Y_t\delta Y_c>-<\delta Y_c><\delta Y_t> \end{bmatrix}$$

Since the matrix elements A_v, B_v, and C_v became calculated, one can analyze the entanglement using Eq. 3.39.

After calculating the incident photons scattering from the target, these photons are reflected back in the atmosphere. So, to complete the quantum radar scenario depicted in Figure 4.4, the atmosphere effect should be applied one more time. In the following, the return signals have to be amplified before detection, suggesting that the active medium effect should be applied as well. The mentioned points, suggesting that the generated microwave entangled photons, are not a necessary condition to detect the entangled photons. In other words, in a quantum radar application, preserving the entanglement between photons is a challenging task. From the latter sections, it was shown that there are a lot of thermally excited photons and noises that critically affect the entanglement between modes. This means that the more thermally excited photons generate in a real medium, the more separability the photons experience. The thermally excited photons directly contribute to the temperature. Unfortunately, one cannot manipulate the operational temperature of the real mediums in the quantum radar system. Then, the converter and the active medium give some degree of freedom to do engineering. In the results and discussions section, it is shown that the entangled microwave photons that are generated at high temperatures can easily endure the noise effect applied from the real mediums and finally maintain the entanglement properties. This is the idea of the next part in which a new and novel converter is designed (called an optoelectronic converter) to produce entanglement at high temperatures.

4.2. Design of the optoelectronic converter for entangled photons generating in a typical quantum radar

In this part, the concentration mainly sat on the optoelectronic converter design in a quantum radar to improve critical characteristics such as modes non-classicality at high-temperature. It

will be discussed in the later section that the "electro-opto-mechanical converter" high-temperature operation is so essential for preserving two modes entanglement. As shown in the results and discussion section, the main problem is issued because of the mechanical part operating at low-frequency. Due to that fact, so many photons excited due to the thermal effect are generated and can destroy the entanglement. Thus, we significantly focus on that point and substitute the mechanical part with an optoelectronic part to solve the problem. A general schematic for such a system is depicted in Figure 4.8.

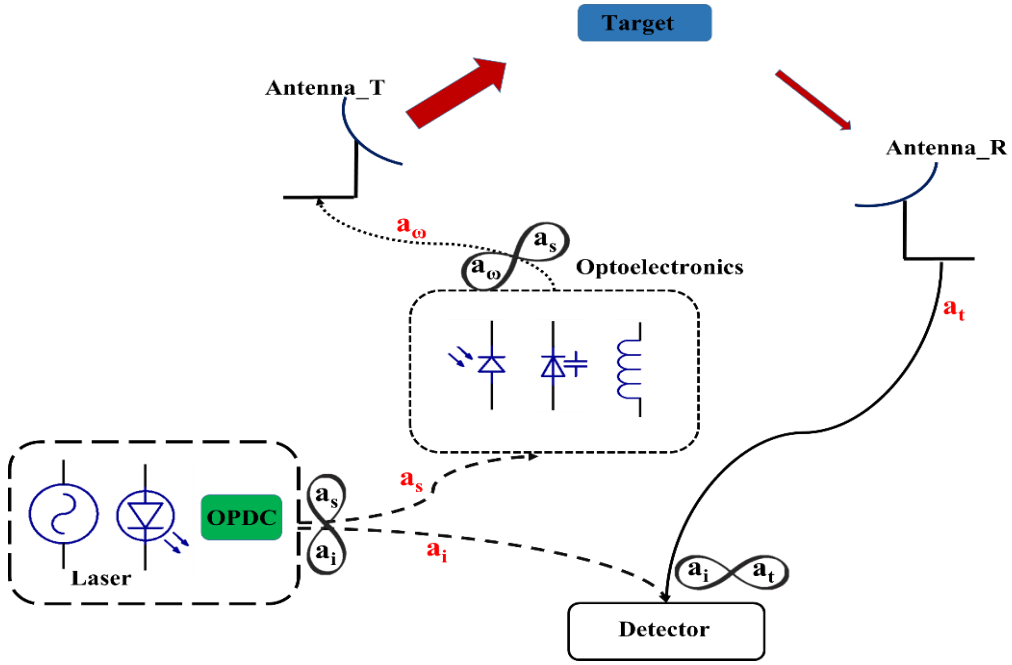

Figure 4.8. A general schematic for a quantum radar using an optoelectronic converter, transmitter antenna, receiving antenna, and detector [67].

It is clear that quantum radar fundamentally works in the same way with a classical radar, both of which use microwave photons to detect the target. Nonetheless, in quantum radar entanglement phenomenon plays an indispensable role. In a typical quantum radar, the operation starts with the generation of the entangled optical photons shown with a_s and a_i in Figure 4.8. After that, $\mathbf{a_s}$ is applied to an optoelectronic circuit to generate the entangled microwave photons $\mathbf{a_\omega}$, while $\mathbf{a_i}$ is kept in the laboratory to be following processed. The generated entangled microwave photons are broadcasted toward the target through the transmitter antenna (Antenna_T), and then the scattered photons are collected by the receiver antenna (Antenna_R), and finally, the detected signals are sent to accomplish the signal processing. In the processing section, the correlation

between a_i and a_t is analyzed. The main goal is to maintain and preserve the entanglement between a_i and a_t, which is strongly affected by the real medium impacts such as attenuation due to the atmosphere, scattering loss because of the target, and also electronic noises in the detection unit.

An optoelectronic converter is theoretically designed to produce the entanglement between photons. In this system, OC is linked to MC via a Varactor diode (VD) which is excited by a photodetector. Initially, optical cavity modes excite the photodetector, and then flowing current with a functionality of the incident light triggers the Varactor diode. The flowing current due to the OC coupling with a photodetector (PD) causes a drop voltage across the diode. This creates a functionality between the drop voltage across the diode and OC modes. In this dissertation, the effect of some critical quantities is deeply studied to engineering the system. One of the mentioned quantities is the photodetector coupling factor (μ_c) to the microwave cavity that makes a dramatic difference between the opto-mechanical converter and the new design. It is shown in the results and discussions section that by engineering the coupling between PD and VD, the entanglement preserved up to 5500 mK. In the following, we first define the system and completely determine how the parts of the system complete each other to maintain the entanglement at high temperatures.

4.2.1. Optoelectronic converter system definition

First of all, to completely analyze the quantum radar [22,67], it is necessary to fully describe the optoelectronic converter schematically illustrated in Figure 4.9, which also is a compact illustration of the step-by-step of the work. It is clear from Figure 4.9a that the laser light is first coupled to OPDC and generates the optical photons (called signal and idler) entangled with each other. The signal mode couples to OC, and consequently, PD is excited by OC outcoming wave. Therefore, flowing current through PD is a function of the incident photons energy. It means that flowing current through the PD is strongly dependent on OC modes. That current causes a voltage drop across VD, leading to a change in the VD's capacitance. That means that the capacitance generated by VD is a function of OC mode intensity. Figure 4.9a shows that MC resonant frequency is manipulated by the change of VD capacitance. Therefore, the modes of MC are influenced by OC modes with coupling between PD and VD. The design of the

optoelectronic converter gives us double key factors to engineer the MC and OC coupling to improve the output modes' nonclassicality correlation. OC coupling to PD is one of the critical factors used to engineer the current flow rate in the converter. In the system analysis, the mentioned factor has to be theoretically calculated. Another factor that is so important contributes to the VD and MC coupling by which MC electronic properties are affected. This coupling factor is created due to the change of the MC capacitance with coupling to PD. As a brief and obvious result, it can be stated that the output modes entanglement is manipulated by altering the discussed factors.

In a quantum radar, one can manipulate the subsystem observed in Figure 4.9a to engineer the photons' non-classicality; after that step, schematically shown in Figure 4.9b, Figure 4.9c, and Figure 4.9d, there is no degree of freedom to control and change the entanglement behavior. Thus, entangled microwave photons generating via an optoelectronic converter propagate in the atmosphere to detect an object. The atmosphere channel effects are analyzed by modeling the atmosphere with the BS series configuration [28], as illustrated in Figure 4.9b. As discussed earlier, each BS has two inputs (c_{i-1}: incident wave and b_i: thermally generated photons) and two outputs (a_{si}: noise and c_i: desired output). The photons induced due to the thermal effect are strongly dependent on the change of temperature in the atmosphere (185~300 K). Also, the atmosphere height is another affecting factor that one should consider its effect on the quantum properties. Regarding the above mentioning parameters, it is clear that the atmosphere disturbs the photons' non-classicality, and then the incident entangled photons treat as classical photons. Consequently, the target scattering effect is applied to the incident photons (Figure 4.9c). Since the propagated signals contain both entangled and separable photons incident on the target, the target's atom fields interact with both of them. The target's materials causing reflection and diffraction severely affect the backscattering photons amplitude and frequency with respect to the incident photons. This is contributed to the quantum field of target atoms manipulating the incident photons properties. Finally, in Figure 4.9d, the backscattering photons endure the atmosphere effect one more time, similar to Figure 4.9b. Nevertheless, there is a difference between the atmosphere effect in Figure 4.9b and Figure 4.9d. In Figure 4.9b, the input mode $\mathbf{c_\omega}$ contains more entangled photons, while in Figure 4.9d, the input mode is $\mathbf{c_t}$ having a few entangled photons and losing a lot of entanglement due to the scattering from the target. It is

indicating that in Figure 4.9d, the atmosphere can easily destroy the entanglement properties. Additionally, in this figure, quantum dot (QD) photodetector [11] sensitivity enhanced by the quantum effect is employed to sense the OC incoming wave. In the simulation part, the QD is supposed as a two-level energy system.

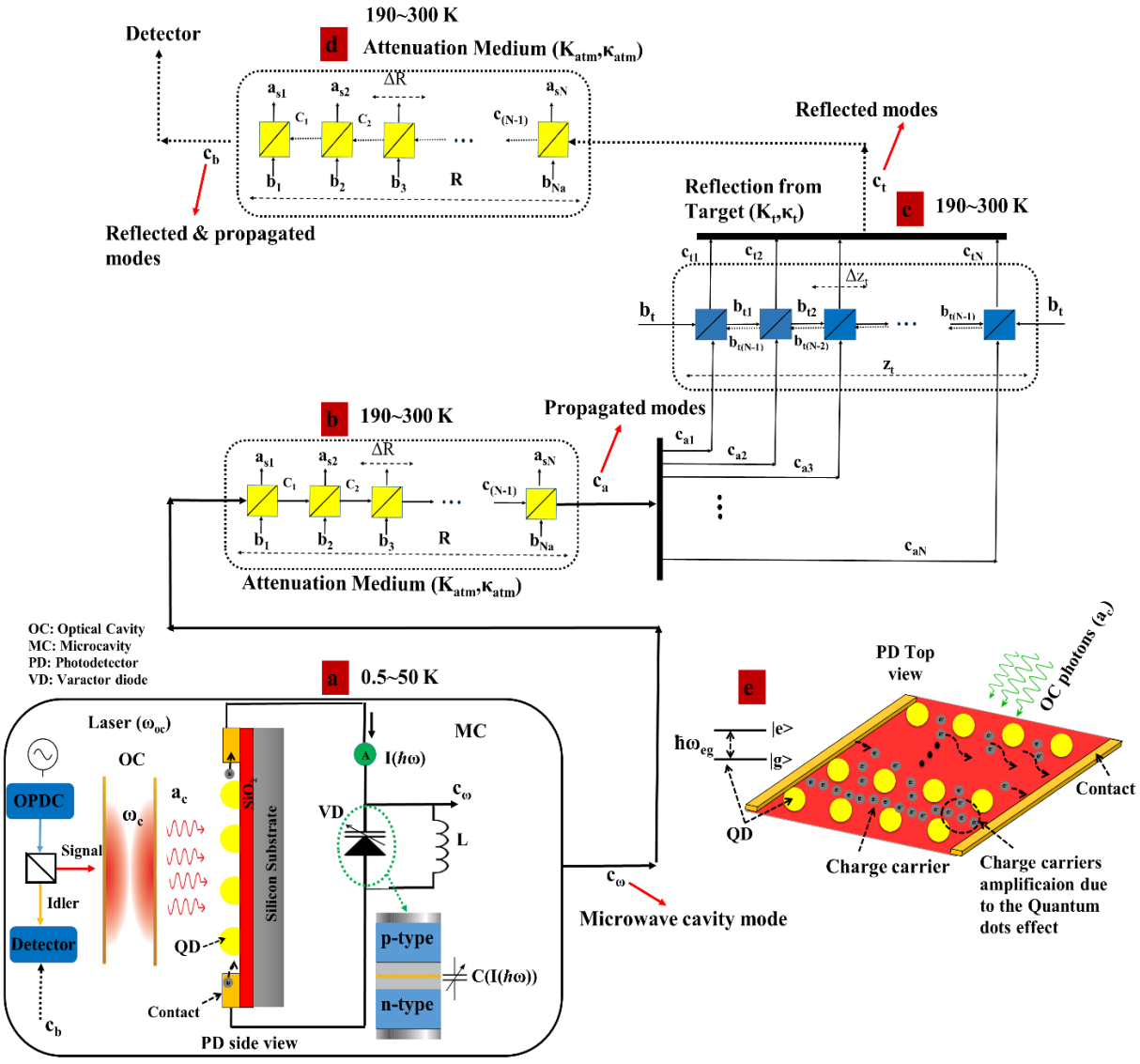

Figure 4.9. Quantum radar schematics using optoelectronic converter; a) Interaction of laser light with an OPDC to generate optical entangled photons and generation of microwave entangled photons using MC coupling to OC through PD, b) Atmosphere medium modeling using BS, c) Target scattering modeling with BS, d) Effect of the atmosphere on the backscattering signals, e) QD using in PD to increase the sensitivity [67].

In the following, an optoelectronic converter is theoretically designed in the same way with the latter section (design of the electro-opto-mechanical converter to generate the entanglement modes). The significant goal is to fully compare the two systems results and find out which system can safely preserve the entanglement between modes and also by which method one can increase the nonclassicality correlation between modes. Since this thesis mainly focuses on providing a sustainable entanglement, therefore, it needs to design a suitable system to do the favor.

4.2.1. Design of a typical optoelectronic converter to generate the entangled states

The quantum radar using the optoelectronic converter illustrated in Figure 4.9a is theoretically analyzed using "canonical quantization method" [18]. In this method, in contrast to the dipole approximation [68,69], the incident and atom's quantum field interaction is underlined.

In general, defining the dynamics of a quantum system needs the contributed Hamiltonian expressed as:

$$
\begin{aligned}
H_{OC} &= \frac{\varepsilon_0}{2}(E^2 + \omega_c{}^2 A^2) \\
H_{PD} &= \frac{P^2}{2m_{eff}} + \frac{1}{2} m_{eff}\, \omega_{eg}{}^2 X^2 \\
H_{MC} &= \frac{Q^2}{2C_0} + \frac{\phi^2}{2L} + \frac{C_d v_d}{C_0} Q \\
H_{OC-PD} &= \alpha_c \frac{AP}{m_{eff}} \\
H_{MC-PD} &= \frac{-C'(x)}{C_0{}^2} \left\{ \frac{Q^2}{2} + C_d v_d Q \right\} X
\end{aligned}
\tag{4.31}
$$

In this equation, the (**X**, **P)**, (**A**, **E)**, and **(Φ**, **Q)** are the PD electron-hole position and momentum operator, optical cavity vector potential and electric field, and the phase and charge operators of MC, respectively. Also, the constants α_c, v_d, C'(x), and C_d, are OC-MC coupling coefficient, the MC driving field, variable capacitor, and capacitor between MC driving field and cavity, respectively. The next step needs to determine the operators **A**, **X**, and **Φ** conjugate variables to express the Hamiltonian based on the raising and lowering operators. This is done regarding a classical approach defining the conjugate variables [29]; so the Hamiltonian is presented as:

$$H_{OC} = \hbar\omega_c \hat{a_c}^{+} \hat{a_c} + j\hbar E_c[\hat{a_c}^{+} e^{(-j\omega_{oc}t)} - \hat{a_c} e^{(j\omega_{oc}t)}]$$

$$H_{PD} = \frac{\hbar\omega_{eg}}{2}(\hat{P_x}^2 + \hat{q_x}^2)$$

$$H_{MC} = \hbar\omega_\omega \hat{c_\omega}^{+} \hat{c_\omega} - j|v_d|C_d\sqrt{\frac{\hbar\omega_\omega}{2C_0}}[\hat{c_\omega} e^{(-j\omega_{o\omega}t)} - \hat{c_\omega}^{+} e^{(j\omega_{o\omega}t)}] \quad (4.32)$$

$$H_{OC-PD} = \hbar\sqrt{\frac{\alpha_c{}^2\omega_{eg}}{2\varepsilon_0 m_{eff}\omega_c}}(\hat{a_c}^{+} + \hat{a_c})\hat{P_x}$$

$$H_{MC-PD} = -\frac{\hbar\mu_c\omega_\omega}{2d}\sqrt{\frac{\hbar}{\omega_{eg}m_{eff}}}\hat{q_x}\hat{c_s}^{+}\hat{c_s}$$

In Eq. 4.32 ($\mathbf{a_c}^{+}$, $\mathbf{a_c}$), and ($\mathbf{c_\omega}^{+}$, $\mathbf{c_\omega}$) are, respectively, optical and microwave cavities creation and annihilation operators. Additionally, ($\mathbf{P_x}$, $\mathbf{q_x}$), E_c, g_{op}, and d are normalized quadrature operator, driving rate of optical cavity input, and the depletion layer width of VD's capacitor, respectively, and moreover $\mu_c = C'(x)/C_0$. In this design, MC modes resonate around ω_ω = 2.75 GHz (S-band); the reason is because of the decreasing the thermally excited photons in MC. In $H_{MC\text{-}PD}$, which is the interaction Hamiltonian between microwave cavity and photodetector, the related coupling factor is concluded as $g_{o\omega} = (\mu_c\omega_\omega/2d)\times\sqrt{(\hbar/\omega_{eg}m_{eff})}$; it is a critical factor by which it will be possible to preserve the entanglement even at high temperatures. The mentioned point will be discussed in detail in the results and discussions section. Also, $g_{op} = \sqrt{(\omega_{eg}\alpha_c{}^2/2\omega_c\varepsilon_0 m_{eff})}$ is OC-PD coupling rate. In Eq. 4.32, the MC field Hamiltonian and its driving are expressed altogether in H_{MC}. One of the critical tasks here is the calculation of g_{op}. To do so in unit volume, one can use the "first-order perturbation theory", and the result is expressed as [11]:

$$g_{op} = \frac{\pi\omega_c}{\varepsilon_0 V_m}\mu^2 g_J(\hbar\omega_{eg})L(\omega_{eg}) \rightarrow \alpha_c = \sqrt{\frac{2\omega_c\varepsilon_0 m_{eff}}{\omega_{eg}}}\frac{\pi\omega_c}{\varepsilon_0 V_m}\mu^2 g_J(\hbar\omega_{eg})L(\omega_{eg})$$

(4.33)

where $g_J(h\omega_{eg})$, μ, and $L(\omega_{eg})$ are, respectively, the PD density of state, dipole momentum, and Lorentzian function. To know precisely how g_{op} is derived for a typical photodetector, one can find the material in Appendix A. Using Eq. 4.33, one can guess about α_c, which is strongly dependent on the electrical and optical properties of the PD. Thus, converter engineering, specifically PD engineering, gives a chance to manipulate the coupling between OC and PD. For example, on can use the plasmonic-based photodetector [11] to enhance the coupling factor.

At last, this key factor is employed as a critical factor to engineer the cavity modes coupling and find out how much the factor can affect the nonclassicality correlation between modes. After Hamiltonian calculation, the contributed dynamic equation of the motion is introduced using "Heisenberg-Langevin equation". To complete the dynamic equation, it needs to add the damping rate and noise effects because of the system and real medium interaction. Also, using RWA, one can define the detuning frequencies of MC, OC, and PD are defined as $\Delta_\omega = \omega_\omega - \omega_{o\omega}$ and $\Delta_c = \omega_c - \omega_{oc}$, and $\Delta_{eg} = \omega_{eg} - \omega_c$, respectively. Finally, the dynamic equation of motion of the new converter is given by:

$$\begin{aligned}
\dot{\hat{a}}_c &= -(j\Delta_c + \kappa_c)\hat{a}_c - jg_{op}\hat{P}_x\hat{a}_c + E_c + \sqrt{2\kappa_c}\,\hat{a}_{in} \\
\dot{\hat{c}}_\omega &= -(j\Delta_\omega + \kappa_\omega)\hat{c}_\omega + jg_{\omega p}\hat{q}_x\hat{c}_\omega + E_\omega + \sqrt{2\kappa_\omega}\,\hat{c}_{in} \\
\dot{\hat{q}}_x &= \Delta_{eg}\hat{P}_x + g_{op}(\hat{a}_c^{+} + \hat{a}_c) \\
\dot{\hat{P}}_x &= -\gamma_p\hat{P}_x - \Delta_{eg}\hat{q}_x + g_{\omega p}\hat{c}_\omega^{+}\hat{c}_\omega + \hat{b}_{in}
\end{aligned} \tag{4.34}$$

In this equation, the parameters κ_c, γ_p, and κ_ω are the damping rates of the optical cavity, photodetector, and microwave cavity, respectively. In the same way with a real system, the cavities interact with the environment; thus, to support the indicating effect, some quantities such as $\mathbf{b_{in}}$, $\mathbf{a_{in}}$, and $\mathbf{c_{in}}$ as the noise sources are defined to model the environment effect on cavities.

In the following, the entanglement will be analyzed as a fluctuation mode for the continuous modes of OC and MC around the fixed operational point that the cavities are driven. Under this condition, it is possible to linearize the converter equation of motion by expanding to the driven field as a fix point [23,27]. The linearization of Eq. 4.34 is done in the same way with Eq. 4.3 as ($\mathbf{a_c} = A_s + \boldsymbol{\delta a_c}$, $\mathbf{c_\omega} = C_s + \boldsymbol{\delta c_\omega}$, $\mathbf{q_x} = X_s + \boldsymbol{\delta q_x}$, and $\mathbf{P_x} = P_s + \boldsymbol{\delta p_x}$). In fact, to calculate the nonclassicality correlation between modes, the fluctuation parts should be considered. Nonetheless, it is necessary to calculate the linearized equation in the steady-state. In the steady-state condition, applying a few assumptions such as $\mathrm{Re}\{A_s\} \gg 1$ and $|C_s| \gg 1$ satisfy the stability. Herein, the quantum fluctuation is noticed and the related equation is solved. The cavity modes quantum fluctuations are defined around the DC points as:

$$
\begin{aligned}
\dot{\delta a}_s &= -(j\Delta_c + \kappa_c)\,\hat{\delta a}_c - jg_{op}\{A_s\,\hat{\delta p}_x + P_s\,\hat{\delta a}_c\} + \sqrt{2\kappa_c}\,\hat{\delta a}_{in} \\
\dot{\delta c}_\omega &= -(j\Delta_\omega + \kappa_\omega)\,\hat{\delta c}_\omega + jg_{\omega p}\{\hat{\delta q}_x\,C_s + X_s\,\hat{\delta c}_\omega\} + \sqrt{2\kappa_\omega}\,\hat{\delta c}_{in} \\
\dot{\delta q}_x &= \Delta_{eg}\,\hat{\delta p}_x + g_{op}\{\hat{\delta a}_c^{+} + \hat{\delta a}_c\} \\
\dot{\delta p}_x &= -\gamma_p\,\hat{\delta p}_x - \Delta_{eg}\,\hat{\delta q}_x + g_{\omega p}\{C_s\hat{\delta c}_\omega^{+} + C_s^{*}\,\hat{\delta c}_\omega\} + \hat{\delta b}_{in}
\end{aligned}
\tag{4.35}
$$

The CV entanglement can be generated due to the interaction among cavities [23-27]. For the aim of OC-MC entanglement analysis, it is necessary to define the related cavities quadrature fluctuation as the fundamental modes. The matrix form of the equations is expressed as:

$$
\begin{bmatrix} \dot{\delta q}_x \\ \dot{\delta p}_x \\ \dot{\delta X}_c \\ \dot{\delta Y}_c \\ \dot{\delta X}_\omega \\ \dot{\delta Y}_\omega \end{bmatrix}
=
\underbrace{\begin{bmatrix}
0 & \Delta_{eg} & \sqrt{2}g_{op} & 0 & 0 & 0 \\
-\Delta_{eg} & -\gamma_p & 0 & 0 & \sqrt{2}g_{\omega p}C_{sr} & -\sqrt{2}g_{\omega p}C_{si} \\
0 & \sqrt{2}g_{op}A_{si} & -\kappa_c & \Delta_c + g_{op}P_s & 0 & 0 \\
0 & -\sqrt{2}g_{op}A_{sr} & -\Delta_c - g_{op}P_s & -\kappa_c & 0 & 0 \\
-\sqrt{2}g_{\omega p}C_{si} & 0 & 0 & 0 & -\kappa_\omega & \Delta_\omega - g_{\omega p}q_s \\
\sqrt{2}g_{\omega p}C_{sr} & 0 & 0 & 0 & -\Delta_\omega + g_{\omega p}q_s & -\kappa_\omega
\end{bmatrix}}_{A_{i,j}}
\times
\underbrace{\begin{bmatrix} \delta q_x \\ \delta p_x \\ \delta X_c \\ \delta Y_c \\ \delta X_\omega \\ \delta Y_\omega \end{bmatrix}}_{u(0)}
+
\underbrace{\begin{bmatrix}
0 \\ \delta b_{in} \\ \sqrt{2\kappa_c}\,\delta X_c^{in} \\ \sqrt{2\kappa_c}\,\delta Y_c^{in} \\ \sqrt{2\kappa_\omega}\,\delta X_\omega^{in} \\ \sqrt{2\kappa_\omega}\,\delta Y_\omega^{in}
\end{bmatrix}}_{n(t)}
\tag{4.36}
$$

In Eq. 4.36, $\mathbf{\delta X_c^{in}}$, $\mathbf{\delta Y_c^{in}}$, $\mathbf{\delta X_\omega^{in}}$, and $\mathbf{\delta Y_\omega^{in}}$ are the noises quadrature operator. The solution of Eq. 4.36 produces an equation with a form as "$u(t) = \exp(A_{nm}t)u(0) + \int(\exp(A_{nm}s).n(t-s))ds$", where n(s) is the noise. One can see Eq. 4.8 to get more information about the noise correlation function.

The entanglement between cavity mods can be analyzed using "Symplectic eigenvalue" [33,35]:

So far, the quantum radar system utilizing optoelectronic converter's dynamic is analytically derived employing the "canonical quantization method" and "Heisenberg-Langevin equations" and also "Symplectic eigenvalue" was applied as a suitable criterion to study the modes entanglement. After converter modes entanglement analysis regarding the procedure demonstrated in Figure 4.9, it needs to consider the real mediums and target effects on the out coming photons. As the primary goal of this part, the new converter illustrated in Figure 4.9a should be brought forth in a way that other effects, such as real medium effects, have a slight impact on entanglement. Besides a crucial difference between the optoelectronic converters with the electro-opto-mechanical converter, there is an interesting point about the system illustrated in Figure 4.9. That is ignoring the amplifier or active medium in this system. There are some

references [16, 65] stating that it is critical to amplify the entangled photons to produce more photons to remain entangled and bring out extra problems that may disturb the entanglement between photons in reality. So, it needs to show how the optoelectronic converter in the quantum radar can work without an amplifier to detect a target and, more importantly, how it can preserve the entanglement of photons before detecting the backscattering photons. With this short introduction, in the following, the atmosphere effect and target scattering are theoretically shortly investigated. Of course, one can find the same material in detail in sections 4.1.3, 4.1.4, and 4.1.5. However, the effect of the real mediums on propagation modes is just listed.

4.2.2. Quantum mechanically analyzing the effect of the active and passive medium on the generated entangled photons

The effects of the lossy mediums are studied in the same way with section 4.1.3. The atmosphere medium is modeled with an array of scattering centers. These scattering centers using QED are modeled with BS depicted in Figure 4.9b. For n^{th} BS, ($c_{a\omega j}$, b_j) is the input, and ($c_{a\omega(n+1)}$, a_{sn}) is the output. Therefore, the output mode continuous form using $|t(\omega)|^2+|r(\omega)|^2 = 1$ is expressed as:

$$\hat{c_a}(\omega) = e^{[\,jKatm-\kappa_{atm}(\omega)]R}\,\hat{c_\omega}(\omega) + j\sqrt{2\kappa_{atm}(\omega)}\int_0^R dz\, e^{[\,jKatm+\kappa_{atm}(\omega)](R-z)}\,\hat{b}(\omega,z) \qquad (4.38)$$

The first part of Eq. 4.38 reveals that the input mode operator is exponentially attenuated because of the scattering agents, and the second part introduces the effect of the noise operator. Using Eq. 4.38 creates the possibility to calculate the modes entanglement between $\mathbf{c_a}(\omega)$, $\mathbf{a_c}$.

In the same way considered for the attenuation medium effect, the QED is used to model the scattering effect. The modeling of the reflection from a typical target is illustrated in Figure 4.9c. From the quantum point of view, the target reflection is defined as the target's atoms scattering. The photons excited thermally in the system have an essential role during the scattering from the target, by this critical factor, the entanglement behavior is severely distorted. To initialize the process, a reflection agent is selected as j^{th} BS, and so the input and output operator continuous form relationship is given as:

$$\hat{c_t}(\omega) = \left\{ t(\omega)e^{[\,jKt\Delta z_t\,]} + 2\kappa_t(\omega)\sqrt{\Delta z_t}\int_0^{z_t} dz\left\{t(\omega)e^{[\,jKt-\kappa_t(\omega)]}\right\}^{(z_t-z)}\right\}\hat{c_a}(\omega) + j\sqrt{\kappa_t(\omega)\Delta z_t}\,e^{[\,jKt-\kappa_t(\omega)]z_t}\,\hat{b_t}(\omega) \qquad (4.39)$$

In this equation, the first term shows the target's dielectric constant imaginary part effect, whereas second part defines the effect of the thermally excited photon. The crucial effect in this

equation is the phase raising because of the photons excited thermally in the second part by which the entanglement between modes is strongly distorted. After analyzing the target reflection, the scattering photons from the target are scattered back in the atmosphere. Thus, it is obligatory to consider the effect of the atmosphere one more time before the signal detection.

So far, the two different quantum radar systems fundamentally emphasizing the generation of the sustainable entanglement between returned mode and the mode kept in the lab are theoretically designed. It is necessary to involve all of the parameters that can affect the correlation between modes, including real medium effect, interaction with the environment, and noises.

Before considering the simulation results of the quantum radar utilizing electro-opto-mechanic and optoelectronic converters and comparing the finding, the last essential task in this study is introduced as radar cross-section calculation. It is very important to complete the radar system. In this dissertation, a novel method is introduced that can be comparable with the quantum radar cross-section (dipole approximation-based method), and also a new numeric-based method is defined to satisfy the proposed theory. In fact, for the aim of RCS calculation, two quantum theories to define the RCS using different methods are investigated. In recent years, "quantum radar cross-section" (QRCS) has been calculated by employing "dipole approximation method", and the results showed that it is possible to improve the interference pattern sidelobe. Thus, it is impossible to attain such a degree of freedom using classical methods. With knowledge of QRCS, the "canonical quantization method" is utilized which is a more complete theory than the "dipole approximation method" to calculate the RCS. A few similarities are found between mentioned methods, but some crucial parameters and factors that had been ignored using the "dipole approximation method" can be considered as the difference between two approaches. The significant difference between the "dipole approximation" and "canonical quantization methods" to calculate RCS are emanated due to the interaction Hamiltonian. For this reason, the focus specifically sat on that point and derive the interaction Hamiltonian with different methods to find the quantitates that have been ignored in the dipole approximation method. Finally, to testify the mentioned point, a new numerical method is accomplished by which RCS is estimated by inserting the quantum theory in "method of moment" (MoM) called "quantum-method of moment" (QMoM).

5. RCS CALCULATION USING QUANTUM APPROACH

In radar applications, predicting RCS of a target with an arbitrary shape is usually taken as a high priority. This task has been investigated by some exact and numerical methods [43-44, 49-50]. The methods commonly utilize the classical procedure to calculate RCS, called CRCS, in which the classical theory analyzes the RCS by calculation of the scattering electromagnetic fields due to the induced current on the target [70]. In essence, RCS is the target's ability to backscatter the radar signal intercepted by it, and other properties of the target, such as its reflectivity, projected cross-section, and directivity, can affect the RCS [46]. The latter expression emphasizes that RCS cannot be defined as the target's geometric area. In other words, RCS, more technically, is a function of the radar position regarding the target, the geometry of the target and its material composition, the operational radar frequency, the polarization of the radar transmitter and receiver [47,48].

For RCS accurately analyzing, the trend has recently been emphasized on the quantum radar [1,18,22] and "quantum electrodynamics theory" to improving the RCS calculation [1,18, 22,68-69]. The calculation of RCS using QED is called quantum RCS (QRCS). It is found that the calculation of the CRCS and QRCS fundamentally differ from each other. QRCS is based on the intercepted photons' field and atoms' field interaction through the "dipole approximation method" [1,22]. In QRCS, the effect of the diffraction and absorption of the target are ignored [70], through which the accuracy of the calculation can be manipulated. Various studies in the literature have discussed why QRCS provides an enhancement of the sidelobe over CRCS [68]. This point has been theoretically shown that QRCS includes a term $|\cos(\theta)|$, while the CRCS contains a term $\cos^2(\theta)$ [68]. The origin of $\cos^2(\theta)$ in CRCS comes from the induced current density decomposition. We will get back to this critical point in the later subsection. Nonetheless, here in this dissertation, the concentration laid on QRCS using "dipole approximation method"; we think that QRCS, maybe, is an incomplete method. This is due to the fact that it employs an approximation procedure for RCS calculation. Following, the aim is to clarify some critical questions: Can one use "dipole approximation method" as a perfect method for RCS calculation? Is there another approach to improving QRCS?. Canonical quantization method [18,72] is used rather than the dipole approximation to answer the questions asked

above. Using that approach, the scattering photons-related wave function is derived, and the results are compared with the wave functions of photons calculated by "dipole approximation method" [68-69]. It is found some main differences between the methods indicating that the RCS calculation can be improved using "canonical quantization method". Also, in the following, to confirm the theory mentioned, a novel numerical method is established in which the quantum theory is merged into the MoM [43, 44] for RCS calculation. In the following, a short introduction is given about the MoM and introduce our new approach.

RCS predicting an arbitrary perfect conductor (PEC) using MoM has been studied in the literature [43, 44]. Through this method (MoM), the integral equation of the electric field is solved. It is clear from MoM approach that the tangential electric field on the PEC surface is zero. Based on the approach, the PEC surface is initially defined by subdomains division such as rectangles or triangles and choosing a suitable basis function and weighting function. Then, the integral is reformed to a simple matrix form. The scattering field can be calculated by solving the matrix containing the unknown coefficients, leading to examining the current density [45]. Then, RCS is calculated through the current density employing. However, a new method is introduced as QMoM. In this method, the current density operator is utilized in MoM (recognizing as QMoM) in contrast to the classical MoM for scattering field calculation. Using the current density operator [69, 72] introduces a few degrees of freedom un-deliberately relinquished in the classic approach employing the current density average. The results are so interesting when QMoM predicts the sidelobe enhancement, which is in agreement with QRCS. Additionally, QMoM shows a main-lobe enhancement has not been estimated and predicted by QRCS calculation. In fact, that result certifies the difference between two discussed methods discussing in the next section.

5.1. Scattering photons wave function theoretically deriving using Canonical quantization method

RCS calculation using two different methods, "dipole approximation" and "canonical quantization", are calculated and compared with the associated results. For this reason, the system schematic is illustrated in Figure 5.1. The procedure is as follows: a wave with intensity I_0 propagates in the atmosphere to the incident upon a target, and the backscattering signals are

detected. The receiving signals from the target are analyzed using two quantum approaches to compare the results. The emphesis is specifically laid on "canonical quantization" method and derive $\Psi_c(\Delta R,t)$ as the scattering photons wavefunction and compare the result with $\Psi_D(\Delta R,t)$ derived using "dipole approximation" method [68, 69].

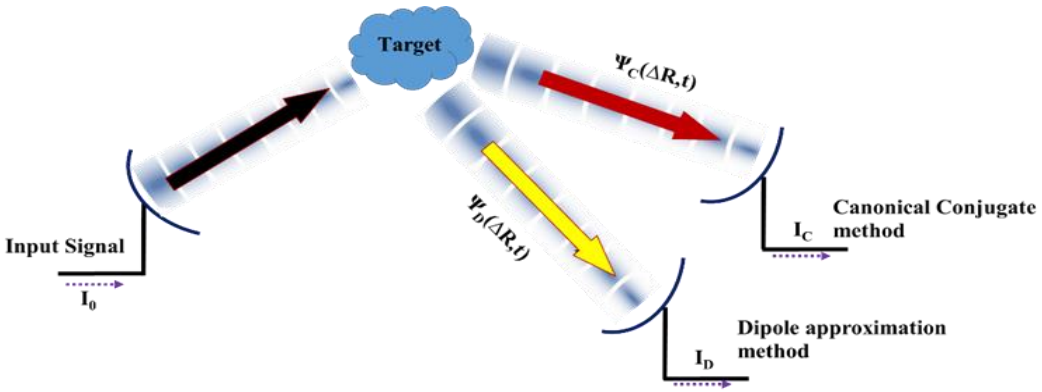

Figure 5.1. A typical schematic of a target excitation by incident photons and detection signals analyzing with two different quantum-based methods canonical quantization method and dipole approximation [51].

Herein, the task is to show the step-by-step derivation of the wave function for a single photon emitting from the target's atom using "canonical quantization" method. The approach starting point is to clarify the interaction Hamiltonian (light-matter interaction). In the canonical quantization method, the matter is assumed as an atomic medium (harmonic polarization field). Thus, the Hamiltonian for the proposed system [51] is given by:

$$H_0 = \varepsilon_0(E^2 + \omega_n^2 A^2)$$
$$H_m = m\omega_m^2 X^2 + \frac{P^2}{m} \quad (5.1)$$
$$H_{\text{int}} = \alpha \frac{AP}{m}$$

In this equation, $\mathbf{H_0}$, $\mathbf{H_m}$, and $\mathbf{H_{int}}$ are the incident field Hamiltonian, atom's field Hamiltonian, and the interaction Hamiltonian, respectively. Moreover, the parameters in the equation m, $\omega_n = 2\pi f_n$, $\omega_m = c/\lambda_m$, and α are the oscillator mass, incident angular wave frequency, matter oscillator angular frequency, and the incident and atom's fields interaction coefficient, respectively. With introducing raising and lowering operators ($\mathbf{a}^+$, $\mathbf{a}$) and ($\mathbf{b}^+$, $\mathbf{b}$) for the incident and polarization fields, respectively, the Hamiltonians expressed in Eq. 5.1 is represented as:

$$H_0 = \hbar\omega_n(a^+ a + \frac{1}{2})$$

$$H_m = \hbar\omega_m(\hat{b}^+ \hat{b} + \frac{1}{2}) \tag{5.2}$$

$$H_{\text{int}} = -\alpha \frac{j\hbar}{2m}\sqrt{\frac{m\omega_m}{\varepsilon_0\omega_n}}(a^+ + a)(\hat{b} - \hat{b}^+)$$

In Eq. 5.2, by dropping the energy non-conserving terms using the "rotating wave approximation" (RWA), the interaction Hamiltonian by involving the different modes is given by:

$$H_{\text{int}} = \frac{j\hbar}{2}\sum_n \sqrt{\frac{\alpha^2}{m\varepsilon_0}\frac{\omega_m}{\omega_n}}(a_n \hat{b}^+ e^{-j[\omega_n t - \vec{k}.\vec{r}]} - a_n{}^+ \hat{b} e^{j[\omega_n t - \vec{k}.\vec{r}]}) \tag{5.3}$$

where the term $\sqrt{(\alpha^2/m/\varepsilon_0)}$ defines the incident and polarization fields interaction rate. The calculation of the wave function of the emitting photon using $<0|\mathbf{E}^+(\boldsymbol{r},t)|\gamma_0>$ emphasizes examining the time evolution of the atom's state interacting with the incident field $|\gamma_0>$. The incident photons interaction state with the atoms is obtained by superposition between the excited state of the atoms when there is no photonic mode and all photonic mode state since the atom remains in the ground state expressed by:

$$|\gamma_0(t)>= C_b(t)|b,0> + \sum_n C_a(t)|a,1_n> \tag{5.4}$$

In Eq. 5.4, C_b and C_a stand the for probability of the atoms finding in state $|b>$ (excited state) without exciting photons and the probability of finding atoms in ground state $|a>$ because of the photonic mode interaction with mode k, respectively. For the state time evolution calculation, Schrödinger equation is used as:

$$\begin{aligned} &|\dot{\gamma_0}(t)>= \frac{-j}{\hbar} H_{\text{int}}|\gamma_0(t)> \\ &\dot{C_b}(t)|b,0> + \sum_n \dot{C_a}(t)|a,1_n> = \sum_n \sqrt{\frac{\alpha^2}{4m\varepsilon_0}\cdot\frac{\omega_m}{\omega_n}}\left\{\sum_n C_a(t)e^{-j[\omega_n t - \vec{k}.\vec{r}]}|b,0> - C_b(t)e^{j[\omega_n t - \vec{k}.\vec{r}]}|a,1_n>\right\} \end{aligned} \tag{5.5}$$

Eq. 5.5 can be re-expressed as a coupled equation with regard to the sweep of incident frequency:

$$\begin{cases} \dot{C_a}(t) = -\sqrt{\dfrac{\alpha^2}{4m\varepsilon_0}\dfrac{\omega_m}{\omega_n}}C_b(t)e^{j[(\omega-\omega_n)t - \vec{k}.\vec{r}]} \\ \dot{C_b}(t) = \displaystyle\sum_n \sqrt{\dfrac{\alpha^2}{4m\varepsilon_0}\dfrac{\omega_m}{\omega_n}}C_a(t)e^{-j[(\omega-\omega_n)t - \vec{k}.\vec{r}]} \end{cases} \tag{5.6}$$

Through integrating each side of the first part of Eq. 5.6 and replacing in the second part, that equation becomes:

$$\dot{C_b}(t) = -\sum_n \frac{\alpha^2}{4m\varepsilon_0}\frac{\omega_m}{\omega_n}\int_0^t dt' C_b(t') e^{j(\omega-\omega_n)(t-t')} \tag{5.7}$$

Due to the modes closely spreading, the summation can be replaced by integration over volume V using Eq. 5.7 is re-introduced as:

$$\dot{C_b}(t) = -\frac{2V}{(2\pi)^3}\int dk^3 \left\{ \frac{\alpha^2}{4m\varepsilon_0}\frac{\omega_m}{\omega_n}\int_0^t dt' C_b(t') e^{j(\omega-\omega_n)(t-t')} \right\} \tag{5.8}$$

where $dk^3=k^2\sin(\theta)dkd\theta d\varphi$, $k = \omega_n/c$, $dk = d\omega_n/c$, and supposing that ω_n can be assumed as a constant in the defined bandwidth; so Eq. 5.8 becomes simplified as:

$$\begin{cases} \dot{C_b}(t) = -\frac{2V}{(2\pi)^3}\int_0^{2\pi} d\varphi \int_0^{\pi} \sin\theta d\theta \int_0^t dt' C_b(t') \left\{ \frac{\alpha^2\omega_m}{4m\varepsilon_0}\int_0^{\infty} \frac{\omega_n^2}{c^2} e^{j(\omega-\omega_n)(t-t')} \frac{d\omega_n}{c\omega_n} \right\} \\ \dot{C_b}(t) = -\frac{2V}{(2\pi)^3} 4\pi \frac{\omega_n}{c^3}\frac{\alpha^2\omega_m}{4m\varepsilon_0}\int_0^t dt' C_b(t')\delta(t'-t) \rightarrow -\frac{2V}{(2\pi)^3} 4\pi \frac{\omega_n}{c^3}\frac{\alpha^2\omega_m}{4m\varepsilon_0} C_b(t) \end{cases} \tag{5.9}$$

From Eq. 5.9, $C_b(t) = \exp[-\Gamma_q t/2]$ where $\Gamma_q = (V/4\pi^2)(\omega_n/c^3)(\omega_m\alpha^2/m\varepsilon_0)$. Then, $C_b(t)$ is substituted into the first part of Eq. 5.6 leading to calculate of $C_a(t)$ by:

$$C_a(t) = -\sqrt{\frac{\alpha^2}{4m\varepsilon_0}\frac{\omega_m}{\omega_n}} e^{-j\vec{k}.\vec{r}} \int_0^t dt' C_b(t) e^{-j[(\omega-\omega_n)+\frac{\Gamma_q}{2}]t'} \tag{5.10}$$

So, one can express $C_a(t)$ in the steady-state condition:

$$C_a(t) = j\sqrt{\frac{\alpha^2}{4m\varepsilon_0}\frac{\omega_m}{\omega_n}} \frac{e^{-j\vec{k}.\vec{r}}}{(\omega-\omega_n)+j\frac{\Gamma_q}{2}} \tag{5.11}$$

Eventually, the state of the incident and polarization fields interaction by ignoring $C_b(t)$ is given as follows:

$$|\gamma_0> = j\sum_n \sqrt{\frac{\alpha^2}{4m\varepsilon_0}\frac{\omega_m}{\omega_n}} \frac{e^{-j\vec{k}.\vec{r}}}{(\omega-\omega_n)+j\frac{\Gamma_q}{2}} |1_n> \tag{5.12}$$

Now, one can calculate the wave function of an emitting photon using “canonical quantization” method. The contributed wave function is derived as [1,68]:

$$\Psi_c(\vec{r},t) = <0|E^+(\vec{r},t)|\gamma_0> = <0|E^+(\vec{r},t)|\ j\sum_n \sqrt{\frac{\alpha^2}{4m\varepsilon_0}\frac{\omega_m}{\omega_n}}\frac{e^{-j\vec{k}.\vec{r}}}{(\omega-\omega_n)+j\frac{\Gamma_q}{2}}|1_n> \qquad (5.13)$$

With substituting the quantized form of $E^+(\boldsymbol{r},t)$ in Eq. 5.13, it can be finalized as:

$$\Psi_c(\vec{r},t) = <0|\ j\sum_{n'} \sqrt{\frac{\hbar\omega_{n'}}{2V\varepsilon_0}}e^{-j(\omega_{n'}t-\vec{k}.\vec{r})}a_{n'}\ j\sum_n \sqrt{\frac{\alpha^2}{4m\varepsilon_0}\frac{\omega_m}{\omega_n}}\frac{e^{-j\vec{k}.\vec{r_0}}}{(\omega-\omega_n)+j\frac{\Gamma_q}{2}}|1_n> \qquad (5.14)$$

After some algebra and applying $n = n'$, Eq. 5.14 can be re-written as the form of:

$$\Psi_c(\vec{r},t) = -\sum_n \sqrt{\frac{\hbar\alpha^2\omega_m}{8V{\varepsilon_0}^2}}\frac{e^{-j\omega_n t}e^{j\vec{k}.(\vec{r}-\vec{r_0})}}{(\omega-\omega_n)+j\frac{\Gamma_q}{2}} \qquad (5.15)$$

Through changing summation to integral and making a few algebraic for the sake of simplification, Eq. 5.15 is re-expressed as:

$$\Psi_c(\vec{r},t) = \frac{-2V}{(2\pi)^3}\int dk^3\sqrt{\frac{\hbar\alpha^2\omega_m}{8V{\varepsilon_0}^2}}\frac{e^{-j\omega_n t}e^{j\vec{k}.(\vec{r}-\vec{r_0})}}{(\omega-\omega_n)+j\frac{\Gamma_q}{2}}\xrightarrow{k=\frac{\omega}{c},k_0=\frac{\omega_n}{c}}$$
$$\frac{-1}{(2\pi)^3}\sqrt{\frac{\hbar\alpha^2\omega_m V}{2{\varepsilon_0}^2}}\int_{-\infty}^{\infty}k^2dk\frac{e^{-j\omega_n t}e^{j\vec{k_0}.(\vec{r}-\vec{r_0})}}{c[(k-k_0)+j\frac{\Gamma_q}{2c}]} \qquad (5.16)$$

The integral in Eq. 5.16 is solved using the Residue method, and the result is expressed by:

$$\Psi_c(\vec{r},t) = \frac{j}{(2\pi)^2}\sqrt{\frac{\hbar\alpha^2\omega_m V}{2{\varepsilon_0}^2}}\frac{{\omega_n}^2}{c^3}e^{-j\omega_n t}e^{j\vec{k_0}.(\vec{r}-\vec{r_0})}e^{\frac{-\Gamma_q}{2}.[\frac{\vec{k_0}.(\vec{r}-\vec{r_0})}{c}-t]} \qquad (5.17)$$

Defining $\eta_c = 0.5\times\Gamma_q[\boldsymbol{k_0}'.(\boldsymbol{r}-\boldsymbol{r_0})/c - t]$, Eq. 5.17 is finalized as:

$$\Psi_c(\vec{r},t) = \frac{j}{2(2\pi)^2}\sqrt{\frac{2\hbar\alpha^2\omega_m V}{{\varepsilon_0}^2}}\frac{{\omega_n}^2}{c^3}e^{-\eta_c-j\omega_n t}e^{j\vec{k_0}.(\vec{r}-\vec{r_0})} \qquad (5.18)$$

As the main goal, one can compare the new emitting photon wave function deriving in Eq. 5.18 with the wave function derived using "dipole approximation" method [68] through:

$$\Psi_d(\vec{r},t) = \frac{j}{2(2\pi)^2}\frac{e}{\varepsilon_0}(\vec{d_{ab}}.\vec{\varepsilon_k})\frac{{\omega_n}^3}{c^3}e^{-\eta_d-j\omega_n t}e^{j\vec{k_0}.(\vec{r}-\vec{r_0})} \qquad (5.19)$$

In Eq. 5.19, the term ($\boldsymbol{d_{ab}}.\ \boldsymbol{\varepsilon_k}$) indicates the coupling between the incident field and dipole operator.

As a usual approach, RCS is calculated for two different quantum approaches as $\sigma_d = \lim_{r\to\infty} 2\pi r\times(I_{sd}/I_0)^2$ and $\sigma_c = \lim_{r\to\infty} 2\pi r\times(I_{sc}/I_0)^2$, where I_{sd} and I_{sc} are the contributed scattering photons

intensity (Figure 5.1). In the following, the difference between two analyzing approaches is studied; for this reason, it needs to analyze $\sigma_c/\sigma_d \sim [\Psi_c(\Delta R,t)/\ \Psi_d(\Delta R,t)]^2$:

$$\frac{\Psi_c(\vec{r},t)}{\Psi_d(\vec{r},t)} = \left\{ \frac{\frac{j}{2(2\pi)^2}\sqrt{\frac{2\hbar\alpha^2\omega_m V}{{\varepsilon_0}^2}}\frac{{\omega_n}^2}{c^3}e^{-\eta_c - j\omega_n t}e^{j\vec{k_0}.(\vec{r}-\vec{r_0})}}{\frac{j}{2(2\pi)^2}\frac{e}{\varepsilon_0}(\overrightarrow{d_{ab}}.\overrightarrow{\varepsilon_k})\frac{{\omega_n}^3}{c^3}e^{-\eta_d - j\omega_n t}e^{j\vec{k_0}.(\vec{r}-\vec{r_0})}} \right\} = \frac{1}{(\overrightarrow{d_{ab}}.\overrightarrow{\varepsilon_k})}\sqrt{\frac{2\hbar\alpha^2\omega_m V}{e^2}}\frac{1}{\omega_n}e^{\eta_d - \eta_c} \qquad (5.20)$$

First of all, in a simple way, one can suppose $\eta_d \sim \eta_c$, and also by assuming the electric dipole momentum $\boldsymbol{d_{ab}.\varepsilon_k}$ as same as α (incident and polarization fields coupling). Applying the assumptions for the above equations, Eq. 5.20 is written as:

$$\frac{\Psi_c(\vec{r},t)}{\Psi_d(\vec{r},t)} \sim \sqrt{\frac{2\hbar V}{e^2}\frac{\omega_m}{{\omega_n}^2}} \qquad (5.21)$$

In this equation, $V = 4\pi {R_r}^3/3$, where R_r is far-field distance defined by $R_r >= 2D^2/\lambda_k$ and D is the largest scatter dimension. Figure 5.2a shows the simulation results; The simulations are accomplished for the incident wave frequency range of 1.5 GHz $<f_k<$ 60 GHz, far-field distance r >= 200 nm, and scattering dimension D ~ 0.1 mm.

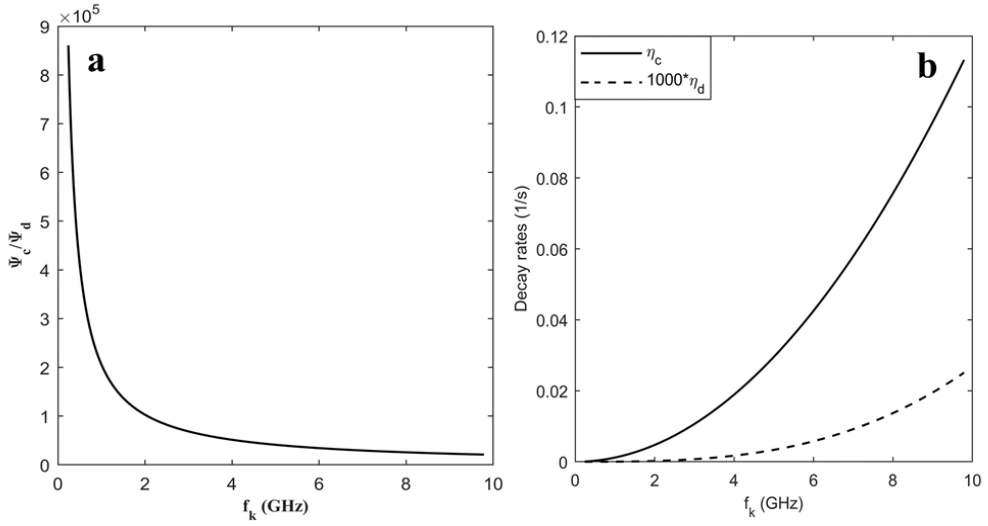

Figure 5.2. a) Comparison between scattering photon wave functions Ψ_d and Ψ_c for $\eta_d \sim \eta_c$ and $\alpha \sim \boldsymbol{d_{ab}.\varepsilon_k}$,b) Comparison between different method decay rates for $\alpha = \boldsymbol{d_{ab}.\varepsilon_k}$

Figure 5.2a shows that the emitting photons calculated via "canonical quantization method" is greater than the "dipole approximation" one in the frequency range less than 2 GHz. It is noteworthy that calculating σ_c/σ_d needs to apply the square power of $[\Psi_c(\Delta \boldsymbol{R},t)/\ \Psi_d(\Delta \boldsymbol{R},t)]$. The

mentioned ratio is dramatically decreased with the increase of the incident frequency. Nonetheless, the result shows the emitting photon calculated by the "canonical quantization method" is approximately ~2×10^5 times greater than the "dipole approximation method" at f_k = 1GHz. The comparison suggests that some critical points, maybe, are ignored as utilizing the dipole approximation method. As an interesting result, Figure 5.2a reveals that RCS main lobe may be enhanced besides the sidelobe. RCS sidelobe enhancement is predicted by QRCS [68-69], while QRCS using the approximated method cannot tell anything about the main lobe. However, for a complete comparison between two quantum-based methods, one needs enough information about Eq. 20. One can initially concentrate on the time constants η_d and η_c in the formula. The comparison between time constants calculated by two different methods is displayed in Figure 5.2b. In this figure, for easy comparison, η_d is multiplied by 1000 because η_d is much less than η_c. Regarding the illustration in Figure 5.2b, η_d and η_c behave in the same way at low frequencies. The results suggest that the decay rates term in Eq. 5.20 could be ignored at a very low frequency. However, η_c becomes dominant by increasing the frequency, meaning that the atom excited state predicting by "canonical quantization method" is decayed sharply rather than the dipole approximation method at RF frequency. Furthermore, for completely analyzing Eq. 5.20, the behavior of $\exp[\eta_d - \eta_c]$ shown in Figure 5.3 should be studied. The simulation results show that $\exp(\eta_d - \eta_c)$ is too close to unity; therefore, the term $\exp[\eta_d - \eta_c]$ can be simply removed in Eq. 5.20 specifically for the frequencies in the range of 0.5~3 GHz.

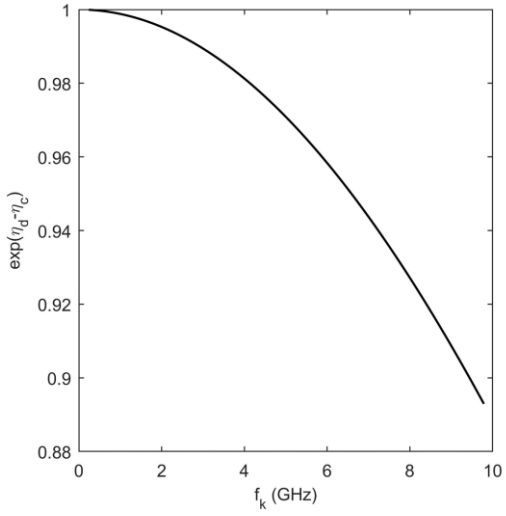

Figure 5.3. Functionality of $\exp[\eta_d - \eta_c]$ vs frequency with the assumption of $\alpha = \boldsymbol{d_{ab}}.\boldsymbol{\varepsilon_k}$

Nonetheless, the main point is the difference between α and $\boldsymbol{d_{ab}.\varepsilon_k}$ that one has to consider to thoroughly compare $\Psi_d(\Delta \boldsymbol{R},t)$ and $\Psi_c(\Delta \boldsymbol{R},t)$. Thus, these two critical terms are considered and study the non-ideal form of $\Psi_c(\Delta \boldsymbol{R},t)$/ $\Psi_d(\Delta \boldsymbol{R},t)$. Semi-classically, $\boldsymbol{d_{ab}}$ is the atom randomly oriented electric dipoles in every direction. For precise analysis, the electric dipole of atoms and also photon's polarization vector are expressed as:

$$\begin{aligned} \overrightarrow{d_{ab}} &= \vec{d} < \sin\xi\cos\zeta, \sin\xi\sin\zeta, \cos\xi > \\ \overrightarrow{\varepsilon_k} &= < \sin\theta\cos\varphi, \sin\theta\sin\varphi, \cos\theta > \end{aligned} \tag{5.22}$$

The spherical coordinates are selected for the presentation in Eq. 5.22. The different azimuth and elevation angles are introduced to distinguish between the direction of the incident photon polarization and atom dipole orientation. In this equation, $\boldsymbol{d_{ab}}$ is the dipole operator of the radial component of the atoms. One can consider a suitable scenario for $\boldsymbol{d_{ab}}$ in which it is supposed a uniform distribution for dipole direction, and therefore each atom has the same average value. Thus, in a common way, the mean($|\boldsymbol{d_{ab}.\varepsilon_k}|^2$) can be used rather than $\sum_{i=1}^{N} |\boldsymbol{d_{ab}.\varepsilon_k}|^2$. Considering the scenario mentioned above, the dipole operator coupling with the photon's polarization can be approximated by a constant regarding the second scenario. After the dipole momentum analyzing α should be expressed in terms of atom's transition momentum. If one defines $\boldsymbol{d_{ab}.\varepsilon_k}$ as a constant, the coupling factor of the atom-field is given by [73]:

$$g_d = \varsigma \frac{|E|}{\hbar} \tag{5.23}$$

In this equation, ς is the transition momentum of an atom equal to the mean value e.($\boldsymbol{d_{ab}.\varepsilon_k}$). Therefore, the atoms eigenstates are shifted by $\hbar g_d$. In this relation, ς is an atom characteristic depending only on the wave function of the electronic states. Also, g_d has a strong functionality of the incident field. It is a critical point to focus on it to relate the coupling constant of "canonical quantization method" to the "dipole approximation" method's characteristics constant. It is obvious from the "canonical quantization method" that the term $\sqrt{(\alpha^2/m/\varepsilon_0)}$ indicates the incident and polarization fields interaction rate. Finally, by substituting the interaction rate in Eq. 5.23, α can be figured out as:

$$\sqrt{\frac{\alpha^2}{m\varepsilon_0}} = \varsigma \frac{|E|}{\hbar} \rightarrow \alpha = \varsigma \sqrt{\frac{m\omega_n}{2\hbar V}} \tag{5.24}$$

Eq. 5.24 shows a clear dependency of ς to α and. Now, one can replace Eq. 5.24 in Eq. 5.20 with exactly $\Psi_d(\Delta \boldsymbol{R},t)$ and $\Psi_c(\Delta \boldsymbol{R},t)$. The results of the analysis for non-ideal form are shown in Figure

5.4. For instance, at a frequency around 2 GHz, $\Psi_c = 40\Psi_d$ concluding to $\sigma_c \sim 1600\sigma_d$. This point shows a larger RCS predicted by the "canonical quantization method" than the "dipole approximation method". Additionally, it is understandable from the figure that the exponential term in Eq. 5.20 has an ignorable impact at the RF frequency range. The results demonstrated above show that RCS calculation through the "canonical quantization method" is strongly enhanced. It is attributed to the different coupling factors that the two quantum-based methods introduce.

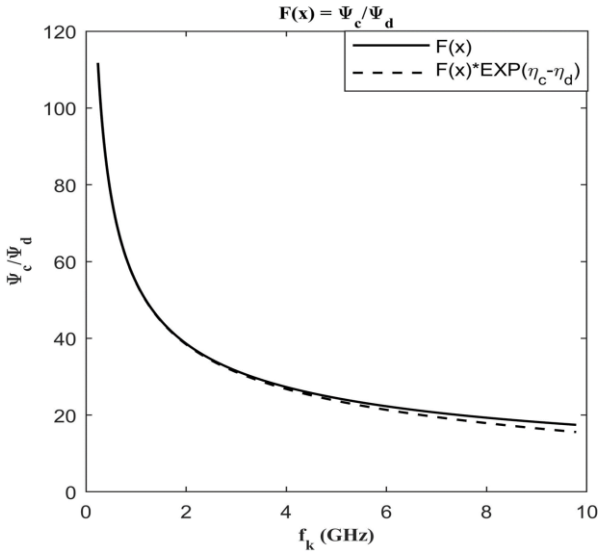

Figure 5.4. Comparison between scattering photon wave functions Ψ_d and Ψ_c; bold: $\eta_d = \eta_c$, dashed: $\eta_d \neq \eta_c$

Also, the relationship $\sigma_c/\sigma_d \sim [\Psi_c(\Delta \boldsymbol{R},t)/\ \Psi_d(\Delta \boldsymbol{R},t)]^2$ reveals the amplitude of the emitting photons as a key factor that RCS severely depends on it. The result $\sigma_c >> \sigma_d$ is easily deduced from $\Psi_c(\Delta \boldsymbol{R},t) > \Psi_d(\Delta \boldsymbol{R},t)$, meaning that RCS estimated by the "canonical quantization method" is strongly enhanced.

So far, it is theoretically derived that the "canonical quantization method" results in the amplitude of the emitting photon greater than the "dipole approximation method". The simulation results demonstrate a few crucial differences between two quantum-based methods. Accepting this point means that the QRCS prediction may be incomplete [1, 68]. In other words, QRCS, maybe, could not forecast the enhancement of the main lobe amplitude as same as the side-lobe. In the following, a new method is accomplished to analyze RCS by the quantum

approach merging in the "Method of Moment" called QMoM. MoM uses the current density operator to calculate the field scattering from the target to study RCS. It is found that using the current density operator [28,47] in QMoM rather than the average current density gives more degree of freedoms ignored in CRCS [70]. It is possible to demonstrate using QMoM that the dipole approximation is not a complete method to calculate RCS.

5.2 The emerging quantum approach in "Method of Moment" for RCS calculation

By illuminating a PEC with an incident field, the incident and scattering fields eventuate the total field. The scattering field includes reflecting, diffracting, and the surface wave components. For initializing MoM approach, one usually uses the principle of "Huygens's equivalence" [74], where the outside medium parameters are replaced with the object ones and then employ the current densities of the equivalent fields (electric and magnetic) on the surface. Because of PEC assumption, the tangential component of $E_{tangential}$ equals zero on PEC surface, resulting in $M_s = 0$. Eventually, J_s is only the parameter that produces the scattering fields. Therefore, we just concentrate on the boundary where $E_{tangential} = 0$; it concludes $\boldsymbol{n}\times(\boldsymbol{E}^{s}_{\text{due to Js}} + \boldsymbol{E}^{i}) = 0$. To complete the approach, Maxwell's equations should be expressed in terms of E^s involving the integration of J_s leading to a Fredholm integral equation. The Fredholm integral equation is generally described as:

$$\vec{E}_z = -\frac{k\eta}{4}\int_{c'} dl' \left\{ \vec{J_z}(\vec{r}\,')H_0^{(2)}(k\,|\,\vec{r}-\vec{r}\,'\,|) \right\} \tag{5.25}$$

where $H_0^{(2)}$ is the second kind of Hankel function with zeroth-order and $\boldsymbol{E_z}$ is the electric field and arisen due to $\boldsymbol{J_z} = I\times\delta(\boldsymbol{r}\text{-}\boldsymbol{r'})$, and $k^2 = \omega^2\mu\varepsilon$. Also, I is the current amplitude, and $(\boldsymbol{r}\text{-}\boldsymbol{r'})$ denotes the distance between source and observation points in space. To apply the MoM approach, it is necessary to re-express Helmholtz as a Fredholm integral form. Then, applying the boundary condition of the tangential field is a necessary case. In other words, if the observation point is moved on the PEC surface and apply the boundary condition, it leads to $\boldsymbol{E_z^s} + \boldsymbol{E_z^i} = 0$ on the PEC surface. Thus, for observation point r on the PEC surface, the 1st kind Fredholm integral equation is expressed as:

$$\frac{k\eta}{4}\int_{c'} dl' \left\{ \vec{J_z}(\vec{r}\,')H_0^{(2)}(k\,|\,\vec{r}-\vec{r}\,'\,|) \right\} = \vec{E_z}^{i}(\vec{r}) \tag{5.26}$$

where $\boldsymbol{J_z(r)}$ is the unknown quantity and $\boldsymbol{E_z^i(r)}$ is the known defined in this study as $\boldsymbol{E_z^i(r)} = e^{-j\boldsymbol{k}.\boldsymbol{r}}$. After that, one can use the traditional MoM approach to calculate $\boldsymbol{J_z(r)}$. However, we don't

follow the classical approach, and instead, $\mathbf{J_z(r)}$ is initially expressed as the current density operator in terms of the quantum state and substitute it into the classical MoM, and then calculate the parameters. The electrons as quantum particles produce current due to their motion. From the quantum point of view, the form of the wave function that describes the state of the particle (electron or photon) defines the associated currents. Therefore, one can define quantum operators to determine the current. It is the quantum motion of the charge that handles charge current, and that motion is probabilistic in quantum mechanics. The main idea is to find a probability current when a wave function satisfies the Schrödinger equation based on the related Hamiltonian [16,17]. For an electron, the related electrical charge density, ρ_e, should satisfy the continuity equation to conserve the charge. It is formulated for an electron as:

$$\frac{\partial \rho_e(\vec{r})}{\partial t} = -\nabla . \vec{j}(\vec{r}) \tag{5.27}$$

where r denotes position. Based on the "Schrödinger equation" $j\hbar(\partial\Psi/\partial t) = \hat{H}\Psi$, where $\hbar$ and $\hat{H}$ are the Planck's constant and Hamiltonian, the wave function $\Psi(r,t)$ is an energy eigenstate of the Hamiltonian. Moreover, the squared wave function gives the density of probability as $\rho_e = e|\Psi|^2$, where e is the electron charge. By substituting ρ_e into Eq. 5.27, it becomes [69, 72]:

$$-\nabla . \vec{j}(\vec{r}) = e\frac{\partial |\psi|^2}{\partial t} = e\left\{\frac{1}{j\hbar}\left[\psi^*(H\psi) - (H\psi)^*\psi\right]\right\} \tag{5.28}$$

Using the nonrelativistic Hamiltonian as $\hat{H} = (1/2m)\,[p - e\boldsymbol{A}(\boldsymbol{r},t)/c]^2 + e\varphi(\boldsymbol{r},t)$, where m, c, $\mathbf{p}$, $\boldsymbol{A}$, and φ are quantum particle with mass m, speed of light, momentum operator, vector potential, and scaler potential, respectively. The bold alphabets are used to denote the operator. In the Hamiltonian defined above, the vector potential $\boldsymbol{A}$ and φ seem to be real because they describe the real electric and magnetic field. To simplify the calculation, it defines a new operator called kinetic operator as $\boldsymbol{\pi} = \mathbf{p} - e\boldsymbol{A}(\boldsymbol{r},t)/c$. From quantum mechanics, the momentum operator is defined as $\mathbf{p} = j\hbar\nabla$, then the new operator re-expressed as: $\boldsymbol{\pi} = j\hbar[\nabla - j(e\boldsymbol{A}(\boldsymbol{r},t)/\hbar c)]$. By substituting $\hat{H}$ in Eq. 5.28, it can be re-introduced as [69, 72]:

$$-\nabla . \vec{j}(r) = \frac{e}{j\hbar}.\frac{(-j\hbar)^2}{2m}\left\{\psi^*[(\nabla - j\frac{e\vec{A}}{\hbar c})^2\psi] - [(\nabla + j\frac{e\vec{A}}{\hbar c})^2\psi^*]\psi\right\} \tag{5.29}$$

From Eq. 5.29, one can derivate the momentum current and gauge current density. The former one depends on ∇^2, while the latter one depends on $-j(\nabla(e\boldsymbol{A}(\boldsymbol{r},t)/\hbar c) - (e\boldsymbol{A}(\boldsymbol{r},t)/\hbar c)\nabla)$. In this

study, for simplicity, the momentum current density is just considered and ignore the other. The momentum current density is given by:

$$-\nabla.\vec{j}(\vec{r}) = \frac{e}{j\hbar}.\frac{(-j\hbar)^2}{2m}\{\psi^*(\nabla^2\psi)-(\nabla^2\psi^*)\psi\} \rightarrow \frac{je\hbar}{2m}\nabla.\{\psi^*(\nabla\psi)-(\nabla\psi^*)\psi\}$$
$$j(\vec{r}) = -\frac{je\hbar}{2m}\{\psi^*(\nabla\psi)-(\nabla\psi^*)\psi\} \xrightarrow{p=-j\hbar\nabla} j(\vec{r}) = \frac{e}{m}\mathrm{Re}\{\psi^* p\psi\} \quad (5.30)$$

Using Eq. 5.30, the classical MoM approach is modified based on the density current operator substituted rather than the current average. With replacing the current density average with the current operator, Eq. 5.26 is re-expressed as:

$$\frac{k\eta}{4}\int_{c'} dl' \left\{\frac{e}{m}\mathrm{Re}[\psi^* p\psi]H_0^{(2)}(k|\vec{r}-\vec{r}'|)\right\} = \overrightarrow{E_z^i}(\vec{r}) \quad (5.31)$$

where $\Psi(\boldsymbol{r})$ can be generally defined as $\Phi(r)e^{(j\boldsymbol{k}.\boldsymbol{r})}$. Eq. 5.31 shows the quantum effect in the Fredholm integral in which the momentum operator is initially applied on quantum wave function and then times to conjugate of the same quantum wave function. Finally, the real part of the result is taken into account. According to the MoM approach, it needs to present $\Phi(\boldsymbol{r})$ as a weighted sum of the basic functions $\Phi(\boldsymbol{r},t) = \sum_{n=1}^{N} C_n F_n(\boldsymbol{r})$, where $F_n(\boldsymbol{r})$ is a basis function and C_n is an unknown quantity used to calculate the current density. By substituting the expanded form of $\Psi(\boldsymbol{r},t)$ in Eq. 5.31, the final version of the equation becomes:

$$\sum_{n=1}^{N}|C_n|^2\frac{k\eta}{4}.\frac{e\hbar k}{m}\int_{\Delta C'_n} dl'\left\{|F_n(\vec{r}')|^2\, H_0^{(2)}(k|\vec{r}-\vec{r}'|)\right\} = \overrightarrow{E_z^i}(\vec{r}), \quad (5.32)$$
$$F_n(\vec{r}') = \begin{cases} \dfrac{\sin(\vec{k}.\vec{r}')}{\sin(k\Delta C'_n)} & \vec{r}' \in \Delta C'_n \\ 0 & elsewhere \end{cases}$$

where ΔC_n is the length of line segmentation usually approximated by $\Delta C_n <= \lambda/10$. Choosing Delta Dirac function as a weighting function $w_i(r_i) = \delta(\boldsymbol{r}-\boldsymbol{r_i})$, Eq. 5.32 is re-formed as:

$$\sum_{n=1}^{N}|C_n|^2\frac{k\eta}{4}.\frac{e\hbar k}{m}\int_{\Delta C'_n} dl'\left\{|F_n(\vec{r}')|^2\, H_0^{(2)}(k|\vec{r}_i-\vec{r}'|)\right\} = \overrightarrow{E_z^i}(\vec{r}_i), \quad (5.33)$$

Eq. 5.33 is the new version (called QMoM) of the MoM presented in the classical picture in Eq. 5.26. From Eq. 5.33, N equations are established for the considered weight function. With N×N matrix construction as $[A]_{nn}[C_n]_{n1} = [bj]_{n1}$, C_n are calculated and with replacing in $\Phi(\boldsymbol{r},t) = \sum_{n=1}^{N} C_n F_n(\boldsymbol{r})$, the current density is estimated. Solving unknown coefficients J_z distribution using

the matrix system, the scattered field is calculated using Eq. 5.25 to RCS estimation. In fact, the same approach is used to analyze the RCS through the newly established numerical method.

In the following part, the simulation results of the quantum radar employing different converters such as opto-mechanic, optoelectronic, and also the results associated with the QRCS are presented.

6. RESULTS AND DISCUSSIONS

The quantum radar analyzed and designed in the latter part is simulated employing both electro-opto-mechanical and optoelectronic converter, and also the results of the QRCS will be presented and discussed.

6.1. Quantum radar utilizing Electro-Opto-mechanical converter

Since mentioned earlier, preserving the entanglement between the photons before detection and the optical photons kept in the lab (retained and returned modes) is the primary purpose of this study. Thus, it is necessary to study the non-classicality of the modes in quantum radar illustrated step-by-step in Figure 3.1. The designed converter simulation is done based on data in Table. 1. Firstly, the simulation results of the intra-cavity modes are illustrated in Figure 6.1 and Figure 6.2. Figure 6.1 demonstrates the entanglement between the considered modes around $\Delta\omega/\omega \sim 0$ as system uses opto-mechanical converter (λ_c = 808 nm, m = 18 ng, γ_m = 120 1/s). It reveals that if the entanglement is created between microwave cavity and optical cavity photons, then it has a necessary condition to transmitting the MC output photons in the atmosphere.

Table 1. Parameters of quantum radar's opto-mechanical converter operating at L-band (1.5 GHz) [12, 19, 23]

α_c	[0. 025-0.26]
λ_c	808×10^{-9} m
γ_m	120 Hz
m	[18-22] $\times10^{-9}$ g
L	15×10^{-12} H
κ_c	$[0.01\omega_m\text{-}0.03\omega_m]$
κ_ω	$[0.01\omega_m\text{-}0.03\omega_m]$
ω_m	$2\pi\times10^{6}$ Hz
$C(x_0)$	590×10^{-12} F
C_d	20×10^{-12} F
P_c	30×10^{-3} W

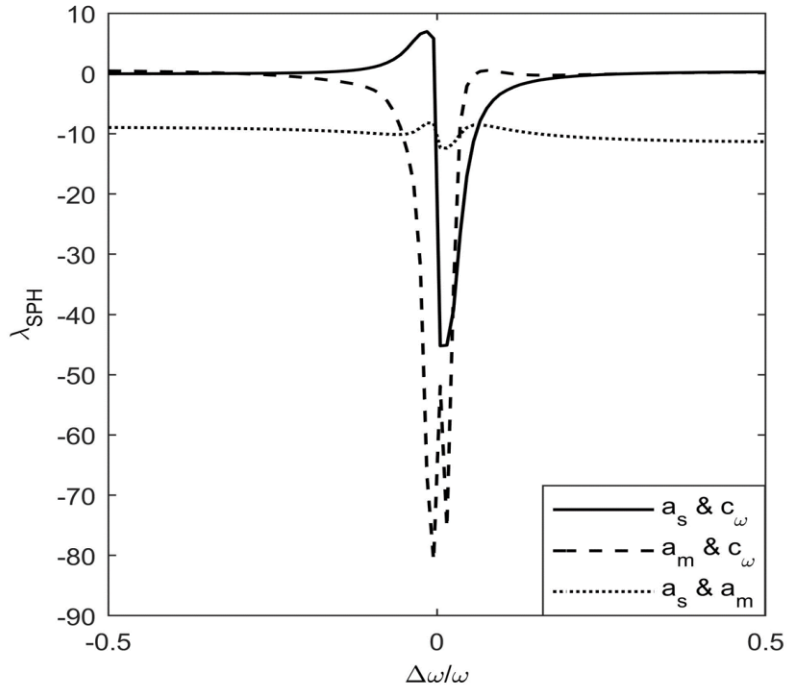

Figure 6.1. λ_{SPH} vs. $\Delta\omega/\omega$, cavities modes entanglement at T = 200 mK.

For a quantum radar application, it is necessary to investigate some critical parameters influencing on the cavity modes entanglement to improve the converter performance. The effect of the designed opto-mechanical crucial parameters as the damping rate of MR, the operational temperature, and incident wavelength to excite the OC are explored on the entanglement of the cavity modes. The operational temperature effect of the opto-mechanical converter (i.e., temperature that the converter system works with) is shown in Figure 6.2a. It is clear that increasing converter operational temperature cause dramatically reducing the modes entanglement. The graphs related to the 200 mK and 300 mK can be seen in detail in an exaggerated inset figure. It is found that the main reason to confine the electro-opto-mechanical converter temperature is MR cavity operational frequency. In this converter, MR modes oscillate around $\omega_m = 2\pi\times10^6$ Hz; from Eq. 4.8, it is clear that the high noise is dominant at a relatively low frequency. Therefore, it is found that the MR system is a critical case that dominantly confines the tripartite system to operate at high temperatures. In fact, it was considered as a factor to improve our design in the optoelectronic-based quantum radar based on removing the MR subsystem. Of course, some different approaches are used to solve the problem. One of the

suggesting methods is engineering the frequency bandwidth [21, 22] and the other method is MR substituting with the optoelectronic device operating at high frequency [12, 23]. However, since the MR subsystem is used in the quantum illumination system, it enforced to confine the operational temperature below 1200 mK to preserve the entanglement. Additionally, the other critical factor is excitation source wavelength that can affect the entanglement. As shown in Figure 6.2b, incident wave wavelength changing leads to a change of the entanglement. This figure again proves that at high frequency, the effect of environmental noise is negligible. So, by increasing the wavelength up to 808 nm, the graph shows a tendency toward modes separability. It is attributed to the effect of the thermally excited noise on output modes entanglement. Also, in Figure 6.2c, the effect of the MR damping rate is investigated on the OC and MC cavity modes, and the result reveals that the more increase in damping rate leads the more increase in the separability of the modes. This is related to the OC and MC cavities coupling, and this factor is effectively manipulated by MR damping rate. To profoundly understanding the point, one can consider the result illustrated in Figure 6.2d. This figure clearly shows that MR damping rate increasing causes to kill the entanglement which is due to the decrease of the coupling between MR and OC cavities.

Up to now, the entanglement between modes of the opto-mechanical converter is just noticed. Following the external medium, effects are considered, and their effects are applied on the entanglement between modes transmitting through the mediums. We again come back to the figure illustrated in Figure 3.1 for entanglement property studying. The general data for all simulation in this section are listed as "T = 200 mK, R = 10 km, λ_c = 808 nm, m = 18 ng, γ_m = 120 1/s, κ_a = 8.7 1/m, $\kappa_{atm} = 5.2\times10^{-7}$ 1/m, κ_t = 18.2 1/m". First of all, quantum radar operation emphasizes studying the OC and MC modes entanglement illustrated in Figure 6.3a. Subsequently, the system uses an active medium to amplify the MC modes. Figure 6.3b (solid line) shows the entanglement distortion by the active medium effect. It is contributed to the real medium effect to increasing the entanglement fragility. In other words, any real medium can strongly affect the non-classicality of the modes, whereas an active medium has been classically used to amplify the signals but not to boost the entanglement. In other words, the active medium amplifies the signals; nonetheless, the intensification of entangled photons remains critical. Sequentially, the lossy medium effect is investigated, and the result is depicted in Figure 6.3b.

Comparison between results (solid- and dashed-lines) indicates that the modes separability are dramatically increased due to the attenuation medium. Therefore, one can conclude that the different parameters of the attenuation medium, such as (temperature, pressure, and so on) [30], which are not controllable, can easily kill the quantum property considered an essential factor for a quantum radar. It should be noted that there are no controls (i.e., degrees of freedom) on the atmosphere and its effect on modes, whereas, in the previous step, one could engineer, for example, the active medium length and materials to manipulate the effects. It indicates that one should focus on the tripartite and active medium subsystems to create some robust signals. Finally, the scattering effect from a target is studied. A completely flat target madding Aluminum is used. The simulation result is shown in Figure 6.3c. The reflected signal's amplitude is dramatically decreased due to the target material attenuation factor. However, the output modes remain slightly entangled around $\Delta\omega/\omega \sim 0$. Nonetheless, it is predictable that a target with different materials and shapes can distort the modes entanglement. It means that RCS affecting parameters can distort the entanglement in the quantum radar.

In the following, the signals reflecting from the target experience the influence of the attenuation medium one more time, and then the modes are intensified before returning signal detection. The mentioned effects are depicted in Figure 6.3d. It is clearly shown the entanglement between returned and retained modes before the detection. That is an impressive achievement the study is expecting for it. It is noteworthy to mention that the results were attained for the ideal conditions. Therefore, for a better examination, it should apply some actual conditions and then evaluate the performance of the design.

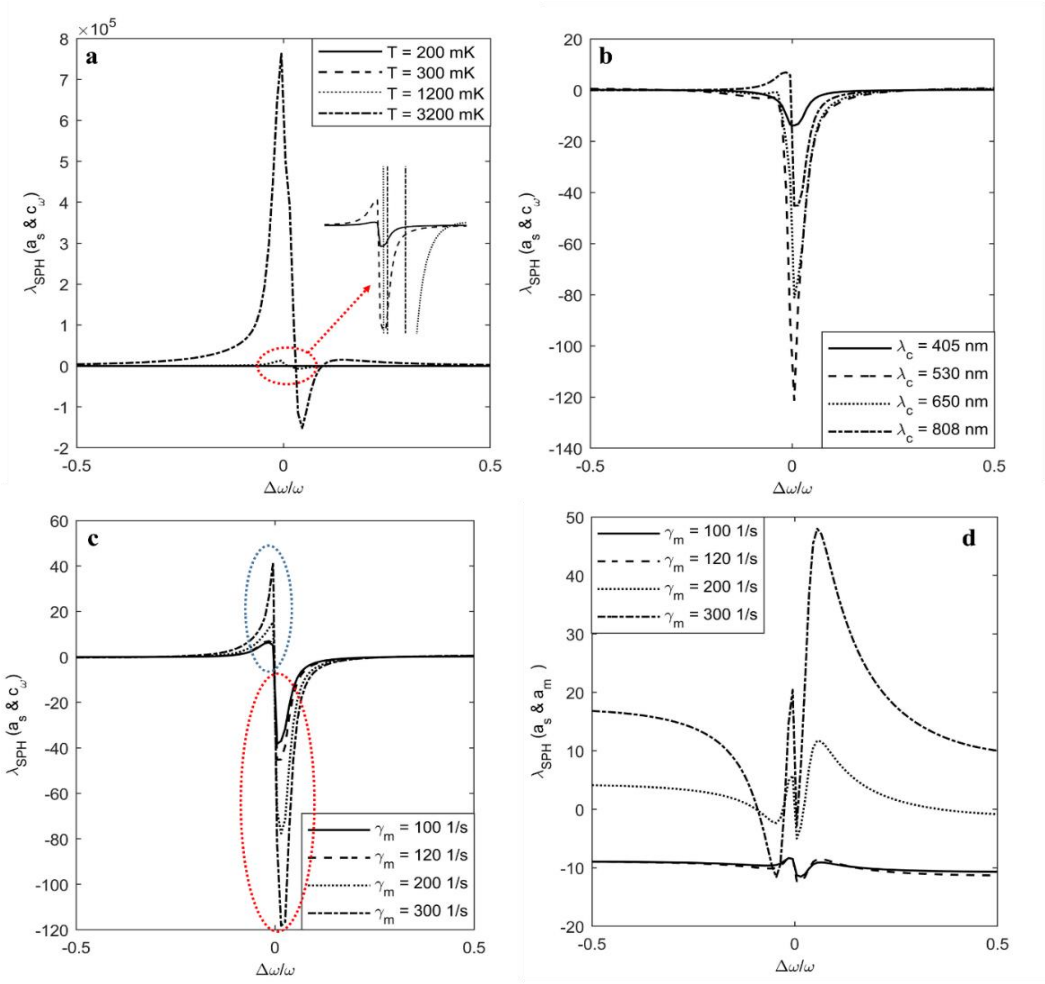

Figure 6.2. λ_{SPH} vs. $\Delta\omega/\omega$, OC and MC modes entanglement (a) Temperature effect and (b) incident source wavelength effect, and (c), (d) study of the effect of the MR damping rate.

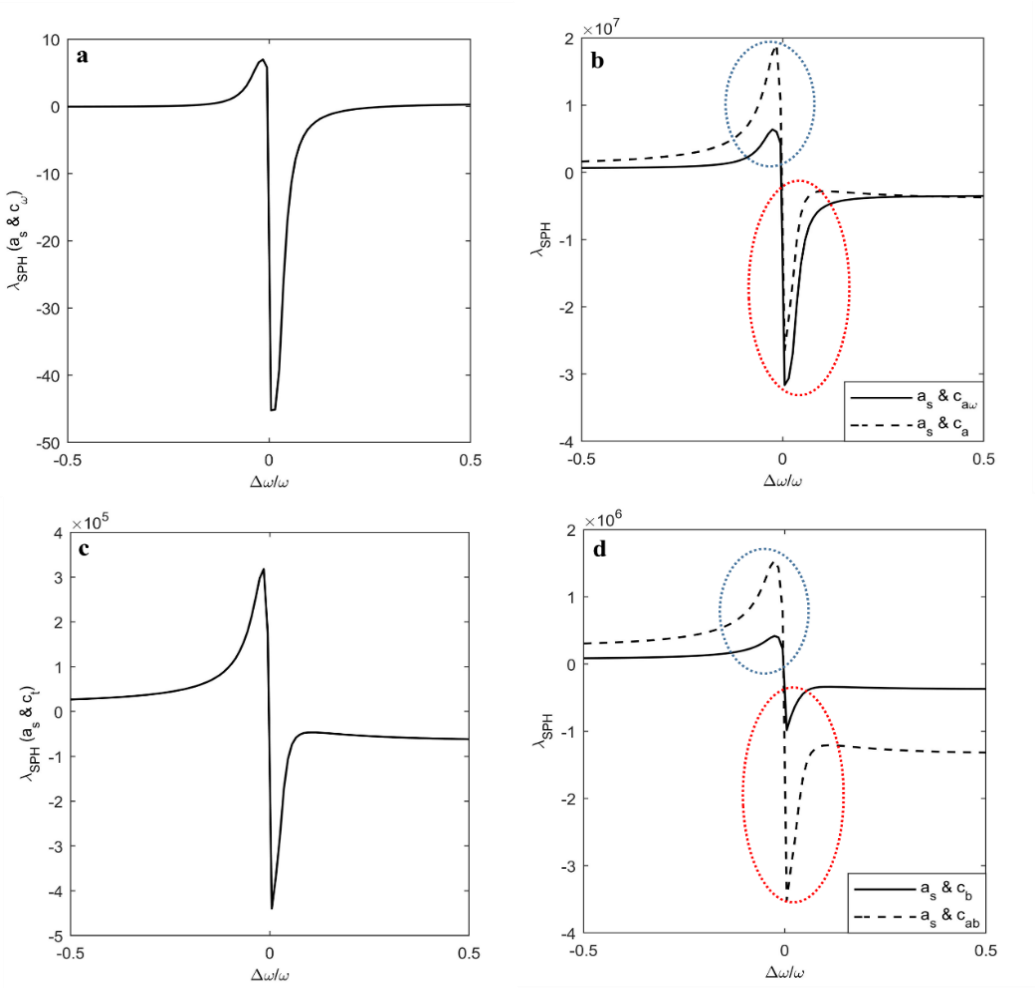

Figure 6.3. λ_{SPH} vs. $\Delta\omega/\omega$ for different modes entanglement at different level of a typical quantum radar at R = 100 km.

So far, it is supposed that the C_s and q_s in Eq. 4.5 were real and studied the system for an ideal condition. It seems a sufficient assumption regarding the section of the phase references [19]. Nevertheless, it is necessary to apply the dielectric constant imaginary part effect as a critical parameter affecting a real system design. Thus, the constants C_s and q_s are supposed as the complex numbers. The entanglement created mainly around $\Delta\omega/\omega \sim 0$ is shown in Figure 6.4a. Also, the resonance at some off-detuning frequencies is shown. As a predictable case, the result illustrated in Figure 6.4a demonstrates a difference in comparison with Figure 6.3a. It is due to the effect of the imaginary part of C_s and q_s ignored in the previous section. As the next step in quantum radar, the entangled photons have to experience some steps as follows: amplification by an active medium, propagation through a lossy channel as atmosphere, reflection from a target,

backscattering into the atmosphere again, and then amplification before detection (Figure 6.4b). Also, the constants C_s and q_s are supposed to be complex. From Figure 5.8b, the microcavity signals entangled with OC modes are intensified, indicating with solid black-line in the figure showing that the entanglement between modes is largely killed due to the medium effect. Also, the microwave photons started to strongly oscillation at $\Delta\omega/\omega \neq 0$. This indicates that the active medium severely distorts the correlation between modes; nevertheless, it helps to intensify the level of the signals to avoid the background noises. After that, the entanglement behavior of the modes is distorted because of the attenuation medium effect, and this is indicated with a dashed black-line in the figure. In other words, lots of propagating photons lose non-classicality due to the real medium effect. Then the attenuation medium output photons interact with a target causing to kill some more reflecting photons (dotted black-line). For better presentation, the important section of the figure is exaggerated and indicated with a red-dashed arrow. The back-scattering signal oscillation with minute amplitude is interesting to note about it. Finally, the returned photons before detection are indicated with the blue line in the graph. There is a slight similarity between the blue-colored signals (returned signals) with the transmitting signal (solid black-line). This is contributed to the target reflection effect and also the impact of the attenuation medium factors, including the length of the atmosphere and attenuation factor of the medium on the signal. Thus, to know how a real medium such as the atmosphere can affect the entanglement, some simulations are accomplished and the results completely analyze the effect. The atmosphere channel effect on the entanglement is investigated, and Figure 6.4 and Figure 6.5 demonstrate the results. In Figure 6.5, the channel length is decreased to 10 km. The result shows that the entanglement (blue-color graph) is preserved even if κ_{atm} is drastically increased. For better illustration, one can consider an inset figure depicted on the right-hand side of Figure 6.5. This figure clearly demonstrates the reflecting signals (dotted-line), propagating signal (dashed-dotted line), and intensifying signal (blue solid-line) before detection.

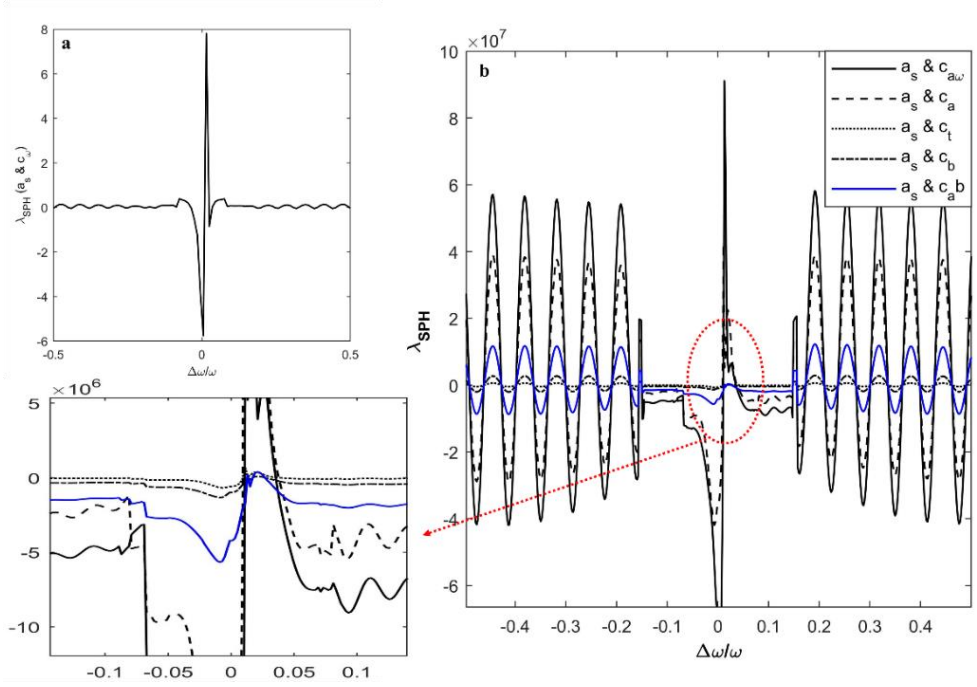

Figure 6.4. λ_{SPH} vs. $\Delta\omega/\omega$, entanglement between modes at different level of a typical quantum radar for κ_a = 10.7 1/m, $\kappa_{atm} = 20\times10^{-7}$ 1/m, R = 100 km.

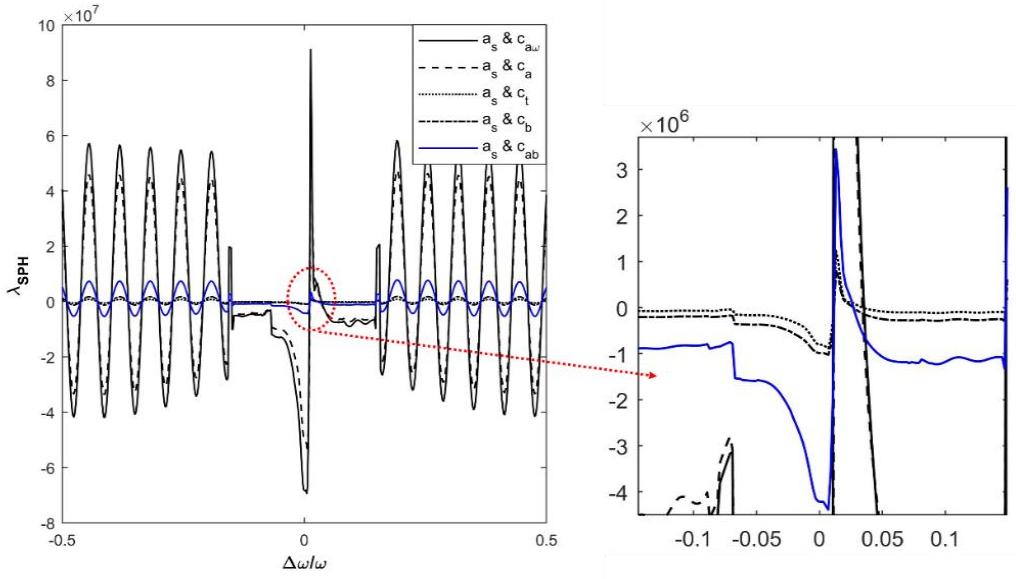

Figure 6.5. λ_{SPH} vs. $\Delta\omega/\omega$, entanglement between modes at different level of a typical quantum radar for κ_a = 10.7 1/m, $\kappa_{atm} = 100\times10^{-7}$ 1/m.

To confirm the points mentioned above, a few other simulations are accomplished with different temperatures at 500 mK (Figure 6.6) and 1500 mK (Figure 6.7). At each figure, the entanglement behavior is dramatically changed at on-detuning frequencies as compared to Figure 6.5. Those figures also demonstrate a separable state at off-detuning frequencies. Nonetheless, it is forcing to focus on a very narrow band of frequency around on-detuning frequencies $\Delta\omega/\omega \sim 0$ to effectively preserve the entanglement. Fortunately, the results are appeared to be so different close to the on-detuning region shown in Figure 6.6 and Figure 6.7. The effect of different mediums on the entanglement is clearly demonstrated in inset figures. The results indicate that temperature increasing up to 1500 mK leads to a slight deformation of the detecting signal (solid blue-line) because of the medium effects; however, the entanglement between modes is still slightly maintained. Also, it is shown that the incident photons mostly missed the related entanglement, meaning that it has to be to consider only the classical correlation among photons after entanglement's miss. The latter conclusion suggests that the entangled transmitting photons will be largely killed in a real system. This can be because of the uncontrollable atmospheric conditions, target shape effect, target material type effect, incident angle, target's reflection and diffraction angles, the noise effect of the receiver and transmitter, and the idler photons degradations. In order words, in a real system, many parameters can distort the entanglement between photons. Of course, it should be noted that the fragility of the entangled photons is the main reason which makes the photons so vulnerable to the real medium effects. That is why quantum radar design is so challenging than the classical radar system. In the classical radar, the main point is to keep the signal-to-noise ratio high, acceptable level, while in the quantum radar system, besides that, we should pay special attention to the correlation between the received photons. Another challenging point about the quantum radar is that one has to just focus on the tripartite system and active medium to make a robust entanglement, while other real mediums are not accessible either to manipulate or to control, rather than they originally disturb the correlation between photons. In the latter part, the effect of the tripartite system is shortly discussed on the entanglement. Also, one examines the effects of the active medium; it is because the active medium is a case that one can manipulate its characteristics to get the best results. It has been concluded that real mediums such as atmosphere and target reflection can strongly distort the "phase estimation errors" and "phase responsivity" [1, 4].

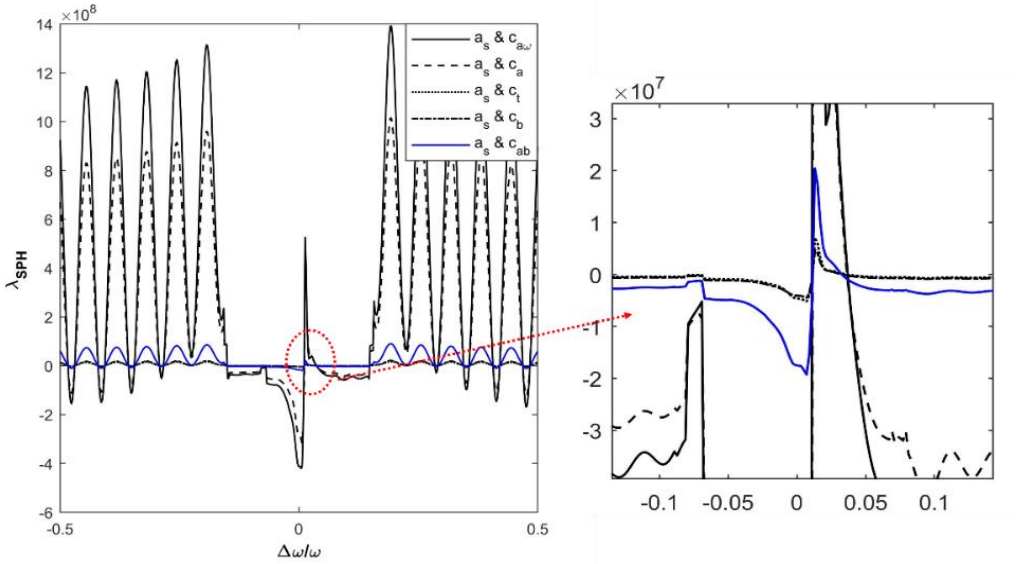

Figure 6.6. λ_{SPH} vs. $\Delta\omega/\omega$, entanglement between modes at different level of a typical quantum radar for T = 500 mK, κ_a = 10.7 1/m, $\kappa_{atm} = 100\times10^{-7}$ 1/m.

From the classical radar operation, it is found that the active medium (transmitter) is an indispensable part of a quantum radar. By ignoring the active medium effect (zero gain), the phase estimation errors can close to the "Heisenberg limit". Nonetheless, the entanglement between modes is strongly affected through nullifying the gain of the active medium; this is a trade-off between entanglement enhancing and approaching the Heisenberg limit. Now, the main question of this study is recalled which is how the entanglement sustainability can be satisfied? To answer the questions, some simulations are conducted and depicted in Figure 6.8. Figure 6.8a shows the entanglement between the opto-mechanical converter cavity modes around $\Delta\omega/\omega \sim 0$. To know about the active medium in quantum radar, the MC output photons are transmitted in the atmosphere without any amplification. First of all, the impact of the transmitting channel is investigated. Figure 6.8b clearly demonstrates the attenuation medium dramatic effect on the entanglement, and also due to that fact, the detected modes (solid-blue) become entirely separable. In fact, most of the transmitted microwave photons entangled with optical cavity photons lose the entanglement. For better understanding, the results of Figure 6.8b with Figure can be compared.

As a significant result, one should note that the simulations in Figure 6.8b clarifies a trade-off existed between the improvement of the estimation errors and entanglement. If one pays particular attention to catch the Heisenberg limit by nullifying the active medium gain, it will effectively lose the entanglement and vice versa. It is a critical point that any quantum radar designer should delicately consider.

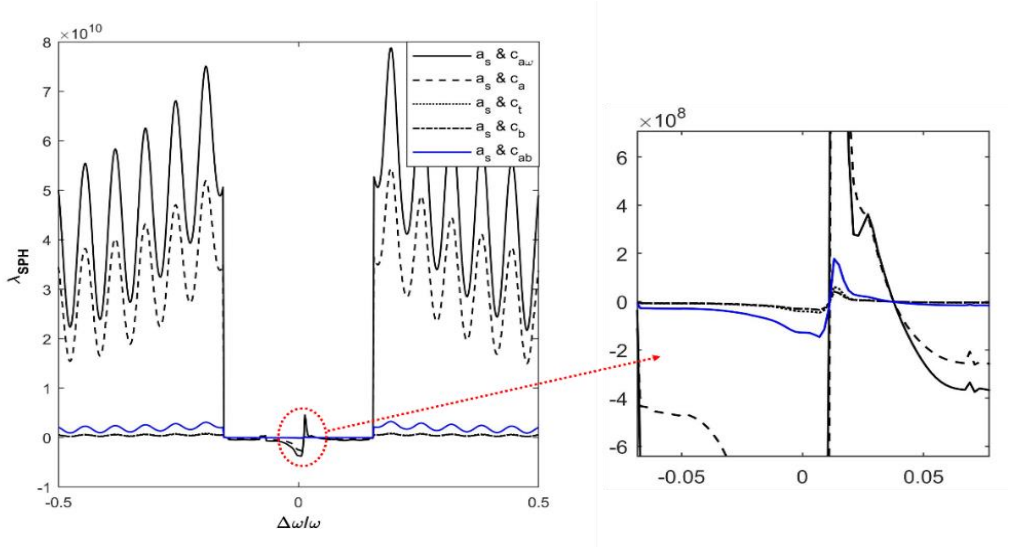

Figure 6.7. λ_{SPH} vs. $\Delta\omega/\omega$, entanglement between modes at different level of a typical quantum radar for T = 1500 mK, κ_a = 10.7 1/m, $\kappa_{atm} = 100\times10^{-7}$ 1/m.

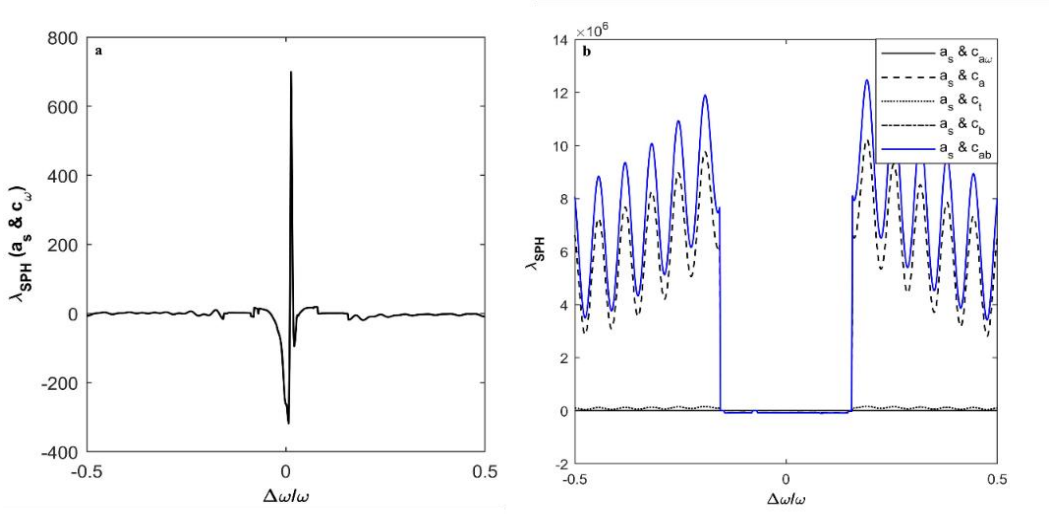

Figure 6.8. λ_{SPH} vs. $\Delta\omega/\omega$, entanglement between modes at different level of a typical quantum radar for T = 1500 mK, κ_a = 0.0 1/m, $\kappa_{atm} = 100\times10^{-7}$ 1/m.

6.2. Optoelectronic based quantum radar

After a discussion about the opto-mechanical based quantum radar results, in this section, the emphasis is laid on the optoelectronic quantum radar. It was shown that MR was a critical subsystem by which some crucial issues arose, and that was why the latter version of the quantum radar couldn't work well. Also, due to that subject, we had to use the active medium to intensify the signals before broadcasting into the atmosphere. Even though using an active medium helps to enhance the signal level, but it, in essence, add some noises to the signals that can disturb the correlation between modes. It means that adding an active medium to the system helps to enhance the signal classically. Nonetheless, it was shown that the backscattering photon's entanglement was completely disturbed without the active medium. Thus, since theoretically demonstrated in section 5.2, the design is completely changed in which the MR subsystem was entirely ignored. Rather than, the optoelectronic-based subsystem is utilized to drive make the optoelectronic quantum radar. In the following, the simulated results associated with that design will be presented.

The data given in Table. 2 used to simulate the typical quantum radar shown in Figure 4.9. Firstly, temperature as one of the critical parameters affecting the operation of the converter modes entanglement is analyzed. The entanglement between cavity modes $\mathbf{a_c}$ and $\mathbf{c_\omega}$ and also the transmitting and receiving modes $\mathbf{a_c}$ and $\mathbf{c_b}$ are examined for MC-PD coupling factor $\mu_c = 0.0002$ and $D_{td} = 20$ m where D_{td} is transmitter-detector distance. Figure 6.1 demonstrates the results of the entanglement between cavity modes (2η) depicting versus the detuning frequency of PD. It is demonstrated in Figure 6.9a that the cavity modes preserve entanglement even though the temperature T_c is increased up to 2500 mK. This is an astonishing result and remarkable compared to Figure 2 of [14] and Figure 2a of [15] that create entanglement between microwave photons at too limited temperatures such as 15 mK and 30 mK, respectively. The mentioned references [14, 15] have used the electro-opto-mechanical converter to produce the entanglement between microwave photons. The electro-opto-mechanical converter problem to operate at high temperatures originates from the mechanical oscillator operating at low frequency. The lower frequency operating results in the higher generating thermally excited photons through which the entanglement is profoundly affected. Since the entangled photons generating by MC are sent in the atmosphere for target detection, one cannot manipulate the atmosphere to subside the lossy medium effect. The lossy medium and target reflection effects are theoretically formulated in

Eqs. 4.38 and 4.39, and also the simulation results are depicted in Figure 6.1b. Regarding theory estimation, the returned field entanglement is completely killed and becomes separable at temperatures such as T_c> 1000 mK. For T_c<~ 500 mK, in contrast, the modes remained entangled, suggesting that the newly designed optoelectronic converter operates well with respect to the latter converter utilizing the mechanical part [14]. The atmosphere and backscattering from the target are uncontrollable manners. Nonetheless, it is possible focus on the design of a suitable converter (Figure 4.9a) operating safely at high temperatures and creating entangled photons. Utilizing a new approach, it seems possible to severely decrease the atmosphere and target scattering harmful effects to partially enhance the entanglement.

Table 2. Parameters for Quantum radar's optoelectronic converter operating at S-band (2.7 GHz) [14-15], [23-27]

v_d	0.1 mV
μ_c	0.0002
m_0	9.109383×10^{-31} Kg
m_{eff}	$0.45m_0$
κ_c	$0.08\omega_{ref}$
κ_ω	$0.02\omega_{ref}$
ω_{ref}	$2\pi\times10^6$ Hz
P_c	30 mW

The coupling factor of MC-PD $g_{\omega p}$ manipulating by μ_c can be considered as a critical factor in designing such a system to operate at high temperatures. An important note about this factor $g_{\omega p}$ is that it can be controlled by different parameters in the system such as d, m_{eff}, $\omega_{\omega,}$ and ω_{eg}. Some simulations have done to study $\mathbf{a_c}$ and $\mathbf{c_\omega}$ entanglement at T_c = 5000 mK, shown in Figure 6.10. The results show that the idea works well in which the entanglement between modes is improved in amplitude because of the MC and PD coupling factor increasing. The coupling factor mentioned above as critical to engineer the optoelectronic converter creates an ignorable difference between this converter and others [14-15], [23], [27]. So, it can give an unavoidable glue in the converter designing when one compares the results of Figure 6.10 with Figure 2 shown in [14]. In the latter work, the operational temperature is confined to T = 15 mK, and also with a coupling factor around μ = 0.013, the entanglement is created. In contrast, in the former

one the entanglement is produced for $\mu = 3.09\times10^{-4}$ at 5000 mK. The important region of Figure 6.10 is zoomed in for better presentation and depicted as an inset figure. Eventually, it is found as an important conclusion that the optoelectronic converter as a new design in contrast to the electro-opto-mechanical converter can preserve the entangled states since the operational temperature is increased. Thus, it is shown using simulation results that the entangled photons generating at a higher temperature lead to significantly alive the entanglement at different levels of quantum radar. In a simple word, the entangled photons generation at high temperature guarantees the returned signals non-classicality.

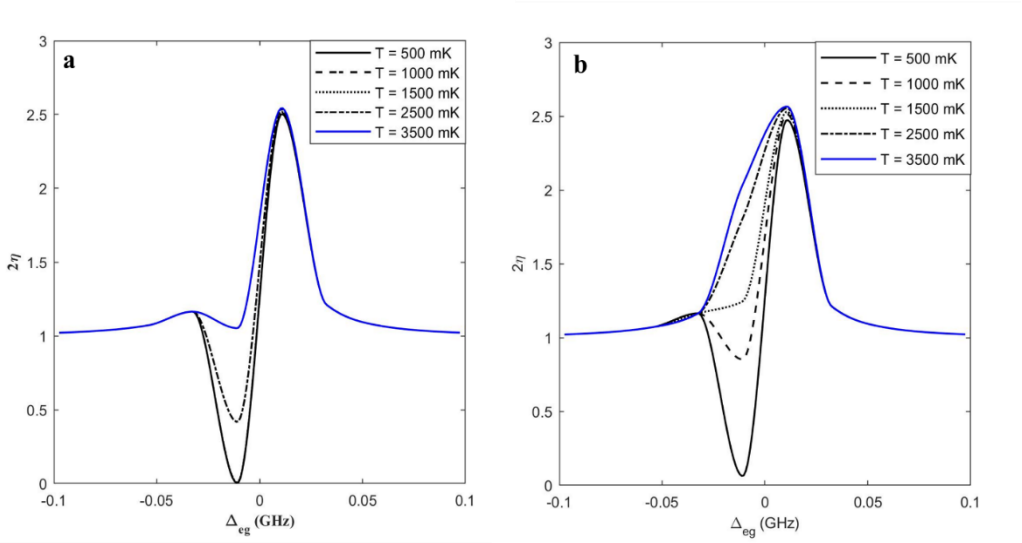

Figure 6.9. (2η) vs. Detuning frequency (Δ_{eg}), a) $\mathbf{a_c}$ and $\mathbf{c_\omega}$, b) $\mathbf{a_c}$ and $\mathbf{c_b}$.

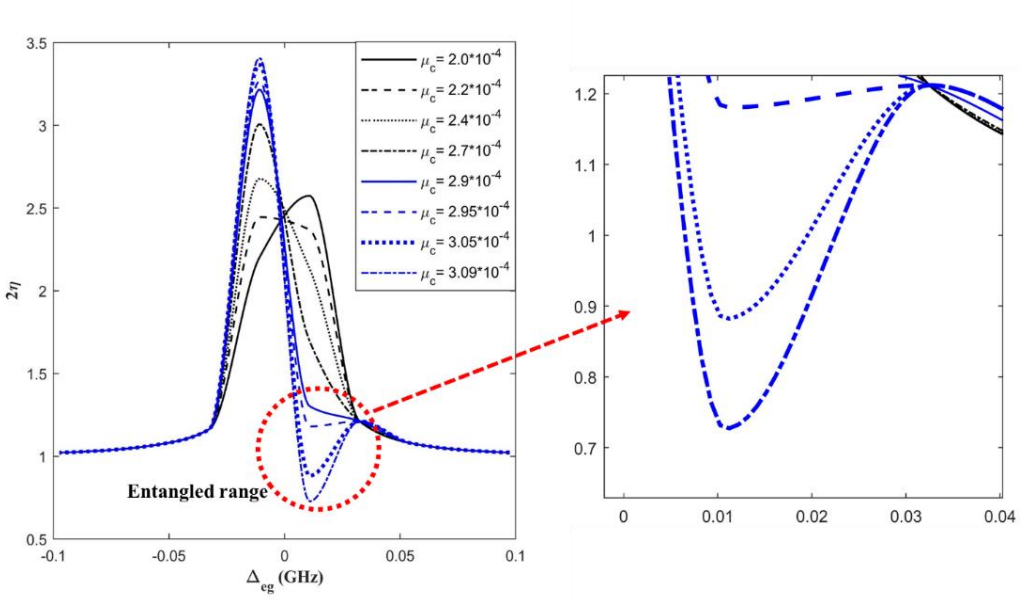

Figure 6.10. (2η) vs. Δ_{eg}, MC-PD coupling effect at T_c = 5000 mK.

The transmitter-detector (D_{td}) distance is another vital parameter studied in this dissertation, shown in Figure 6.11. According to the theoretical formula expressed in Eqs. 4.38 and 4.39, increasing D_{td} leads to an increase of the thermally excited photons. This eventuates to entanglement disturbing between modes. Moreover, as D_{td} is increased to 2000 m, shown in Figure 6.11d, the entanglements between all modes entirely leak away, and the photons before detection become separable. This is attributed to the thermally excited photons and noise effect on the fragility of the entangled states. Losing all of the non-classicality of the photons before detection suggests that the designer has to study the quantum correlation between signals (retained and returned) rather than the entanglement. The returning signal entanglement with the idler is mostly lost due to the propagation loss and target scattering effects. In the following, the results contributed to the optoelectronic converter are illustrated, and these results are definitely regarded as a chief contribution of the new design to generate the entanglement used in quantum radar application.

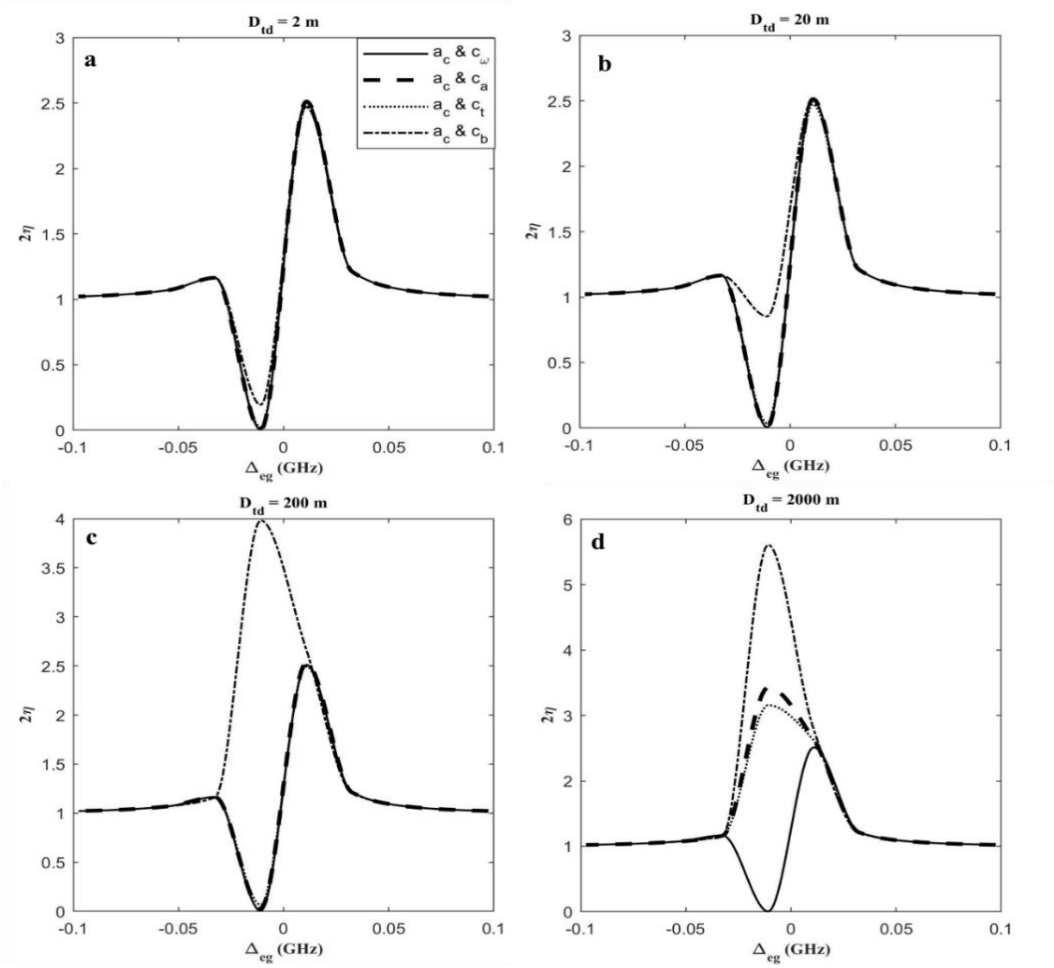

Figure 6.11. (2η) vs. Δ_{eg}, a) D_{td} = 2 m, a) D_{td} = 20 m, a) D_{td} = 200 m, a) D_{td} = 2000 m, for μ_c = 0.0002, T_c = 1000 mK.

The foundation of this dissertation, as the main aim, emphasizes the design of an optoelectronic converter to preserve entanglement between modes, even though the operational temperature is increased. Therefore, it is specifically focused on the MC-PD coupling factor engineering to manipulate the entanglement. Figure 6.12 shows that all modes become separable by increasing T_c around 3500 mK for a weak coupling between MC and PD cavities. As an important point to design a suitable system, it should be noted that the entanglement between $\mathbf{a_c}$ and $\mathbf{c_\omega}$ is directly affected by MC-PD coupling factor. Thus, it is clear that the retained and returned fields non-classicality can be manipulated as a robust functionality based on the mentioned coupling factor. To prove the latter mentioning point, one can pay special attention to the results illustrated in Figure 6.13, in which the simulations were done in the same condition with Figure 6.12 except

μ_c to controlling the coupling strength. According to results illustrated in Figure 6.13, the entanglement is partially preserved between $\mathbf{a_c}$ and $\mathbf{c_b}$ at a very high temperature up to 50 K. This is contributed to the unique design of the optoelectronic converter. The enhancement of the MC and PD coupling factor may generate so strong non-classicality correlated photons even though the propagation inside the real mediums can slightly affect them and cannot kill all of the entanglement between photons. Thus, as a short conclusion, the returned modes non-classicality maintaining is strongly dependent on the conditions that MC modes are created to be entangled with the optical cavity photons. If the MC photons entanglement with OC mode is accomplished at a very high temperature, then the retained (idler) and returned modes remained entangled.

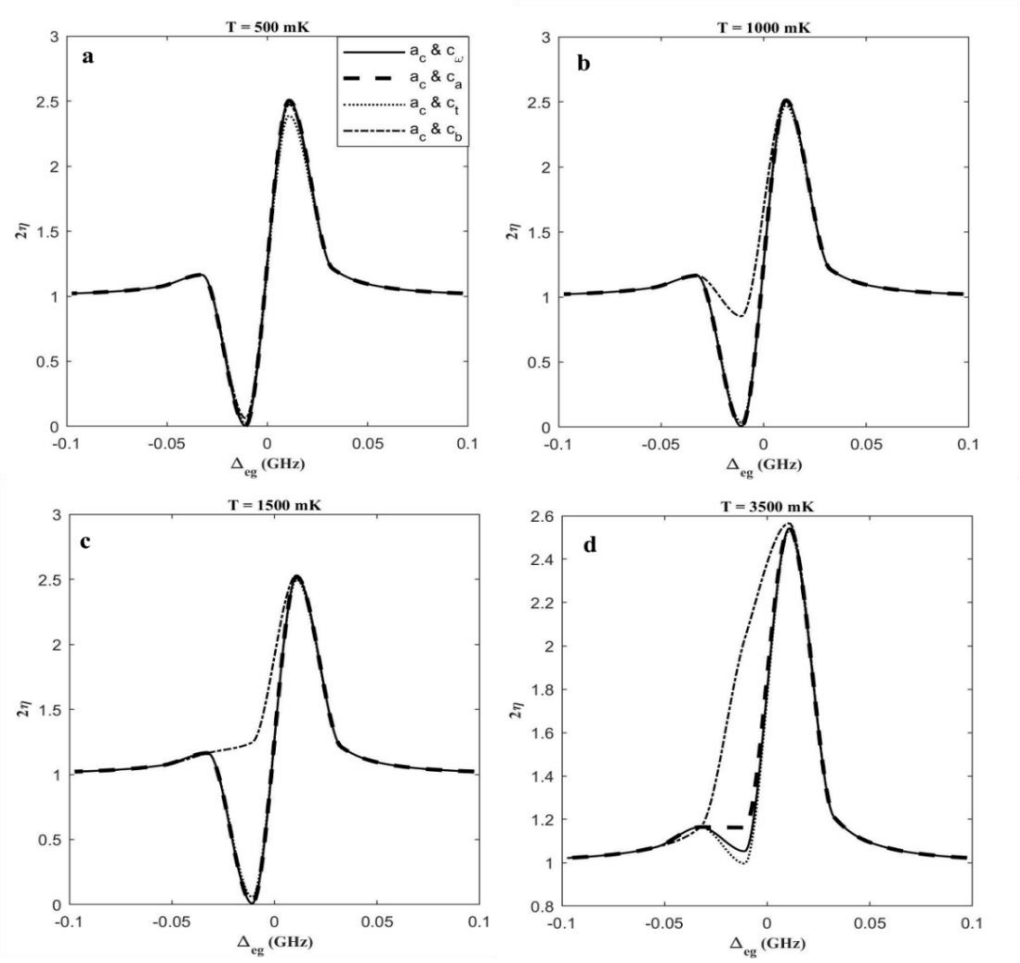

Figure 6.12. (2η) vs. Δ_{eg}, a) T_c = 500 mK, a) T_c = 1000 mK, a) T_c = 1500 mK, a) T_c = 3500 mK.

A dashed circle is used in Figure 6.13 to clarify the region that the photons remained entangled. Also, for a clear presentation, a few crucial regions of the figure are exaggerated and depicted as an inset on the main figure. Figure 6.13 shows that it is possible to create the entanglement between modes at a high temperature around 5 K. Nonetheless, it doesn't mean ignoring the effect of the optoelectronic converter as an efficient system to create robust non-classicality for the photons at high temperatures. Another important point in the design of the optoelectronic converter is MC and PD coupling factor, which is entirely different than the electro-opto-mechanical converter [14-17]. The latter converter is designed regarding the change of the capacitor's layer distance. That has been done by applying the optical pressure from the optical cavity. In contrast, in the optoelectronic converter, the depletion layer gap's width of VD

introduces the capacitance. The depletion layer width changing because of the photocurrent flowing leads to shifting μ_c, which affects the drop voltage across VD. In this procedure, the MC and PD coupling factor μ_c is implicitly manipulated via OC modes. While in the traditional converter, it is optical pressure generating by OC that plays the prominent role to displace the capacitor's electrodes to manipulate the MC cavity resonance. The mechanical part in the system limits the operational frequency because the injecting noises because of thermal effect as a crucial factor confines the operational temperature [14-17]. The other significant point studied in this work is the role amplifier or active medium before the signal propagation in the atmosphere. It is clear from the simulation results that increasing D_{td} destroys the entanglement between modes. This is attributed to the fact that in the new design, there is no active medium to amplify the signals. It is because the entangled photons amplification to produce more photons entangled with the origin ones is a crucial task [16,65]. The task is so challenging because the amplifier stage can easily kill the entangled photons. So, it is deliberately preferred to design a typical quantum radar without of amplifier.

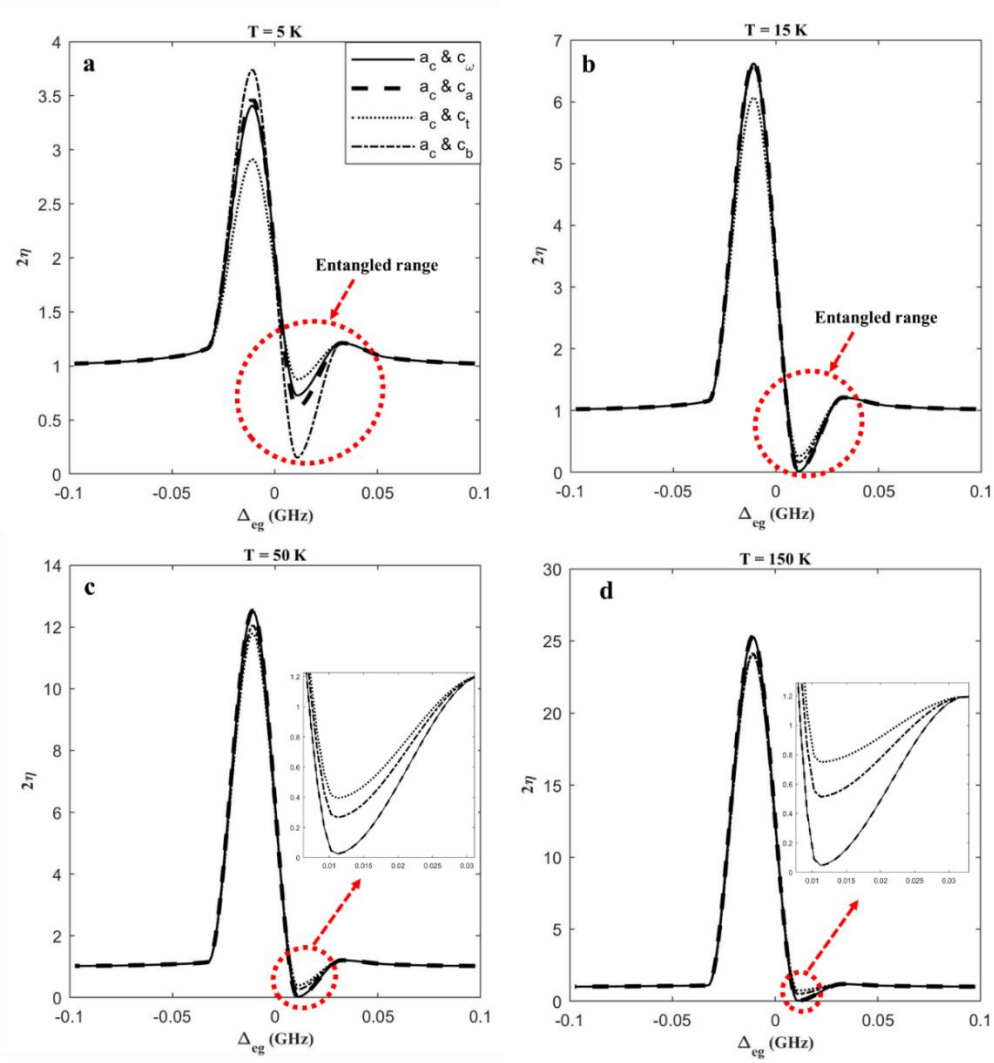

Figure 6.13. (2η) vs. Δ_{eg}, a) T_c = 5 K, a) T_c = 15 K, a) T_c = 50 K, a) T_c = 150 K.

6.3 Quantum Radar Cross-section

In the previous section, the electro-opto-mechanical and optoelectronic converters are discussed to produce the entangled photons. Also, the trade-offs in the systems are studied by which the designed converters can enforce to the system and consequently introduce a suitable system. This section aims to raise the associated results to the radar cross-section calculated with a new method compared to the classical ones. In other words, we want to discuss the QMoM method specifically introduced briefly in the previous section (5.2). To examine QMoM and also to answer an important question that can QMoM do in the same way as MoM, a metal plate with 1m×1m illuminating via an incident field is supposed and illustrated in Figure 6.14a. To testify

QMoM results with MoM results, a simple geometric shape is selected [69]. Also, there are some numerical and theoretical modeling results of RCS calculated for a metal square plate [69, 70]. Figure 2.2b reveals the main lobe increase of QMoM beside the side-lobe. This figure demonstrates the RCS calculated by MoM and QMoM for the considered geometry at f = 1.2 GHz and $\theta_i = 0$, $\varphi_s = \varphi_i = 0$. The difference between two methods indicated in the figure by a dashed circle showing the main lobe enhancing as well as the side-lobe. This means that the main lobe improvement could not be predicted by QRCS. We think that this fact is arisen because of the difference between $\Psi_c(\Delta R,t)$ and $\Psi_d(\Delta R,t)$. It was discussed in detail in the previous section. Also, in QMoM, the current quantization derived in Eq. 5.30 has a critical role that can strongly affect the results. The current density operator expressed in Eq. 5.30 causes the wave function imaginary part effects besides its real part.

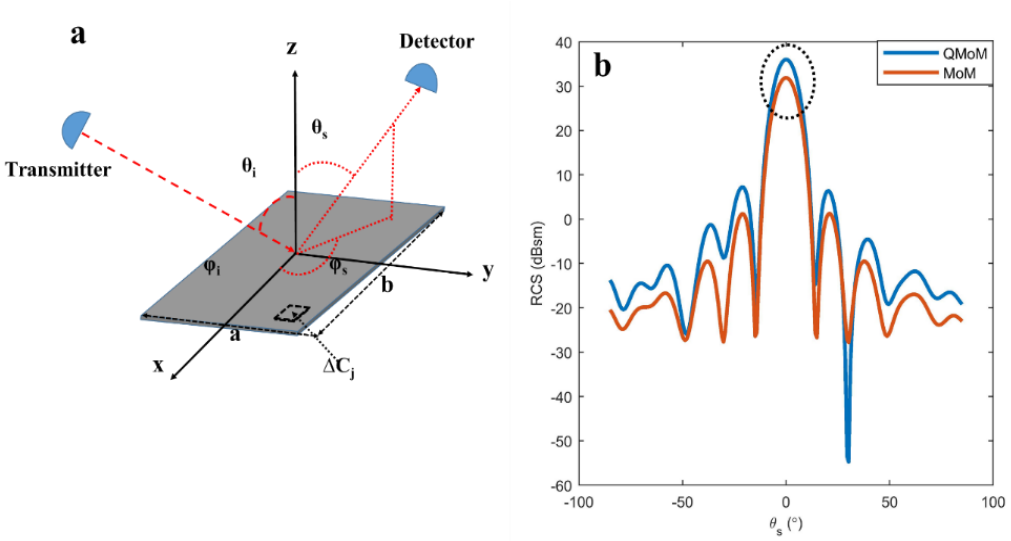

Figure 6.14. Square plate geometry and the illumination of the microwave photons with angle θ_i, φ_i and scattering angle θ_s, φ_s. ΔC_j stands j^{th} unit of the segmentation used in MoM; b) QMoM and MoM comparison for the calculation of RCS of $1m^2$ rectangular target illuminated at f = 1.2 GHz and $\theta_i = 0$, $\varphi_s = \varphi_i = 0$..

As a routine approach to certify the QMoM with respect to MoM, the effect of some parameters are investigated on RCS, such as frequency of the incident wave, the incident wave angle, and target geometrical shape. It is shown in Figure 6.15 that by frequency increasing, both the main lobe peak and the nodes number of the interference pattern are increased accordingly. In order to

show the frequency increasing effect on the main lobe, the related part of the figure is exaggerated and illustrated as the inset figure. It is shown that by increasing frequency, the amplitude of the main lobe is increased, and according to MoM approach, increasing the frequency enhances the main lobe amplitude; thus, QMoM operates in the same way as MoM when the frequency is changed. The comparison between the results of the standard method like MoM with QMoM satisfies the calculation accuracy of the new approach.

For further study about the QMoM approach, the incident angle effect on RCS are investigated at f = 1.2 GHz, $\varphi_s = \varphi_i = 0$. Similar to RCS and QRCS, as the incident photon deviates from the normal incident angle $\theta_i = 0$, the attributed scattering main lobe shifts from the normal position. This point is studied, and the simulated results are depicted in Figure 6.16. These simulation results are in agree with RCS and QRCS results [44, 68-69].

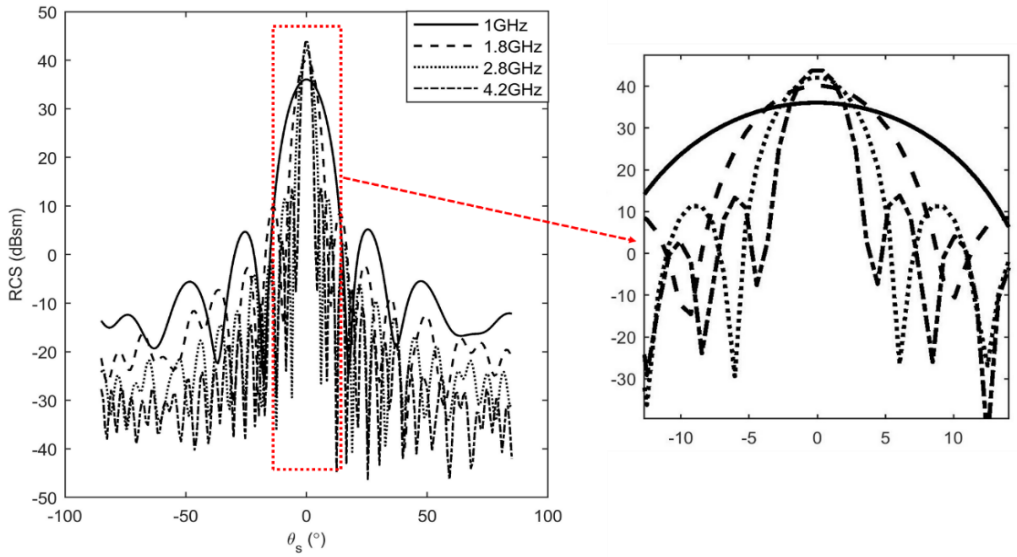

Figure 6.15. Frequency effect in QMoM approach on RCS vs pitch angle changing (θ_s) at $\theta_i = 0$, $\varphi_s = \varphi_i = 0$.

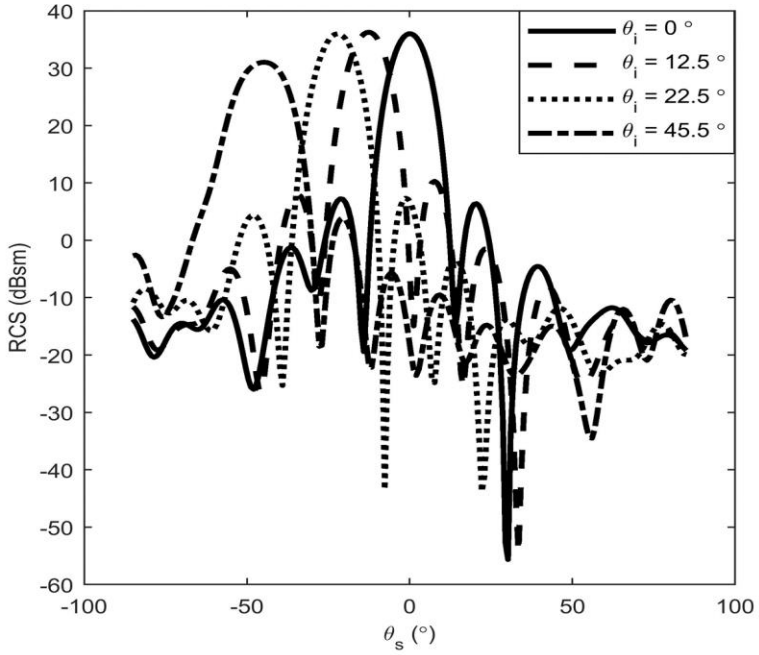

Figure 6.16. Incident angle effect in QMoM approach on RCS vs pitch angle (θ_s) at f = 1.2 GHz, $\varphi_s = \varphi_i = 0$.

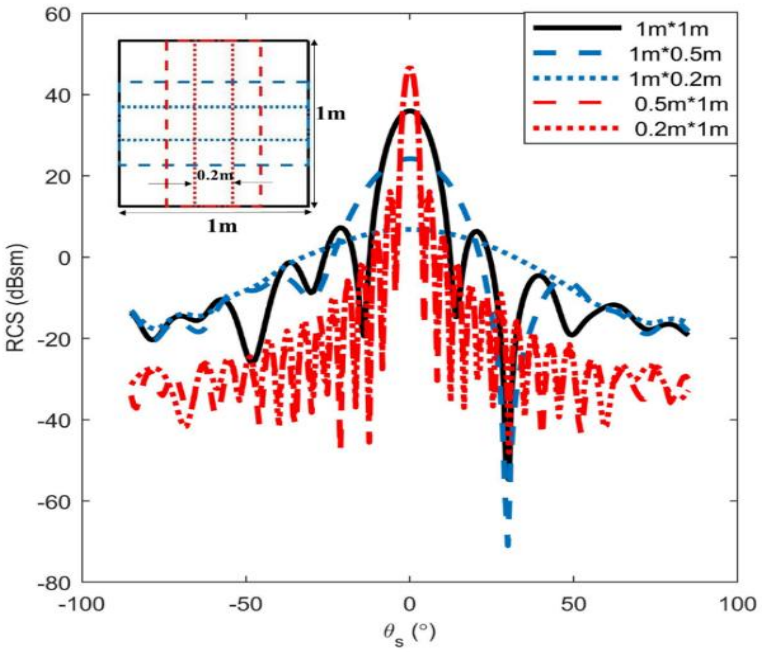

Figure 6.17. Intercepted Shape effect in QMoM approach on RCS vs pitch angle (θ_s) at f = 1.2 GHz, $\theta_i = 0$, $\varphi_s = \varphi_i = 0$.

Finally, the geometrical shape effect on RCS using with QMoM approach is studied, and the results are depicted in Figure 6.17. It is shown that by changing the target shape in terms of incident angle, the RCS profile is significantly altered, and the main lobe amplitude is changed. By decreasing the width, e.g., 0.5m×1m and 0.2m×1m, as shown respectively with red dashed and red dashed-dotted in the figure, the main lobe amplitude is severely increased. In other words, it operates like increasing the incident frequency that means the related wavelength has to be decreased. In contrast, by reducing the length, e.g., 1m×0.5m and 1m×0.2m shown respectively with blue dashed and blue dashed-dotted, with respect to $\theta_i = 0$, the magnitude of the RCS is significantly decreased. It acts as the incident frequency decreasing or increasing the associated wavelength. As an important point, it is interesting to note again that QMoM has perfect harmony with MoM analyzing method, which suggests that the theory behind it works well. Nonetheless, it indicates the main lobe enhancing in RCS that has not been predicted by the QRCS. That is an astonishing point about this study that increases the popularity of the QMoM analyzing method. So, here, it is possible to conclude that the RCS calculation by canonical quantization methods is a perfect method than the dipole approximation, and also QMoM can be employed rather than the classical MoM to calculate and analyze the RCS.

7. CONCLUSIONS

In the last part of this dissertation, a short conclusion about the designed converters, electro-opto-mechanical and optoelectronic, and also RCS calculation using quantum theory is presented as follows.

First of all, a quantum radar with a traditional electro-opto-mechanical converter operating at L-band (MC output resonance frequency is around 1.5 GHz) is theoretically designed to study the behavior of the entanglement at the different stage of a quantum radar, such as the generation of entangled photons, intensification of entangled photons to produce more photons, propagation of the microwave entangled photons, and finally the target reflection. As a common point, it is obvious that a quantum radar advantage is due to the utilization of entangled photons. Nonetheless, it had been proved that the entangled states are so unstable and can be easily broken. For this reason, the entanglement behavior as a major purpose of the study is thoroughly examined. Firstly, an electro-opto-mechanical converter is designed using the canonical conjugate method, and all of the contributed theory was derived. It is shown that the modes of the optical and microwave cavities remained entangled for such a design. After this, the microwave cavity photons (entangled and separable photons) experience the effect of the active medium, then propagate inside the atmosphere channel, and finally endure the reflection from the target. The effects of the different mediums listed above are theoretically studied using the QED theory. The results demonstrate the entanglement sustainability through engineering the system. It is contributed to the utilization of the active medium that was used in the system. In fact, in the design of the electro-opto-mechanical converter, it is supposed that the active medium could amplify the entangled photons while preserving entanglement. Also, the effect of the mechanical cavity damping rate, atmosphere channel-related absorption and scattering coefficient, and system operational temperature are studied on entanglement behavior between modes. As an interesting result, if the electro-opto-mechanical converter operational temperature is limited to around 200 mK, and with the assumption of a bad atmospheric condition with contributed coefficient $\kappa_{atm} = 20\times10^{-7}$ 1/m, the returned photons from a target at R = 10 km exhibit slightly the entanglement. However, the entanglement between the incident and

backscattering photons is completely lost at other frequencies. It is noteworthy to mention that the active medium has a critical effect on entanglement conservation. It is shown that without the active medium in the system, the entanglement between modes is completely lost. Another critical point about the designed quantum radar with electro-opto-mechanical converter was the operation of the converter at very low temperatures, e.g., 30 mK. It is contributed to the mechanical part that the converter used to couple the OC to the MC. To solve the temperature problem of the latter mentioned design, another converter is proposed and called "optoelectronic converter" replaced rather than the mechanical part.

Thus, a new quantum radar utilizing an optoelectronic converter to create the entangled photons is theoretically designed, modeled, and analyzed. In this design, the MC frequency of the optoelectronic converter is increased to 2.7 GHz, and it is because we mainly concentrated on limiting the thermally excited photons generated in MC. The latter mentioned converter as a significant part of the designed quantum radar operating at S-band was analyzed using the "canonical quantization method". This method gives some degrees of freedom to manipulate every quantity in the system, such as MC and PD coupling. This gives some abilities for the system to preserve the entanglement behavior. Additionally, applying this approach actually answers one of the main questions of this dissertation that is: "which parameter specifically subsides the temperature effect on the entanglement between retained and returned modes". Using the new converter, it is shown that it is possible to effectively decrease the temperature effect on the cavity modes entanglement by engineering the MC and PD coupling factor. Accordingly, the returning modes non-classicality is preserved at some detuning frequencies meaning the entanglement between returned and retained modes when the temperature is raised around 5000 mK. The modes remain entangled even though the returned signals experienced the atmosphere channel loss and additionally the loss related to the target scattering. This is an interesting result in the field of quantum radar that the retained modes non-classicality is indispensably dependent on the conditions associated with the optoelectronic converter. In other words, if the entanglement between cavity modes into the converter is created at a very high temperature, the probability of the retained (idler) and returned modes entanglement is strongly increased. As the most important and remarkable achievement of this thesis, it is notable to mention that the entanglement establishing at high temperature is accomplished just by utilizing the optoelectronic subsystem.

After investigating the quantum radar and the associated converters, also full quantum theory is studied to calculate the RCS. In fact, RCS is calculated using the "canonical quantization method," seeming that it is a more complete theory than the "dipole approximation method". The emphasis is laid on making a comparison between two theories to calculate the RCS. Some similarities between two approaches are found; nonetheless, some key factors were ignored since the "dipole approximation method" is applied. The significant dissimilarity between two quantum-based approaches is issued due to the interaction Hamiltonian. In the interaction Hamiltonian, the coupling factor derived by two approaches creates a considerable difference between two methods. To make a clear comparison between methods, RCS is calculated in the same conditions by the approaches. The simulated results show that the emitting photons calculated by "canonical quantization method" has a greater amplitude than the emitting photons calculated by "dipole approximation method". The RCS interference pattern can be severely affected by this point. To prove that, a new numerical approach is established to emerging quantum theory in MoM to improve the RCS calculation for QRCS. QMoM idea arose from the fact that the current density average employed by MoM can be replaced with the current density operator. Thus, the current density operator is theoretically derived using quantum theory and substituted in MoM. The results show that the new approach enhanced the side-lobe similar to the QRCS, as well as the main lobe intensity improving. The main lobe intensity improvement is not predicted by QRCS approach. In fact, it is the difference between the current density average and the current density operator that play the original role and cause the main difference between two methods (MoM and QMoM). Additionally, to test the accuracy of QMoM method, some parameters effect such as frequency, incident angle, and geometry effect are studied. The results show full compatibility between MoM and QMoM in accuracy. As a significant result, it can be suggested that the "dipole approximation method" is not a complete one to calculate RCS. Although the dipole approximation method may improve the accuracy of the RCS calculation with respect to CRCS, it cannot be considered a perfect method for analyzing.

REFERENCES

[1] M. Lanzagorta, J. Uhlmann, Quantum Radar, Morgan & Claypool Publishers series, **2012**.

[2] S. Lloyd, Science, 321 (**2008**) 1463.

[3] K. Lukin, IEEE, 9th International Kharkiv Symposium on Physics and Engineering of Microwaves, Millimeter and Submillimeter Waves (MSMW), 20-24 June 2016, Kharkiv, Ukraine, **2016**, p.25.

[4] C. W. Sandbo Chang, A. M. Vadiraj, J. Bourassa, B. Balaji, and C. M. Wilson, Appl. Phys. Lett. 114 (**2019**) 112601.

[5] Y. Shih, IEEE J. Sel. Top. Quantum Electron, 13 (**2007**) 1016.

[6] A. Salmanogli, H. S. Gecim, Ann. Physics, 394, (**2018**) 162.

[7] A. Salmanogli, H. S. Gecim, E. Piskin, IEEE Sensors Journal, 18 (**2018**) 5723.

[8] U. Las Heras, R. Di Candia, K. G. Fedorov, F. Deppe, M. Sanz, E. Solano, Scientific Reports, 7 (**2017**) 9333.

[9] P. C. Humphreys, N. Kalb, J. P. J. Morits, R. N. Schouten, R. F. L. Vermeulen, D. J. Twitchen, M. Markham, R. Hanson, Nature, 558 (**2018**) 268.

[10] S. Wengerowsky, S. Koduru Joshi, F. Steinlechner, H. Hübel and R.Ursin, Nature, 564 (**2018**) 225.

[11] A. Salmanogli, D. Gokcen, and H. S. Gecim, IEEE Sensors Journal, 19 (**2019**) 3660.

[12] A. Salmanogli, Journal of the Optical Society of America B, 35 (**2018**) 2467.

[13] A. Salmanogli, Phys. Rev. A, 100 (**2019**) 013817.

[14] S. Barzanjeh, M. Abdi, G.J. Milburn, P. Tombesi, and D. Vitali, Phys. Rev. Lett, 109 (**2012**) 130503.

[15] S. Barzanjeh, S. Guha, Ch. Weedbrook, D. Vitali, J. H. Shapiro, and S. Pirandola, Phys. Rev. Lett., 114 (**2015**) 080503.

[16] S. Barzanjeh, S. Pirandola, D. Vitali, and J. M. Fink, Science Advances, 6 (**2020**) 1.

[17] N. Lauk, N. Sinclair, S. Barzanjeh, J. P. Covey, M. Saffman, M. Spiropulu, and Ch. Simon, Quantum Sci. Technol., 5 (**2020**) 020501.

[18] A. Salmanogli, D. Gokcen, H.S. Gecim, IEEE J. Sel. Top. Quantum Electron, 26 (**2020**) 1.

[19] Y. Shih, IEEE J. Sel. Top. Quantum Electron, 9 (**2003**) 1455.

[20] T. Ritz, Procedia Chemistry, 3 (**2011**) 262.

[21] A. Salmanogli, D. Gokcen, Sensors and Actuators A: Physical, 322 (**2021**) 112636.

[22] A. Salmanogli, D. Gokcen, and H. S. Gecim, Phys Rev Applied, 11 (**2019**) 024075.

[23] S. Barzanjeh, D. Vitali, P. Tombesi, G. J. Milburn, Phys Rev A, 84 (**2011**) 042342.

[24] N. Aggarwal, K. Debnath, S. Mahajan, A. B. Bhattacherjee, M. Mohan, International Journal of Quantum Information, 12 (**2014**) 1450024.

[25] C. Genes, A. Mari, P. Tombesi, D. Vitali, Phys. Rev. A, 78 (**2008**) 032316.

[26] D. Vitali, S. Gigan, A. Ferreira, H. R. Böhm, P. Tombesi, A. Guerreiro, V. Vedral, A. Zeilinger and M. Aspelmeyer, Phys. Rev. Lett, 98 (**2007**) 030405.

[27] A. Salmanogli, H. Gecim, IEEE J. Sel. Top. Quantum Electron, 26 (**2020**) 1.

[28] J. R. Jeffers, N. Imoto, R. Loudon, Phys. Rev. A, 47 (**1993**) 3346.

[29] B. Huttner, S. M. Barnett, Phys. Rev. A, *46* (**1992**) 4306.

[30] M. O. Scully, M. S. Zubairy, Quantum Optics, Cambridge University Press, UK, **1997**.

[31] E. Waks, D. Sridharan, Phys. Rev. A, 82 (**2010**) 043845.

[32] A. Salmanogli, Phys. Rev. A., 94 (**2016**) 043819.

[33] R. Simon, Phys. Rev. Lett., 84 (**2000**) 2726.

[34] J. Laurat, G. Keller, J. A. Oliveira-Huguenin, C. Fabre, T. Coudreau, A. Serafini, G. Adesso, F. Illuminati, Journal of Optics B: Quantum and Semiclassical Optics, 7 (**2005**) S577.

[35] W. Ge, M. E. Tasgin, M. S. Zubairy, Phys. Rev. A., 92 (**2015**) 052328.

[36] T. Deesuwan, Entanglement Criteria for Continuous-Variable States, Master of Science Dissertation, Imperial College London, **2010**.

[37] B. R. Mahafza, Radar Systems Analysis and Design Using MATLAB, Chapman & Hall/CR, **2000**.

[38] M.L. Skolnik, Introduction to Radar Systems, Third Edition, McGraw Hill, **2001**.

[39] R. E. Collin, Antenna and Radiowave propagation, McGraw Hill book company, **1985**.

[40] C. A. Balanis, Modern Antenna Handbook, A John Wiley & Sons, INC., Publication, **2002**.

[41] B. M. Oliver, Proceedings of the IEEE, 53 (**1965**) 436.

[42] J. F. Valtuena, J. A. Garrido, J. I. Izpura, IEEE Transactions on Electronic Devices, 45 (**1998**) 1201.

[43] C. J. Reddy, M. D. Deshpande, C. R. Cockrell, and F. B. Beck, IEEE Trans. Antennas Propag, 46 (**1998**) 1229.

[44] H-L. Dong, S.X. Gong, P-F. Zhang, J. Ma, B. Zhao, IET Microw. Antennas Propag, 9 (**2015**) 775.

[45] G. K. Carvajal, D. J. Duque, and A. J. Zozaya, ACES Journal, 24 (**2009**) 487.

[46] I. Nicolaescu, T. Oroian, 5th International Conference on Telecommunications in Modern Satellite, Cable and Broadcasting Service. TELSIKS 2001. Proceedings of Papers (Cat. No.01EX517), 19-21 Sept. 2001, IEEE, Nis, Yugoslavia, (**2002**), 65.

[47] R. Radha Krishna, R. Murali Krishna, R.Gopi Krishna, D.Sekhar, International Journal of Advanced Research in Computer Science and Electronics Engineering, 1 (**2012**) 67.

[48] P. Blacksmith, R. E. Hiatt, R. B. Mack, Proceeding of the IEEE, 53 (**1965**) 901.

[49] P. Pouliguen and R. Hemon, C. Bourlier, J. F. Damiens, J. Saillard, Progress In Electromagnetics Research B, 9 (**2008**) 263.

[50] S. Hatamzadeh-Varmazya, Z. Masouri, Journal of Electromagnetic Waves and Applications, 28 (**2014**) 1360.

[51] A Salmanogli, D Gokcen, IEEE Access, 8 (**2020**) 205487.

[52] Tr. Thang, A study of Entanglement theory, Iowa State University Capstones, Creative Components, **2019**.

[53] L. Susskind and A. Friedman, Quantum Mechanics (Theoretical minimum), Basic Books, **2014**. http://www.basicbooks.com/full-details?isbn=9780465036677.

[54] A. Einstein, American Journal of Physics, 33 (**1965**) 367.

[55] R. Geherenberk, Physics Today, 31 (**1978**) 34.

[56] P. Weinberger, Philosophical Magazine Letters, 86 (**2006**) 405.

[57] Arthur H. Compton, Phys. Rev. 21 (**1923**) 483.

[58] G. Cameron, Authentic African Leadership: Authentic African Leaders Defined and the Techniques That Made Them Great, Real African Publishers, **2014**.

[59] M. E Tasgin, M. Gunay, M.S. Zubairy, Phys.Rev. A., 101 (**2020**) 062316.

[60] R. Simon, E. C. G. Sudarshan, Phys. Rev. A., 36 (**1987**) 3868.

[61] R. Feynman, QED: The Strange Theory of Light and Matter, Princeton University Press, **1985**.

[62] M. Höijer, T. Hult and P. Jonsson, Quantum Radar– A survey of the science, technology and literature, FOI-R--4854—SE, **2019**.

[63] P. Kumar, V. Grigoryan, and M. Vasilyev, Proceedings of the 14th Coherent Laser Radar Conference, 2007, Snowmass, Colorado, USA, (**2007**) 9.

[64] U. Fano, Phys. Rev., 103 (**1956**) 1202.

[65] E. Pomarico, B. Sanguinetti, P. Sekatski, H. Zbinden and N. Gisin, New Journal of Physics, 13 (**2011**) 063031.

[66] S. H. Hashemipour, A. Salmanogli, N. Mohammadian, Key Engineering Materials, 500 (**2012**) 3.

[67] A. Salmanogli, D. Gokcen, IEEE Sensors Journal, 21 (**2021**) 9054.

[68] M. J. Brandsema, R. M. Narayanan, M. Lanzagorta, Quantum Inf Process, 16 (**2017**) 1494.

[69] Ch. Fang, H. Tan, Qi-F. Liu, L.Tao, L. Xiao, Y. Chen, and L. Hua, IEEE Photonics Journal, 10 (**2018**) 7500614.

[70] T. Zhang, H. Zeng, R. Chen, IEEE Access, 7 (**2019**) 154260.

[71] E. L. Rumyantsev, P. E. Kunavin, The quantum mechanical probability density and probability current density operators in the Pauli theory, arXiv:1708.04193 [cond-mat.mes-hall], **2017**.

[72] G. M. Wysin, Probability Current and Current Operators in Quantum Mechanics, Kansas State University, Manhattan, Vicosa, Brazil, **2011**.

[73] G. Rempe, Contemporary physics, 34 (**1993**) 119.

[74] Weng Cho Chew, C. C. Lu, IEEE Trans. Antennas Propag, 41 (**1993**) 897.

[75] S.Y. Wang, M.C. Lo, H.Y. Hsiao, H.S. Ling, C.P. Lee, Infrared Physics & Technology, 50 (**2007**) 166.

[76] G. Konstantotos, E. H. Sargent, Infrared Physics & Technology, 54 (**2011**) 278.

[77] A. Salmanogli, B. Nasseri, E. Piskin, Sensors & Actuators: A. Physical, 262 (**2017**) 87.

[78] E. Waks, D. Sridharan, Phys. Rev. A., 82 (**2010**) 043845.

[79] A. Salmanogli, Phys. Rev. A., 94 (**2016**) 043819.

[80] A. S. Clark, L. G. Helt, M. J. Collins, Ch. Xiong, K.Srinivasan, B. J. Eggleton, M. J. Steel, Nonlinear Optics for Photonic Quantum Networks, All-Optical Signal Processing. Springer Series in Optical Sciences, 194. Springer, Cham, **2015**.

APPENDIXES

Articles

1. Ahmad Salmanogli, Dincer Gokcen, H. Selcuk Gecim, Entanglement Sustainability in Quantum Radar, **IEEE JOURNAL OF SELECTED TOPICS IN QUANTUM ELECTRONICS,** 26, 6, 2020.
2. Ahmad Salmanogli, Dincer Gokcen, Analysis of Quantum Radar Cross-Section by Canonical Quantization Method (Full Quantum Theory), **IEEE Access**, 8, 205487-205494, 2020.
3. Ahmad Salmanogli, Dincer Gokcen, Optoelectronic based Quantum Radar: Entanglement Sustainability Improving at High Temperature, **IEEE Sensor Journal**, 21, 9054-9062, 2021.
4. Ahmad Salmanogli, Dincer Gokcen, Design of quantum sensor to duplicate European Robins navigational system, **Sensors and Actuators A** 322, 112636-112672, 2021.